Oil & Natural Gas Technology

DOE Award No.: DE-NT0006555

First Annual Report

October 2008 to September 2009

USE OF POLYMERS TO RECOVER VISCOUS OIL FROM UNCONVENTIONAL RESERVOIRS

Submitted by:
New Mexico Petroleum Recovery Research Center
New Mexico Tech, 801 Leroy, Socorro, NM 87801

Authored By: Randall Scott Seright (Principal Investigator)
Prepared for:
United States Department of Energy
National Energy Technology Laboratory

October 1, 2009

Office of Fossil Energy

DISCLAIMER

DEDICATION

This report is dedicated to the memory of my great friend Robert Dunn Sydansk. Bob showed extraordinary dedication toward advancing the science, engineering, and application of conformance improvement in reservoirs using polymers and gels. Bob invented the Cr(III)-carboxylate-HPAM gel conformance improvement technology. Weekly (and often daily) technical discussions with him were among the best parts of my job. I miss his insights, vision, and friendship.

ABSTRACT

This technical progress report describes work performed from October 1, 2008, through September 30, 2009, for the project, "Use Of Polymers To Recover Viscous Oil From Unconventional Reservoirs." Fractional flow calculations were performed to examine the potential of polymer flooding for a range of characteristics in viscous oil reservoirs (especially relevant to the North Slope of Alaska). Using these recovery results, a simple economic analysis was performed to make a preliminary assessment of the potential for polymer flooding in reservoirs with viscous oils. The analysis indicated that over a significant range of throughput values, polymer flooding can provide a higher relative profit than waterflooding. The results emphasize that maximizing injectivity of polymer solutions may be key to economic implementation of polymer flooding for recovery of viscous oils.

We determined viscosity (at 7.3 s^{-1}, room temperature) versus polymer concentration for 16 commercially available water soluble polymers (nine synthetic polymers and seven biopolymers) in a number of brines. For polymer solution viscosities above 10 cp, viscosity (μ) versus polymer concentration (C) fit quite well using the relation, $\mu=AC^B$. B values typically ranged from 1.6 to 2.5. This behavior provides a cost advantage when using polymer solutions to displace viscous oils. We characterized the performance in 55-md, 269-md, and 5,120-md cores for nine commercially available EOR polymers, including one xanthan, one diutan, and seven partially hydrolyzed polyacrylamides (HPAM). None of the polymers exhibited severe face-plugging in any of the cores. Xanthan and HPAM solution rheology in porous media correlated very well using the parameter: $u(1-\phi)/(\phi k)^{0.5}$, where u is flux, ϕ is porosity, and k is permeability. At low flux values in a 14.4-cm-long, 55-md Berea sandstone core, both xanthan and HPAM can exhibit resistance factors that are much higher than expected and an apparent shear-thinning behavior that deviates from expectations based on viscosity-versus-shear-rate data. Using xanthan injection into a 122-cm-long core, 57-md Berea core, we showed that this behavior was an experimental artifact that is not expected to materialize and benefit oil recovery in field applications. Future tests will examine this issue for HPAM solutions.

In one North Slope viscous oil reservoir, horizontal wells were calculated to provide injectivities and productivities that are 9-10 times those expected for unfractured vertical wells. The pseudodilatant (viscoelastic) behavior of HPAM polymers could lead to significantly reduced injectivity in unfractured vertical North Slope injection wells (2-8% that of water for the HPAM solutions investigated in this report). In contrast, in North Slope unfractured horizontal wells, injectivity reductions should be significantly less severe (with polymer injectivity 10-15% that of water for most of our cases). The pseudoplastic (shear-thinning) xanthan and diutan solutions have an injectivity advantage over HPAM solutions in unfractured vertical wells, with estimated injectivity values around one-third that of water for the solutions that we examined. For horizontal wells, this advantage is diminished considerably.

Many HPAM/xanthan mixtures in brine show viscosity behavior that is virtually the same as solutions with only xanthan. Since xanthan is considerably more expensive (per kg) than HPAM, this observation suggests a significant economic value in using polymer mixtures in brines instead of a single polymer. Diutan could be competitive for use if it costs 4.39 to 6.23 times the cost of HPAM. Alginate was generally ineffective as a viscosifier, compared with the other polymers.

TABLE OF CONTENTS

LIST OF TABLES

TABLE OF FIGURES

ACKNOWLEDGMENTS

Financial support for this work is gratefully acknowledged from the United States Department of Energy (NETL/National Petroleum Technology Office), the State of New Mexico, CP Kelco, and SNF Floerger. ConocoPhillips was kind in providing information on relevant North Slope viscous oil reservoirs. I greatly appreciate the efforts of those individuals who contributed to this project. Simulation work mentioned in Chapter 2 was performed by Oppong Kwame (graduate student at New Mexico Tech), Guo Chen and Peihui Han (Daqing Oilfield Company, PetroChina), and Bergit Brattekas and Aasmund Haugen (University of Bergen). Kate Wavrik and Breanne Dunaway performed the viscosity measurements in Chapter 3. Tianguang Fan performed the coreflood and viscosity measurements in Chapter 4. Professor Rosangela Balaban (U Federal Rio Grande Do Norte, Brazil) performed the work in and wrote Chapter 6, with help from Kate Wavrik, who measured the viscosities. I especially appreciate the thorough review of this manuscript by Julie Ruff.

EXECUTIVE SUMMARY

This technical progress report describes work performed from October 1, 2008, through September 30, 2009, for the project, "Use Of Polymers To Recover Viscous Oil From Unconventional Reservoirs." The objective of this three-year research project is to develop methods using water soluble polymers to recover viscous oil from unconventional reservoirs (i.e., on Alaska's North Slope). The project has three technical tasks. First, limits will be re-examined and redefined for where polymer flooding technology can be applied with respect to unfavorable displacements. Second, we will test existing and new polymers for effective polymer flooding of viscous oil, and we will test newly proposed mechanisms for oil displacement by polymer solutions. Third, we will develop novel methods of using polymer gels to improve sweep efficiency during recovery of unconventional viscous oil.

Fractional Flow/Numerical Analysis. We performed a number of base case simulations to establish confidence in the predictions of various reservoir simulators, including ECLIPSE, VIP, and POLYMER (a variant of UTCHEM). In the first case, we simulated simple one-dimensional displacement of oil (with various viscosities ranging from 1 to 100,000 cp) when injecting 1-cp water. For all three simulators, the results matched predictions from fractional flow calculations reasonably well. However, when two layers were present with different permeabilities, the simulations did not yield credible results. In particular, they predicted that, regardless of mobility ratio, recovery efficiency for cases with crossflow between the layers should be similar to those with no crossflow. Ultimately, we learned the proper formatting of the ECLIPSE simulator to obtain a reasonable match of recovery predictions with those from fractional flow calculations, notably for the free crossflow cases. We performed fractional flow calculations where a polymer flood was implemented to displace 1,000-cp oil. Using these recovery results, a simple economic analysis was performed to make a preliminary assessment of the potential for polymer flooding in reservoirs with viscous oils. The analysis indicated that over a significant range of throughput values, polymer flooding provides a higher relative profit than waterflooding. The results emphasize that maximizing injectivity of polymer solutions may be key to economic implementation of polymer flooding for recovery of viscous oils.

Both with and without crossflow, for 1 pore volume (PV) of polymer injection, oil recovery values increase as a more-permeable layer becomes thicker relative to a less-permeable layer. Without crossflow, large PV throughputs are needed to achieve high recovery values, even when injecting viscous polymer solutions. If only one PV of polymer is injected, relatively low recovery values will be realized if the oil is viscous. Under these conditions (without crossflow), if one PV of polymer solution is injected, most of the recovery benefit is achieved using only a 10-cp polymer solution (i.e., rather than a significantly more viscous solution). In contrast with free crossflow, injection of more viscous polymer solutions (i.e., on the order of the oil viscosity) is needed to achieve high recovery values. With crossflow, nearly 100% recovery can be achieved by injecting 1 PV if the polymer is sufficiently viscous (i.e., the reciprocal of the mobility ratio is greater than or equal to the permeability ratio, k_1/k_2). The free crossflow case may be of most interest for our future considerations. For the permeabilities and viscosities that are likely to be experienced in our target North Slope reservoirs, gravity effects on the positions of polymer fronts will probably not be particularly important.

Polymer Viscosities. We determined viscosity (at 7.3 s^{-1}, 25ºC) versus polymer concentration for 16 commercially available water soluble polymers (nine synthetic polymers and seven biopolymers) in a number of brines. For polymer solution viscosities above 10 cp, viscosity (μ) versus polymer concentration (C) fit quite well using the relation, $\mu=AC^B$. B values typically ranged from 1.8 to 2.5. This behavior provides a cost advantage when using polymer solutions to displace viscous oils. Several observations were consistent with previous expectations. First, in the brines examined, polysaccharides (such as xanthan) provided a given viscosity level with much less polymer than for HPAM polymers. (Of course, the biopolymers cost noticeably more than the HPAMs.) Second, high Mw HPAMs provided a given viscosity level with less polymer than low Mw HPAMs. Third, for a given HPAM, the polymer requirements to achieve a given viscosity increased with increased salinity. Fourth, for a given xanthan, the polymer requirements to achieve a given viscosity were insensitive to salinity. Fifth, for a given HPAM, the polymer requirements to achieve a given viscosity increased with increased divalent cation content. For the various xanthan polymers examined, some viscosity differences were seen between 500 and 5,000 ppm. However, the variations in viscosity were noticeably less for the range of HPAM polymers. For a given polymer concentration, diutan provided the highest viscosity of any polymer tested. These viscosity results will be used as input for our future modeling studies.

Rheology in Porous Media. An important goal for our work is to determine the rheology in porous media for existing EOR polymers for the range of permeabilities anticipated in North Slope viscous oil reservoirs that might be candidates for polymer flooding. In general, we are trying to determine the most cost-effective polymer (most viscosity for the least cost) that will efficiently enter and flow through North Slope rock. We characterized the performance in 55-md, 269-md, and 5,120-md cores for nine commercially available EOR polymers, including one xanthan, one diutan, and seven partially hydrolyzed polyacrylamides (HPAM) with molecular weights ranging from 6 to 22 million daltons. None of the polymers exhibited severe face-plugging in any of the cores.

We examined polymer solution rheology in porous media over a wide range of flux values: from 0.01 to 1,000 ft/d for xanthan and diutan solutions and from 0.01 to 240 ft/d for HPAM solutions. Consistent with previous literature, our work confirmed that xanthan solutions show shear-thinning or pseudoplastic behavior in porous media. Also consistent with previous literature, we confirmed that HPAM resistance factors increase with increased flux at moderate to high flux values. This behavior was attributed to the viscoelastic character of HPAM and the elongational flow field in porous rock. In these cores, xanthan and HPAM solution rheology in porous media correlated very well using the parameter: $u(1-\phi)/(\phi k)^{0.5}$, where u is flux, ϕ is porosity, and k is permeability. The onset of pseudodilatant (viscoelastic) resistance factors (measured in a core) correlated closely with the transition from Newtonian to shear-thinning viscosity behavior (measured in a viscometer). These correlations will be very helpful in our future work in quantifying the potential for polymer flooding.

At low flux values in a 14.4-cm-long, 55-md Berea sandstone core, both xanthan and HPAM can exhibit resistance factors that are much higher than expected and an apparent shear-thinning behavior that deviates from expectations based on viscosity-versus-shear-rate data. Using

xanthan injection into a 122-cm-long, 57-md Berea sandstone core, we showed that this behavior was an experimental artifact that is not expected to materialize and benefit oil recovery in field applications. We believe that the shear-thinning effect was also an experimental artifact for HPAM. In particular, for SNF 3230S HPAM, we showed that mechanically degraded polymer (resulting from flow through a core at 2,292 psi/ft pressure gradient), exhibited Newtonian behavior at low flux values in 46-md and 17.5-md Berea sandstone. Future tests will further examine this issue for HPAM solutions.

Injectivity. A key issue for polymer flooding in a viscous oil reservoir is whether fluid injectivity will be sufficiently high to allow the oil to be displaced and produced at an economic rate. ConocoPhillips was kind enough to provide oil and data for a North Slope viscous oil reservoir. In this reservoir, horizontal wells were calculated to provide injectivities and productivities that are 9-10 times those expected for unfractured vertical wells. Particulate matter in injected water or polymer solutions was 65 times more likely to plug a vertical well than a horizontal well (assuming that fractures do not open during the course of injection). Using methods that we developed previously and using our experimental polymer rheology in porous media (described above), we estimated the injectivities associated with our polymer solutions under North Slope conditions. The pseudodilatant (viscoelastic) behavior of HPAM polymers could lead to significantly reduced injectivity in unfractured vertical North Slope injection wells (2-8% that of water for the HPAM solutions investigated in this report). In contrast, in North Slope unfractured horizontal wells, injectivity reductions should be significantly less severe (with polymer injectivity 10-15% that of water for our cases). The pseudoplastic (shear-thinning) xanthan and diutan solutions have an injectivity advantage over HPAM solutions in unfractured vertical wells, with estimated injectivity values around one-third that of water for the solutions that we examined. For horizontal wells, this advantage is diminished considerably. For a horizontal well with a vertical fracture that perfectly follows the well and extends to the full formation height (i.e., true linear flow), water injectivity was estimated to be about 19% greater than for an unfractured horizontal injection well. Flux values could typically be 0.01 ft/d or less deep within our target North Slope viscous oil reservoirs. These velocities are sufficiently low that we should further study and clarify polymer solution rheology in porous media at these low rates. Future work will also examine the utility of multiple fractures that may cross a horizontal well (i.e., quantifying improvements in injectivity and sweep efficiency versus possible detriments from accentuated channeling).

Using Mixtures of Different Types of Polymers. With the aim of joining the characteristic properties and advantages of synthetic polymers and biopolymers, a study was started using mixed solutions of the following commercial products. The following binary mixtures were studied: HPAM/xanthan, HPAM/diutan, and HPAM/alginate. All the mixed systems were evaluated in distilled water and brine. Many HPAM/xanthan mixtures in brine show viscosity behavior that is virtually the same as solutions with only xanthan. For example, in brine with 2.3% NaCl and 0.22% $NaHCO_3$, the mixture with 60% HPAM/40% xanthan has almost the same viscosity behavior as 100% xanthan. Since xanthan is considerably more expensive (per kg) than HPAM, this observation suggests a significant economic value in using polymer mixtures instead of a single polymer.

The main goal in investigating mixtures of HPAM and various biopolymers (especially xanthan) is to identify conditions where the use of the mixture might be more cost-effective than HPAM alone. To achieve this goal, the polymer components in the mixture must be compatible (i.e., mix to form a single phase with no suspended material that would plug porous media). All mixtures investigated met this requirement. A second requirement is that the cost-effectiveness of the mixture must be at least as attractive as that for a solution that contains only HPAM. Xanthan would have to cost 50% less than 3830S HPAM to become feasible for use in water with low salinity. Thus, as expected, HPAM alone is necessarily preferred for low-salinity applications. In contrast, for the high-salinity, high-hardness brine (5.8% NaCl, 0.8% $CaCl_2$), xanthan would be competitive if it cost 3.76 to 8.59 times more than 3830S HPAM, depending on the desired viscosity level. Thus, xanthan alone or a HPAM/xanthan mixture might be preferred in this brine.

The brine that was most characteristic of North Slope brines contained 2.3% NaCl, 0.22% $NaHCO_3$. For this brine, the required xanthan cost ranges from 1.31 to 2.78 times the cost of 3830S HPAM. For xanthan only (i.e., no HPAM in the polymer mixture), xanthan must cost no more than 1.85 to 2.23 times the cost of 3830S HPAM. This range of price might be difficult for xanthan suppliers to achieve. However, before becoming too pessimistic about xanthan's potential on the North Slope, the permeability dependence of HPAM performance may need to be considered. A lower molecular weight HPAM may be needed. These lower Mw polymers cost roughly the same as a high Mw HPAM, but more polymer is needed to provide a given viscosity. Since xanthan can readily penetrate into the low-permeability rock, its cost-effectiveness improves relative to the lower Mw HPAMs.

When distilled water is used as a solvent, HPAM does not show a significant pseudodilatant (shear-thickening) behavior even at high polymer concentrations. Presumably, pseudodilatancy occurs because coiled HPAM polymers must untangle to some extent when being forced through a pore throat. In saline brines, HPAM polymers are in a normal coil configuration, and a significant energy is required to untangle the coil (i.e., expand and elongate the polymer molecule). This energy is seen in the form of high resistance factors (i.e., resistance factor increasing with increased flux). For xanthan or for HPAM in distilled water, the polymers are already in an expanded configuration, and much less additional energy is needed to force the molecule through a pore throat—thus, shear thickening is not seen. Pseudodilatant behavior of HPAM in brine occurred at concentrations as low as 25 ppm. A HPAM-xanthan mixture showed displacement of critical flux (for the onset of pseudodilatant behavior) to higher flux values. This behavior could be explained by the elongation of the HPAM backbone. It is conceivable that quaternary structures form between xanthan and HPAM.

Diutan could be competitive for use if it costs no more than 4.39 to 6.23 times that of 3830S HPAM. Alginate was generally ineffective as a viscosifier, compared with the other polymers.

1. INTRODUCTION

A tremendous resource of viscous oil exists in the United States and throughout the world. Usually, thermal methods (e.g., steam flooding) are considered first for recovering this oil. However, circumstances often exist that preclude application of thermal methods. Consequently, we are exploring where polymer flooding can be viable for recovering viscous oil. This report describes research performed during the first year of the project, "Use Of Polymers To Recover Viscous Oil From Unconventional Reservoirs."

Project Objectives

The objective of this three-year research project is to develop methods using water soluble polymers to recover viscous oil from unconventional reservoirs (i.e., on Alaska's North Slope). The project has three technical tasks. First, limits will be re-examined and redefined for where polymer flooding technology can be applied with respect to unfavorable displacements. Second, we will test existing and new polymers for effective polymer flooding of viscous oil, and we will test newly proposed mechanisms for oil displacement by polymer solutions. Third, we will develop novel methods of using polymer gels to improve sweep efficiency during recovery of unconventional viscous oil.

Report Content

In Chapter 2, we examine the old screening criteria for polymer flooding, and we use numerical and analytical methods to examine the potential for polymer flooding of reservoirs with viscous oil. Displacement of oils with up to 100,000 cp is considered. One- and two-layer reservoir models are used, both with and without crossflow and with a range of relative zone thicknesses. Chapter 3 reports viscosity versus polymer concentration for sixteen commercially available water soluble polymers (nine synthetic polymers and seven biopolymers) in a number of brines. This information will be useful in judging the most cost-effective polymers to displace viscous oils. Chapter 4 characterizes the rheology in 55-md, 269-md, and 5,120-md cores for nine commercially available EOR polymers, including one xanthan, one diutan, and seven partially hydrolyzed polyacrylamides (HPAM). The HPAM polymers had molecular weights ranging from 6 to 22 million daltons. We especially consider whether an apparent shear-thinning behavior (seen in short cores during injection of fresh polymer solution) is an effect that can reasonably be expected to occur deep within a reservoir. In Chapter 5, we consider injectivity reductions that are expected when injecting EOR polymers into fractured and unfractured vertical and horizontal wells, especially under North Slope conditions. Chapter 6 examines the rheological characteristics of mixtures of various polymers, including HPAM/xanthan, HPAM/diutan, and HPAM/alginate.

Our latest research results, along with detailed documentation of our past work, can be found on our web site at http://baervan.nmt.edu/randy/.

2. FRACTIONAL FLOW ANALYSIS OF THE POTENTIAL FOR POLYMER FLOODING RESERVOIRS WITH VISCOUS OIL

In this chapter, we use numerical and analytical methods to examine the potential for polymer flooding of reservoirs with viscous oil. First, we examine the old screening criteria for polymer flooding. Second, studies of oil recovery (using waterflooding) are described in one- and two-layer reservoirs (using both fractional flow calculations and three commercial simulators, both with and without crossflow). Comparative calculations are presented, based on relative permeability characteristics from a North Slope reservoir. Next, recoveries from simple polymer floods (that consider only Newtonian, viscosity effects) are described, and simple economic comparisons are made for polymer flooding versus waterflooding. Finally, we consider the effects of heights of the layers in a two-layer reservoir and the effects of gravity segregation on the position of a polymer front.

Reconsideration of Screening Criteria for Polymer Flooding

Alaska's North Slope contains a very large unconventional oil resource—over 20 billion barrels of heavy/viscous oil.[1,2] Conventional wisdom argues that thermal recovery methods are most appropriate for recovering viscous oils.[3,4] However, for viscous oil reservoirs at Alaska's North Slope, a number of factors complicate this thinking. The formations that hold vast viscous oil reserves, Ugnu, West Sak, and Schrader Bluff, are relatively close to permafrost. Steam generation is prohibitive here, with severe cold weather on the surface, heat losses while pumping steam down through 700 to 2,200 ft of permafrost, and heat losses when contacting the cold formation and with environmental considerations.

Miscible gas injection and water-alternating-gas have been proposed and attempted, with some success to reduce the viscosity and enhance displacement in some North Slope reservoirs.[5-7] However, this displacement is characterized by a remarkably unfavorable mobility ratio, so the current technology is confined to the least viscous of the North Slope's heavy oils.[6,7] Also, if a gas pipeline is constructed to the lower 48 states, availability of miscible gas for EOR purposes may be restricted.

Earlier screening criteria[3,4] (from the mid-1990s) indicated that polymer flooding should be applied in reservoirs with oil viscosities between 10 and 150 cp. Two key factors were responsible for this recommended range. First, considering oil prices (~$20/bbl) and polymer prices (~$2/lb for moderate Mw polyacrylamide or HPAM polymers) at the time, 150 cp was viewed as the most viscous oil that could be recovered economically using polymer flooding. (For oil viscosities below 10 cp, the mobility ratio during waterflooding was generally viewed as sufficiently favorable that use of polymer would generally not be needed to achieve an efficient reservoir sweep.) Second, for oil viscosities above 150 cp, the viscosity requirements to achieve a favorable mobility ratio were feared to reduce polymer solution injectivity to prohibitively low values (i.e., slow fluid throughput in the reservoir to the point that oil production rate would be uneconomically low).

Kumar *et al.*[10] examined waterflood performance using unfavorable mobility ratios. They concluded that viscous fingers dominate high-viscosity-ratio floods, that mobile water can significantly reduce oil recovery, and that reservoir heterogeneity and thief zones accentuate

poor displacement performance. Their paper strongly suggested that any improvement in mobility ratio (e.g., polymer flooding) can noticeably improve reservoir sweep and recovery efficiency.

Several important changes have occurred since the previous screening criteria were proposed. First, oil prices have increased to ~$70/bbl, while polymer prices have remained relatively low ($0.90 to $2/lb for HPAM). Second, viscosification abilities for commercial polymers have increased, partly from achieving higher polymer molecular weights and partly from incorporating specialty monomers (e.g., with associating groups) within the polymers. Conventional wisdom from earlier polymer floods was that it was highly desirable to achieve a mobility ratio of unity or less during a polymer flood.[11] However, with current high oil prices, operators are wondering whether improved sweep from polymer injection might be economically attractive even if a unit mobility ratio is not achieved.

In wells that are not fractured, injection of viscous polymer solutions will necessarily decrease injectivity. In order to maintain the waterflood injection rates, the selected polymer-injection wells must allow higher injection pressures. Another important change since the time when earlier screening criteria for polymer flooding was developed[3,4] has been the dramatic increase in the use of horizontal wells. Use of horizontal wells significantly reduces the injectivity restrictions associated with vertical wells.[12] In previous work,[12] we also demonstrated that injector/producer pairs of horizontal wells can dramatically improve areal sweep and lessen polymer use requirements. These factors could have a major impact on extending polymer flooding to reservoirs with more viscous oils.

Open fractures (either natural or induced) will also have a substantial impact on polymer flooding. Van den Hoek *et al.*[13] stated that "It is well established within the industry that water injection mostly takes place under induced fracturing conditions. Particularly, in low-mobility reservoirs, large fractures may be induced during the field life." Because polymer solutions are more viscous than water, injection above the formation parting pressure will be even more likely during a polymer flood than during a waterflood. The viscoelastic nature (apparent shear-thickening or "pseudo-dilatancy") for synthetic EOR polymers (e.g., HPAM) makes injection above the formation parting pressure even more likely.[14-16]

Under the proper circumstances, injection above the parting pressure can significantly (1) increase polymer solution injectivity and fluid throughput for the reservoir pattern, (2) reduce the risk of mechanical degradation for polyacrylamide solutions, and (3) increase pattern sweep efficiency.[15-17] Using both field data and theoretical analyses, we demonstrated these facts at the Daqing Oilfield in China, where the world's largest polymer flood is in operation.[15]

During analysis of polymer flooding in this work, we assume that injectivity limitations will require either use of horizontal wells or that polymer injection must occur above the fracture or formation parting pressure. Consequently, linear flow will occur for most of our intended applications.

One Homogeneous Layer

In assessing the potential of polymer flooding for North Slope applications, we assumed that simulation studies would be necessary. Consequently, we performed a number of base case simulations to establish confidence in the predictions of various reservoir simulators, including ECLIPSE, VIP, and POLYMER (a variant of UTCHEM). In the first case, we simulated simple one-dimensional displacement of oil (with various viscosities ranging from 1 to 100,000 cp) when injecting 1-cp water. These studies assumed incompressible flow, no density or capillary pressure differences between phases, and only one homogeneous layer was present. The relative permeability characteristics were given by Eqs. 1 and 2. The conditions given immediately after Eq. 2 will be labeled our "base case" for this report.

$$k_{rw}=k_{rwo}\,[(S_w-S_{wr})/(1-S_{or}-S_{wr})]^{nw} \quad \text{.....(1)}$$

$$k_{ro}=k_{roo}\,[(1-S_{or}-S_w)/(1-S_{or}-S_{wr})]^{no} \quad \text{.....(2)}$$

k_{rwo}=0.1, k_{roo}=1, S_{or} =0.3, S_{wr} =0.3, nw=2, no=2, k_1=1 darcy, ϕ_1=0.3.

To check the validity of the simulation results, we performed fractional flow analysis, which were used to generate Fig. 1. In this figure, the y-axis plots the percent of the mobile oil that was recovered for a given pore volume (PV) of water injected. (The total mobile oil is given by the difference between the original oil saturation at S_{wr} and the residual oil saturation.) Simulations using ECLIPSE, VIP, and POLYMER (a variation of UTCHEM) all matched the results from the single-layer fractional flow calculations reasonably well.

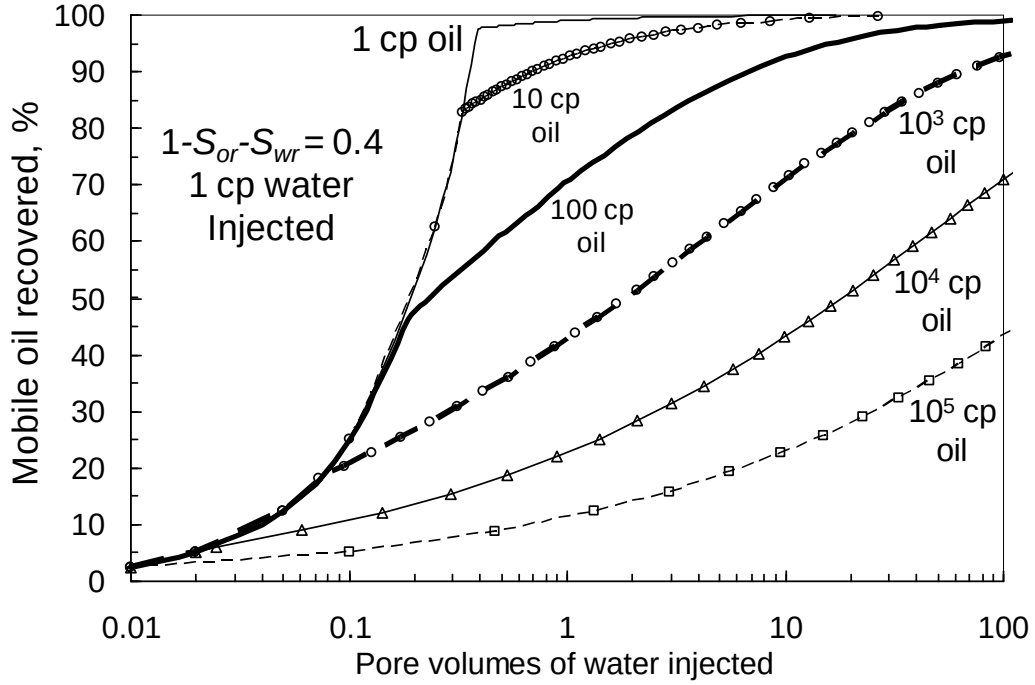

Fig. 1—Fractional flow calculations for water displacing oil, one layer. Base case.

Two Layers with/without Crossflow

For the next set of cases, we considered linear displacement through two layers (of equal thickness), where k_1=1 darcy, ϕ_1=0.3, k_2=0.1 darcy, ϕ_2=0.3. All other parameters and conditions were the same as those used in the one-layer case. We considered two subsets—one with no crossflow between the two layers and one with free crossflow (i.e., vertical equilibrium) between the layers. Accepted reservoir engineering analysis indicates two key expectations.[18-21] First, as the mobility ratio becomes increasingly small (below unity), the vertical sweep efficiency increases for both the crossflow and no-crossflow cases. However, the crossflow cases achieve much higher recovery efficiencies than the no-crossflow cases. Second, as the mobility ratio becomes increasingly large (above unity), the sweep efficiency decreases for both the crossflow and no-crossflow cases. However, the crossflow cases suffer much lower recovery efficiencies than the no-crossflow cases.

For a given oil viscosity, our initial simulations of water displacing oil using ECLIPSE, VIP, and POLYMER all suggested that the recovery efficiencies (versus pore volumes, PV, of water injected) were surprisingly similar with versus without crossflow, regardless of the mobility ratio. This result was simply incorrect. The simulation results were usually close to expectations for the no-crossflow cases. It seems odd that similar incorrect results would be obtained using three different simulators (performed by three different sets of people). One could argue that our personnel that performed the simulations were either insufficiently experienced or in too much of a hurry. However, considering the experience and intelligence levels of these three different sets of people, I can't help but wonder if the manuals/codes/training associated with these simulators do not provide adequate instruction for proper treatment of crossflow cases.

For the two-layer cases, we solved this problem using fractional flow calculations with spreadsheets. The two-layer no-crossflow case was straight forward, since the displacements in the individual layers can be treated separately and then combined to yield the overall displacement efficiency. The free-crossflow case required application of vertical equilibrium[20] between the layers. Figs. 2-4 show results for various crossflow and no-crossflow cases. These results are more credible than our simulation results to date. Consequently, we plan to use our spreadsheet method until we gain more understanding and confidence in the simulation results.

Recently, a graduate student (Oppong Kwame) learned the proper ECLIPSE formatting to yield results that roughly matched the results from the two-layer fractional flow calculations. Still, the simulation results typically over-predict recovery for water injection values below 1 pore volume (PV). Above 1 PV total water injection, the simulation results match the fractional flow calculations reasonably well.

Based on the fractional flow calculations, Table 1 lists the recovery values at 1 PV of water injection. Along with Figs. 1-4, this table hints at the potential for polymer flooding. For any given oil viscosity (e.g., 1,000 cp), one can envision that a 10-fold decrease in the oil/water viscosity ratio (i.e., injecting a 10-cp polymer solution instead of water) could increase oil recovery by a substantial percentage.

Table 1—% mobile oil recovered after 1 PV of 1-cp water injection. Base case.

Oil viscosity, cp	1 layer	2 layers, no crossflow	2 layers with crossflow
1	99	81	99
10	92	59	59
100	70	48	39
1,000	43	32	23
10,000	23	17	12
100,000	12	8	6

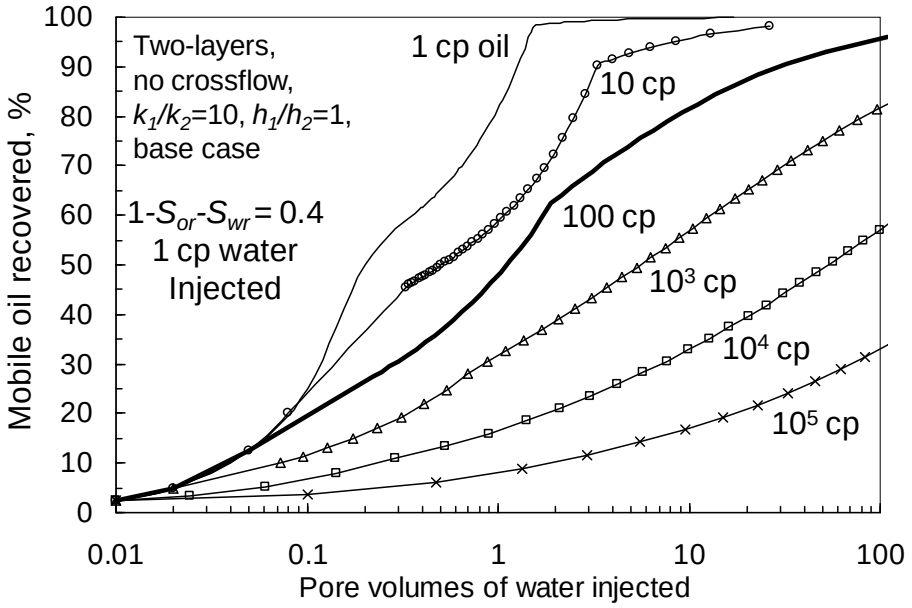

Fig. 2—Fractional flow calculations, two layers, no crossflow. Base case.

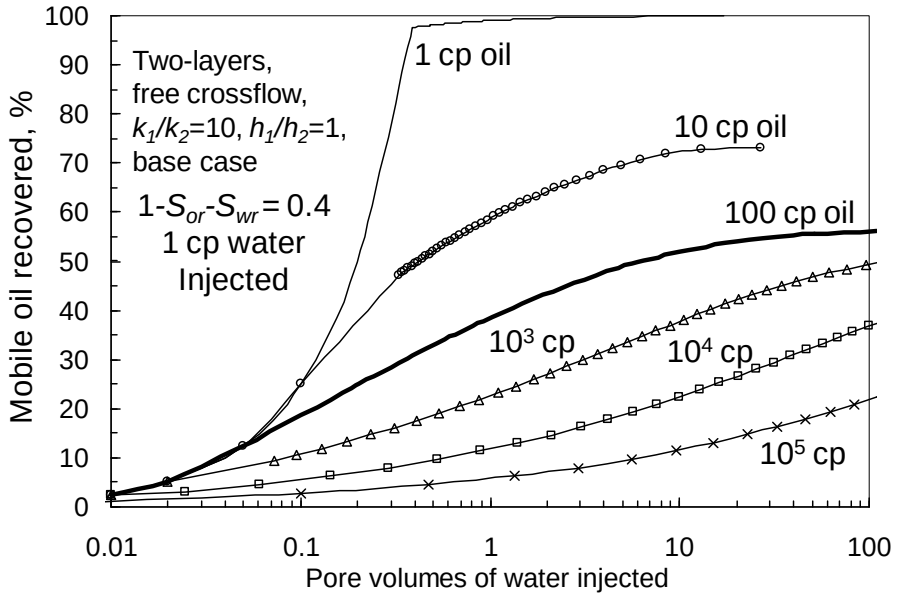

Fig. 3—Fractional flow calculations, two layers, free crossflow. Base case.

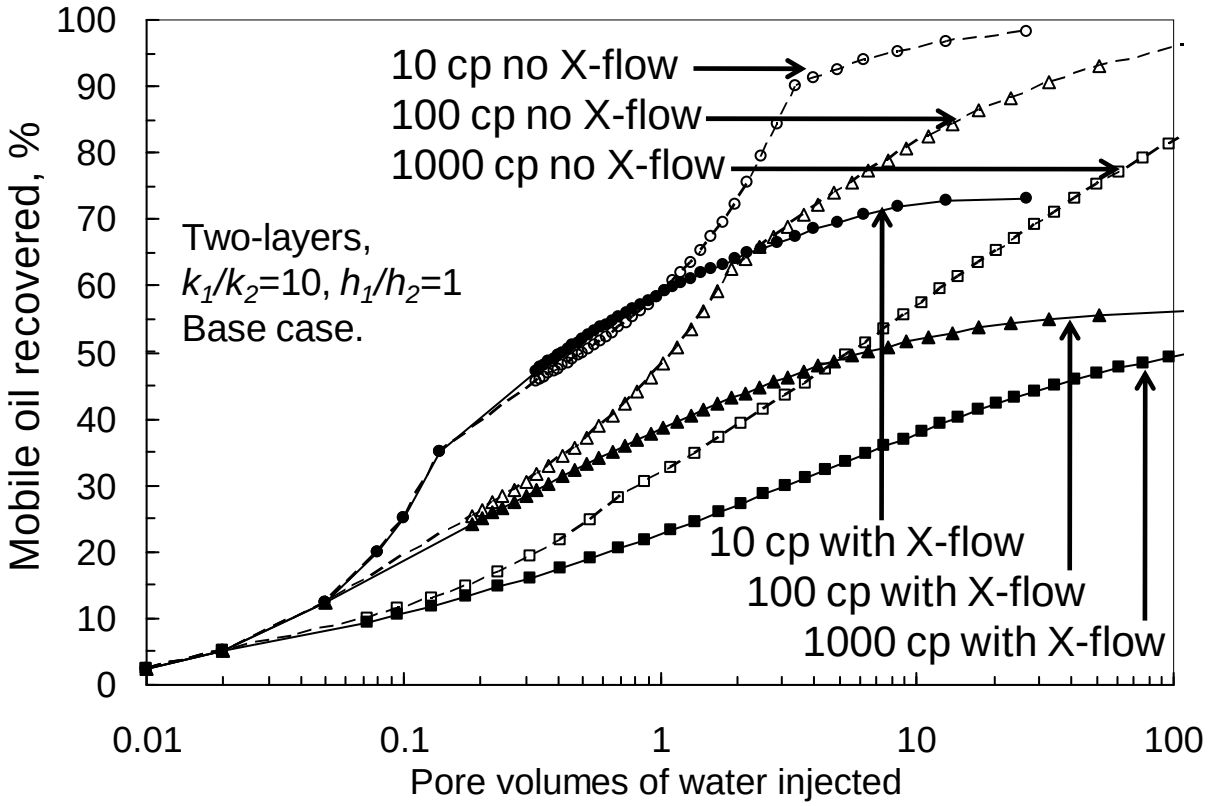

Fig. 4—Fractional flow calculations, two layers, with versus without crossflow.

Runs Using North Slope Relative Permeabilities

ConocoPhillips provided us with relative permeability characteristics that were felt to be representative of those seen in their viscous-oil, North Slope reservoirs. These parameters (for input into Eqs. 1 and 2) were:

k_{rwo}=0.1, k_{roo}=1, S_{or} =0.12, S_{wr} =0.12, nw=4, no=2.5.

We repeated our previous work using these new parameters. Fig. 5 plots results that are analogous to those in Fig. 1. For the North Slope parameters, the mobile oil saturation was considerably larger (1-S_{or}-S_{wr} = 0.76) than for our base case (1-S_{or}-S_{wr} = 0.4). Consequently, there is a much bigger oil "target" for the North Slope case.

Recovery values appear to increase more quickly in Fig. 1 than in Fig. 5. This appearance occurs because the mobile oil saturation is much smaller for our base case (0.4 in Fig. 1) than in the North Slope case (0.76 in Fig. 5). The left part of the curves (that appears exponential) is shifted to the right by a factor of 0.76/0.4 in Fig. 5 versus in Fig. 1. The recovery differences in these figures can be appreciated in Fig. 6. This figure plots the recovery difference between the North Slope case (Fig. 5) and the base case (Fig. 1) when the x-axis was first normalized by dividing original PV by (1-S_{or}-S_{wr}). When expressed in this manner, the waterflood response using the North Slope parameters appears considerably more favorable than for our base case, when the oil viscosity is 100 cp or above.

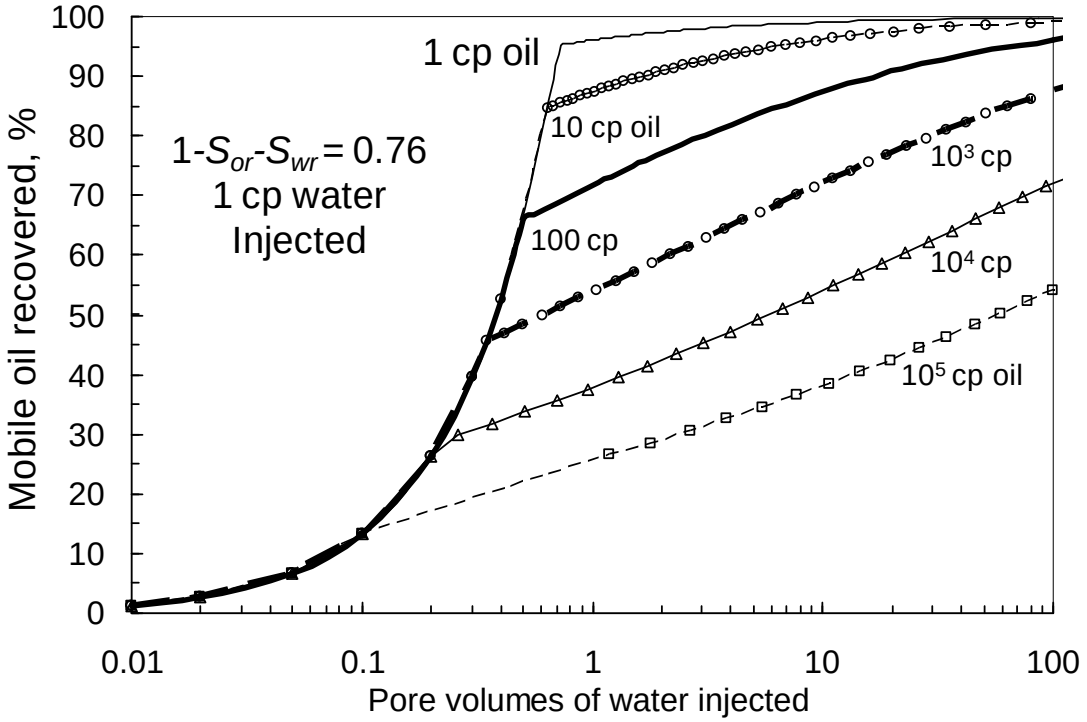

Fig. 5—Fractional flow calculations for water displacing oil, one layer. North Slope case.

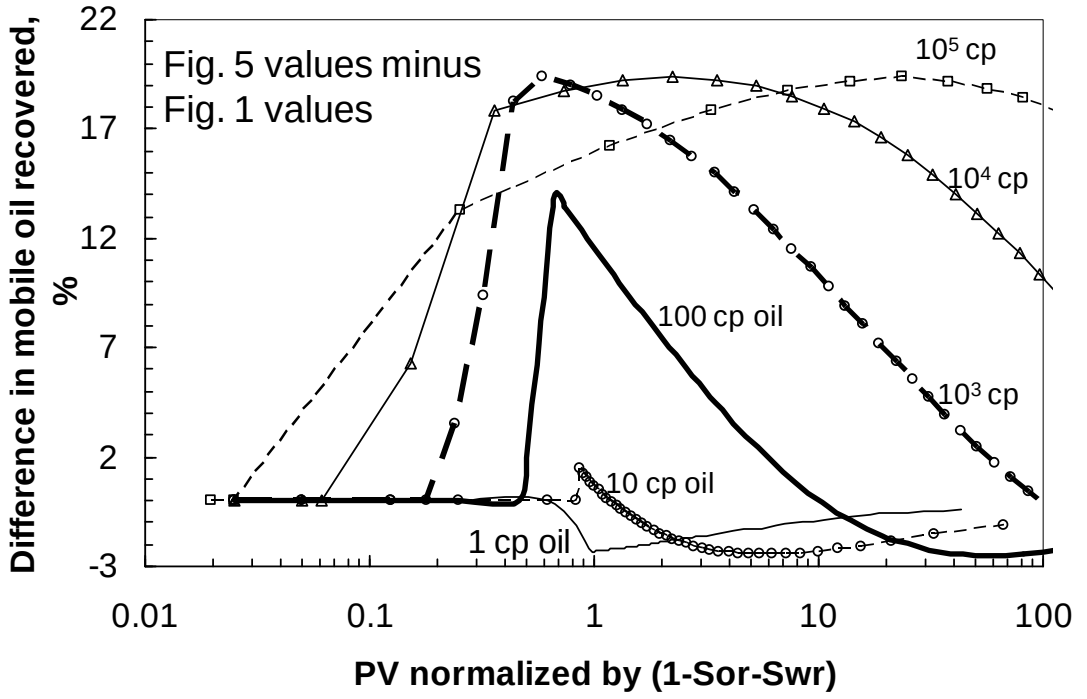

Fig. 6—Difference between North Slope case (Fig. 5) and base case (Fig. 1). *x*-axis normalized by dividing original PV by (1-S_{or}-S_{wr}). Water displacing oil, one homogeneous layer.

For a two-layer reservoir with no crossflow, Fig. 7 is analogous to Fig. 2 except that the North Slope parameters were used instead of the base case parameters. Similarly, for a two-layer reservoir with free crossflow, Fig. 8 is analogous to Fig. 3 except that the North Slope parameters were used instead of the base case parameters. For both the no-crossflow and the free crossflow cases, the left-most portions of the curves for the North Slope plots were shifted to the right by a factor of about 0.76/0.4 compared with those for the base case plots.

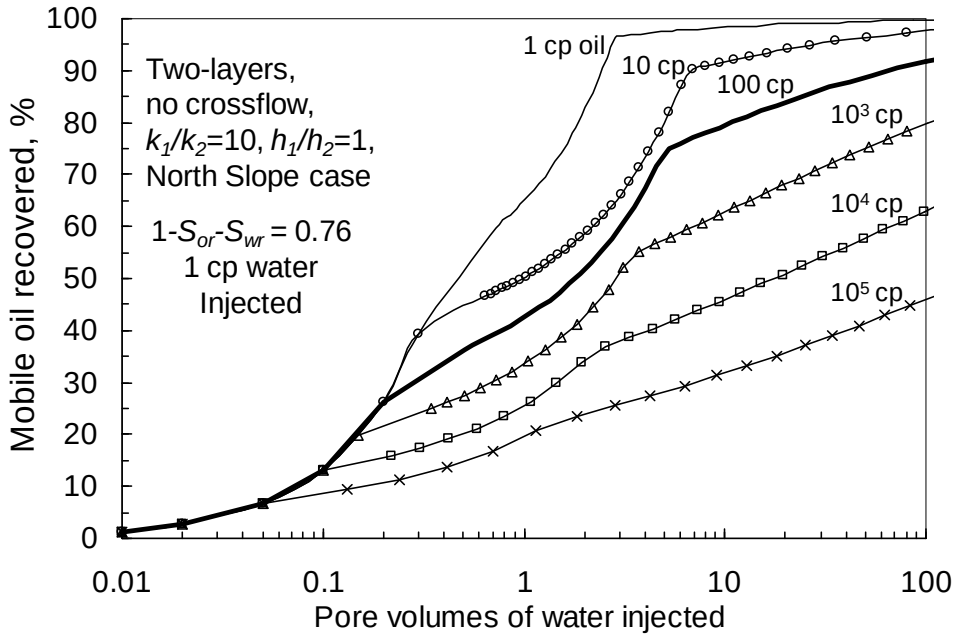

Fig. 7—Fractional flow calculations, two layers, no crossflow. North Slope case.

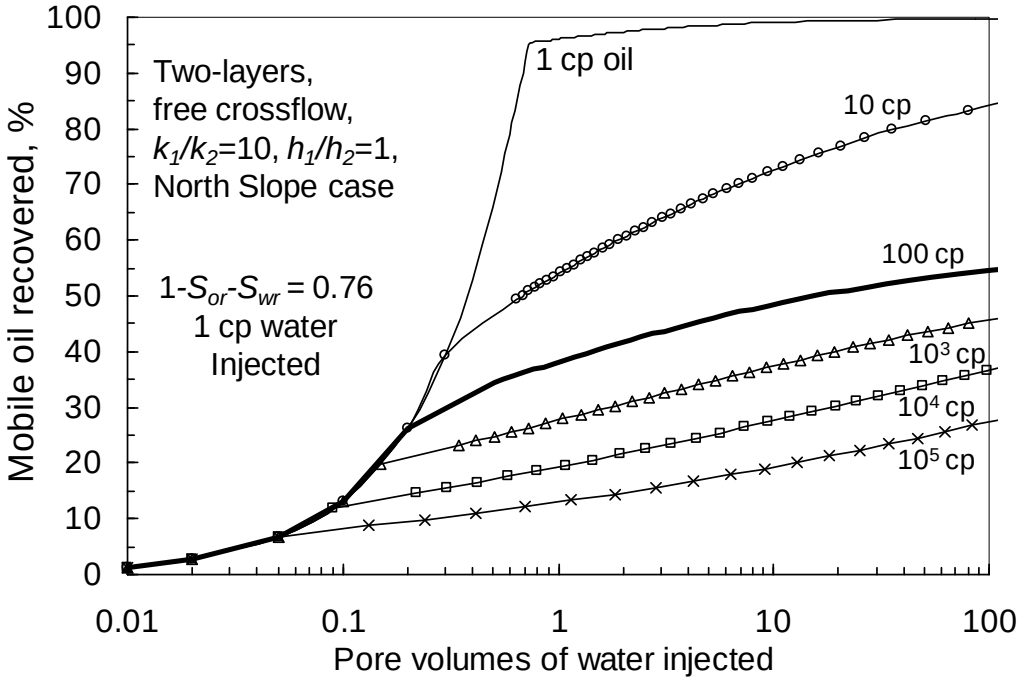

Fig. 8—Fractional flow calculations, two layers, free crossflow. North Slope case.

Polymer Floods

We also performed fractional flow calculations where a polymer flood was implemented to displace 1,000-cp oil. We used the same assumptions given above [specifically using either the relative permeability parameters listed just after Eq. 2 (our base case) or those after Fig. 4 (our North Slope case)], except that polymer solution of a specified viscosity was injected. At the start of the flood, the connate water saturation was either 0.3 (for the base cases) or 0.12 (for the North Slope cases) and water viscosity was 1 cp. (The "mobile" oil saturation was 100% at the start of polymer injection.) For the polymer, we assumed (1) Newtonian (flow-rate independent) behavior, (2) properties were independent of permeability, and (3) polymer retention exactly balanced inaccessible pore volume. Figs. 9 and 10 show displacement results assuming only one homogeneous layer (Fig. 9 for the base case, and Fig. 10 for the North Slope case), while Figs. 11 and 12 show results for two layers (k_1=10k_2, equal layer thickness, same porosity) with no crossflow (Fig. 11 for the base case, and Fig. 12 for the North Slope case). Figs. 13 and 14 show results for two layers (k_1=10k_2, equal layer thickness, same porosity) with free crossflow (Fig. 13 for the base case, and Fig. 14 for the North Slope case). In each figure, we show results for (1) 1-cp waterflooding, (2) 10-cp polymer injection, (3) 100-cp polymer injection, and (4) 1,000-cp polymer injection. Table 2 summarizes the recovery values (% of the original mobile oil saturation recovered) after injecting 0.5 PV of polymer solution. Table 3 provides the same information after injecting 1 PV of polymer solution.

One important observation from viewing Figs. 9-14 and Tables 2 and 3 is that increases in injectant viscosity virtually always leads to a significant increase in oil recovery. As expected, for any given water throughput and polymer solution viscosity (except the 1,000-cp polymer cases), recovery efficiency was substantially better for the one-layer cases (Figs. 9 and 10) than for the two-layer cases (Figs. 11-14). Interestingly, the recovery curves when injecting 1,000-cp polymer solution were quite similar for both the one-layer cases and two-layer cases with free crossflow (thick dashed curves in Fig. 9 versus Fig. 13 and in Fig. 10 versus Fig. 14). This finding is consistent with vertical equilibrium concepts. If the mobility contrast between the displacing and displaced phases [i.e., (1 darcy k_{ro}/1,000-cp oil)/(0.1 darcy k_{rw}/1,000-cp polymer)=10] is greater than or equal to the permeability contrast (i.e., k_1/k_2=10), then the displacement efficiency for two layers will appear the same as for one layer.[21]

For the one-layer cases and the two-layer cases with free crossflow, the waterfloods (i.e., 1-cp polymer) were noticeably more efficient (by 5-12% of the mobile oil) for the North Slope conditions than the base case (see the first data rows of Tables 2 and 3). For the two-layer cases with no crossflow, the waterflood recoveries were quite similar for the North Slope and base cases (27% versus 29% after 0.5 PV and 33% versus 32% after 1 PV).

For a given injection volume and for the cases with no crossflow, the largest increases in recovery generally occurs when increasing the injectant viscosity from 1 cp to 10 cp (Figs. 11 and 12). For the cases with free crossflow (Figs. 13 and 14), the largest increases in recovery occurs when increasing the injectant viscosity from 100 to 1,000 cp. Most previous field polymer floods were directed at reservoirs with oil/water viscosity ratios that were less than 10, although the most successful projects had ratios from 15 to 114.[4] For the world's largest (and most definitive) polymer flood at Daqing, China, the oil/water viscosity ratio was 15, and 10-12% of the original oil in place (OOIP) was recovered, incremental over waterflooding.[4,15,22-24]

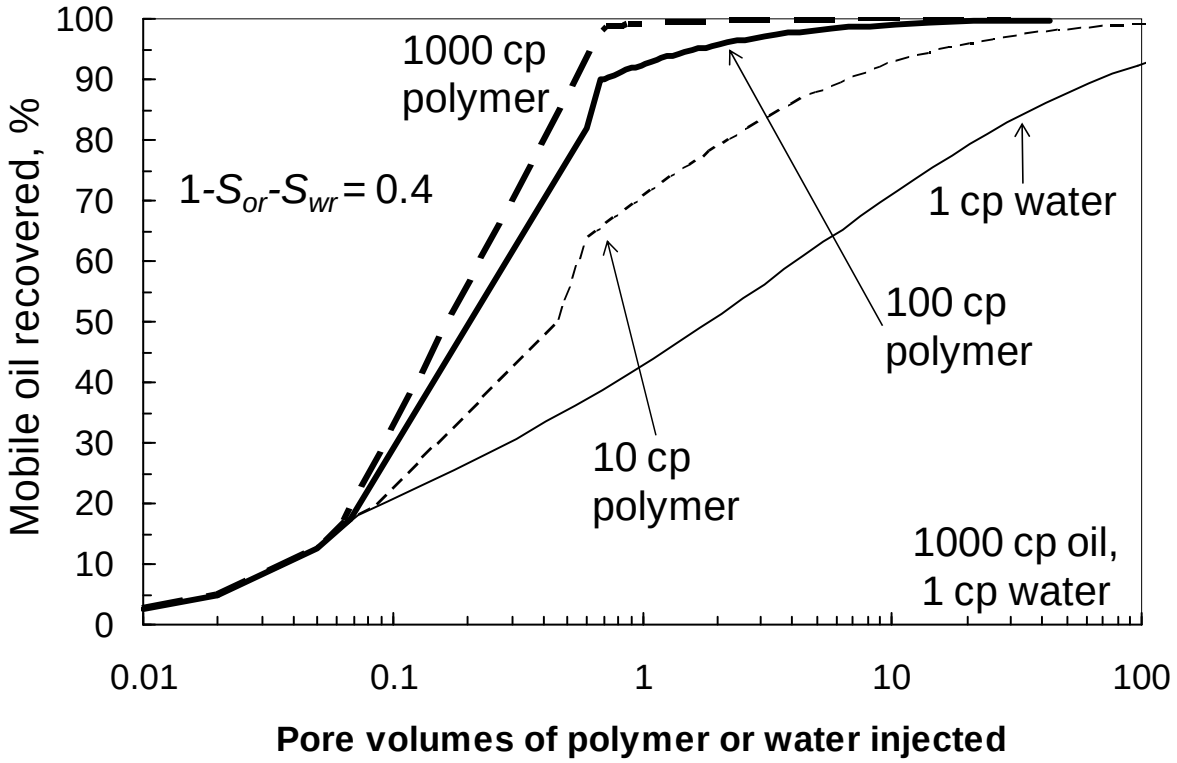

Fig. 9—Polymer flood results for one homogeneous layer. Base case.

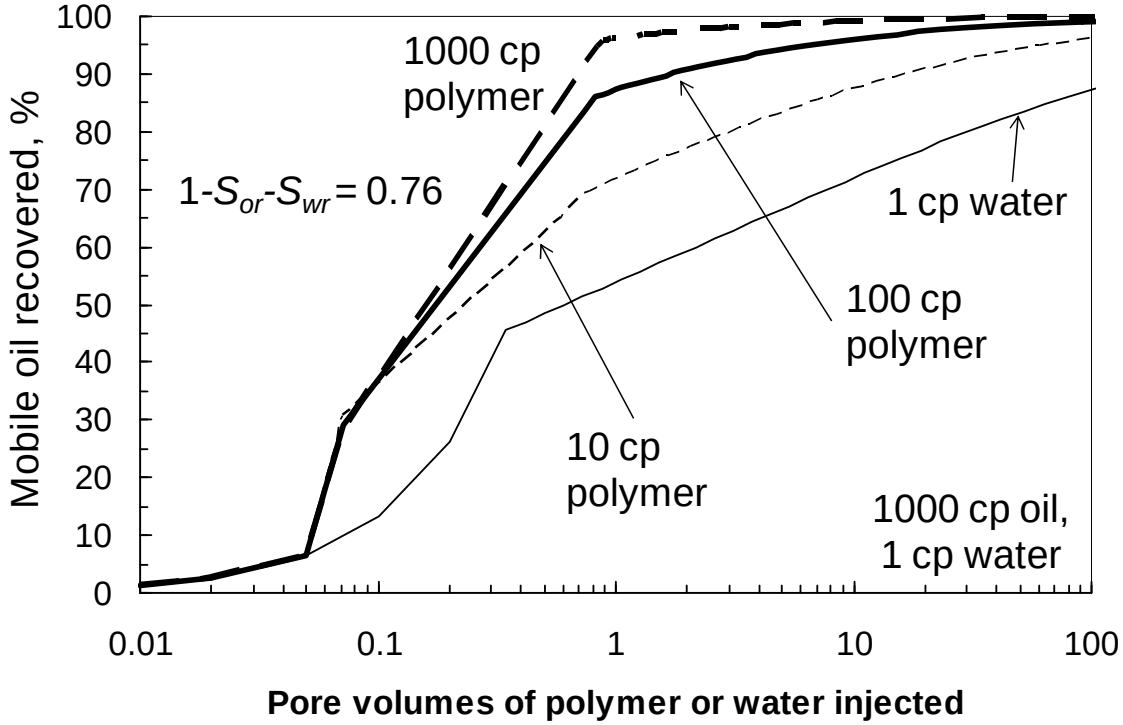

Fig. 10—Polymer flood results for one homogeneous layer. North Slope case.

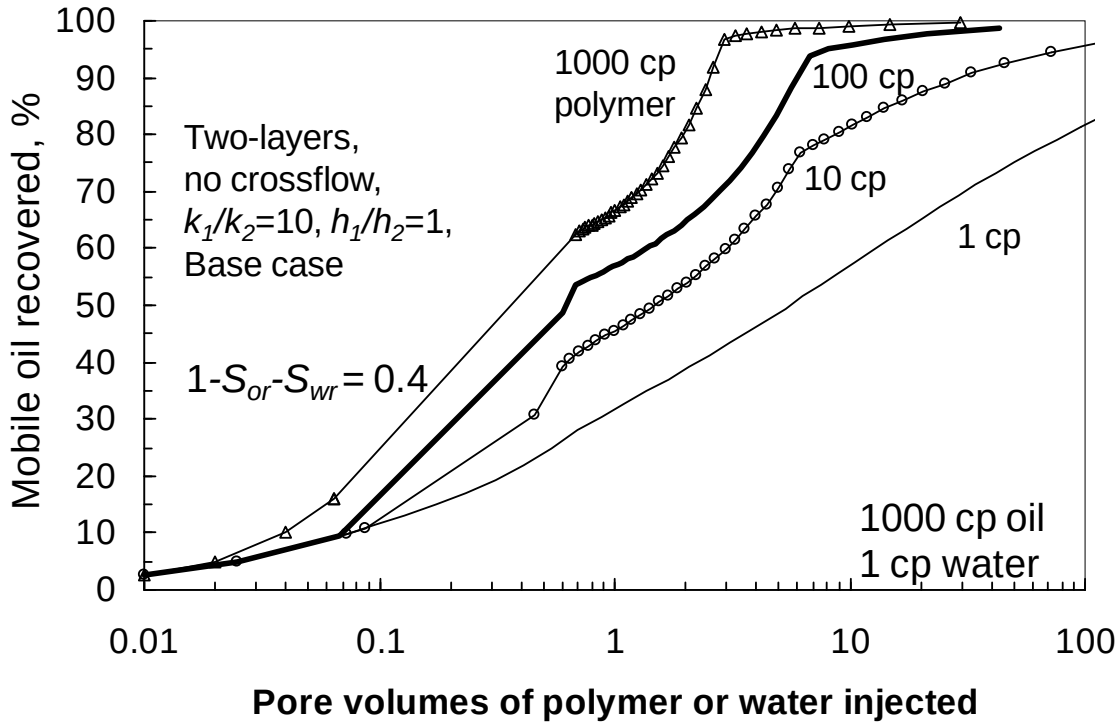

Fig. 11—Polymer flood results for two layers. No crossflow. Base case.

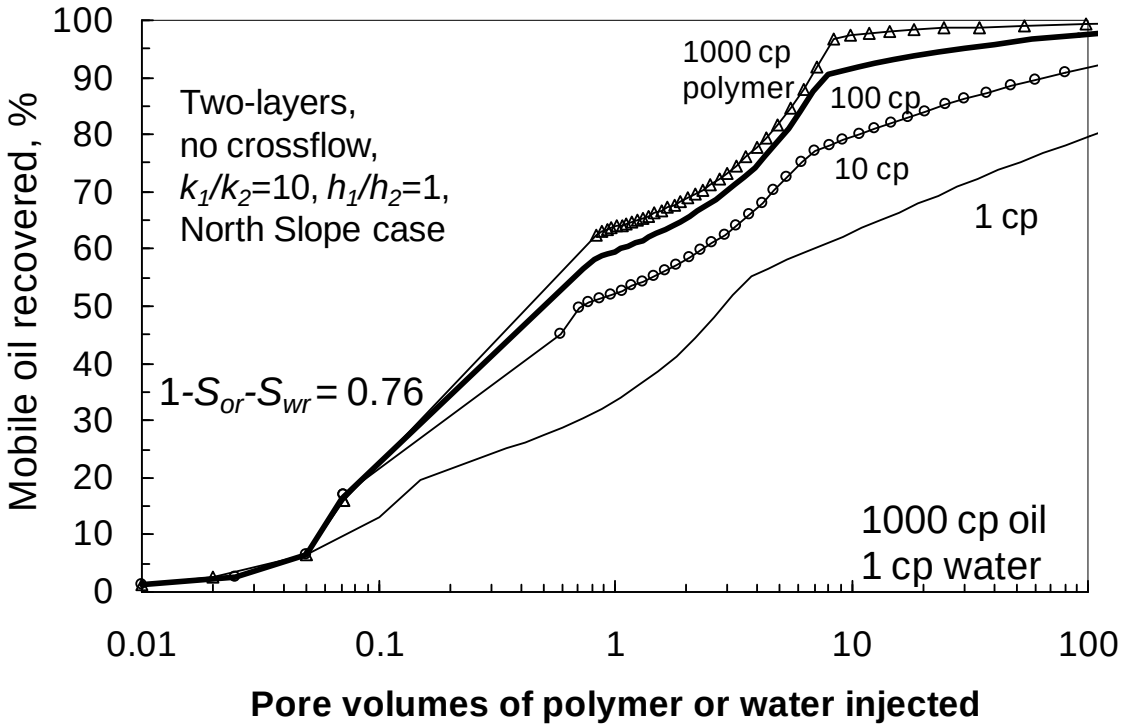

Fig. 12—Polymer flood results for two layers. No crossflow. North Slope case.

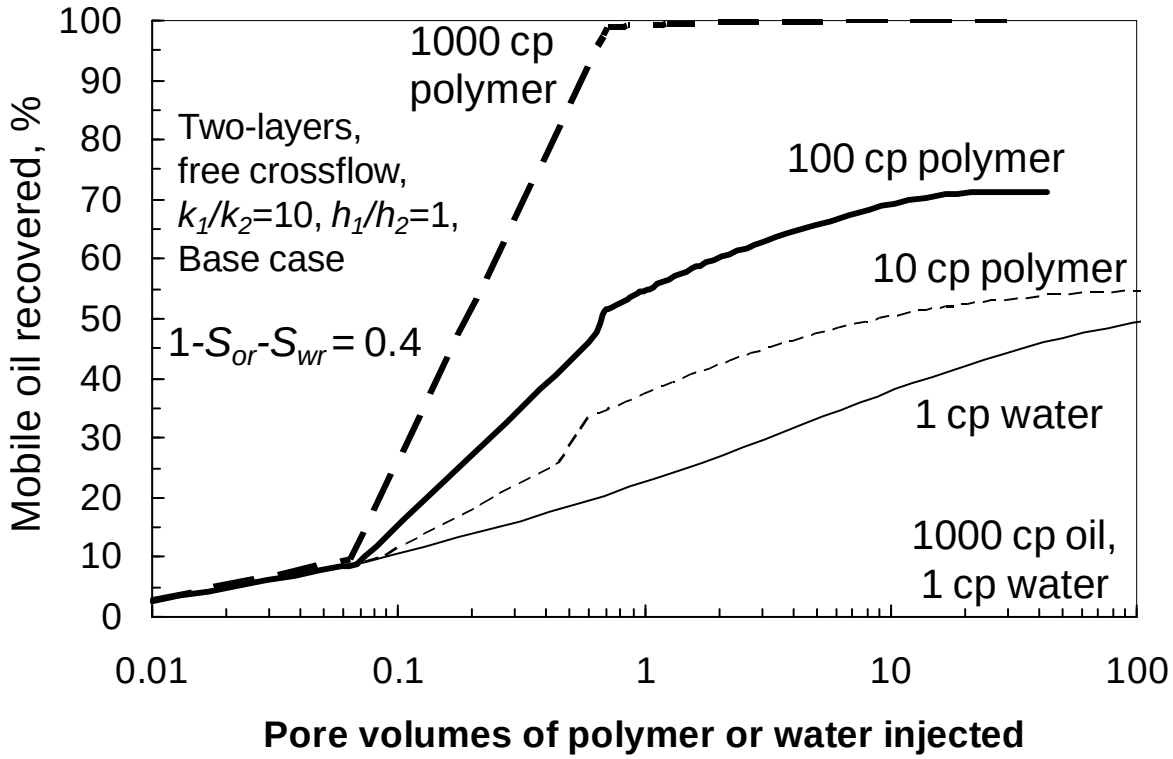

Fig. 13—Polymer flood results for two layers. Free crossflow. Base case.

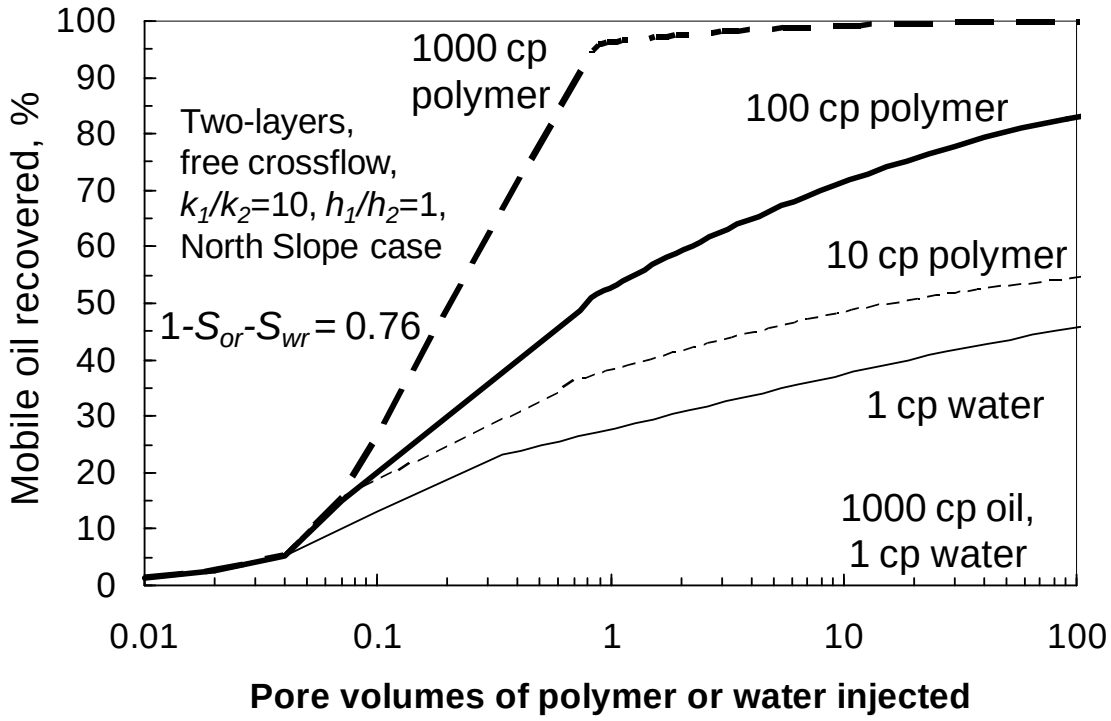

Fig. 14—Polymer flood results for two layers. Free crossflow. North Slope case.

Table 2—% mobile oil recovered after 0.5 PV polymer. 1,000-cp oil.

Polymer viscosity, cp	1 layer		2 layers, no crossflow		2 layers with crossflow	
	Base case	North Slope	Base case	North Slope	Base case	North Slope
1	36	48	29	27	18	25
10	56	62	32	43	27	32
100	76	75	45	50	42	43
1,000	87	81	57	53	86	79

Table 3—% mobile oil recovered after 1 PV polymer. 1,000-cp oil.

Polymer viscosity, cp	1 layer		2 layers, no crossflow		2 layers with crossflow	
	Base case	North Slope	Base case	North Slope	Base case	North Slope
1	43	55	32	33	23	28
10	71	72	45	52	37	38
100	92	87	57	60	55	53
1,000	99	96	66	63	99	96

Preliminary Economic Analysis

Using the recovery results from Figs. 9 through 14, a simple economic analysis was performed to make a preliminary assessment of the potential for polymer flooding in reservoirs with viscous oils. For much of this analysis, we made a pessimistic assumption that oil price was $20/bbl. We also assumed that water treatment/injection costs were $0.25/bbl. We assumed the polymer cost was $1.50/lb and the parameters for SNF Flopaam 3830S HPAM in Chapter 3 (Table 7) described viscosity versus polymer concentration. (No other operating or capital costs were assumed, so of course, this analysis is very preliminary.) Basically, for any given value of water or polymer solution injected, the relative profit is the total value of the oil produced minus the total cost of the polymer injected and also minus the total cost of water treatment to that point.

Figs. 15 through 20 show the results from this analysis. The relative profit from a given North Slope case was typically about twice that from a corresponding base case (compare Fig. 15 versus Fig. 16 and Fig. 17 versus Fig. 18). This result occurs largely because the mobile oil saturation for the North Slope case (0.76 PV) was 1.9 times greater than for our base case (0.4 PV). For most cases, in Figs. 15-18, the peak in profitability was noticeably greater when injecting polymer solution than for waterflooding. Also over a significant range of throughput values, polymer flooding provided a higher relative profit than waterflooding.

Fig. 19 is analogous to Fig. 18, except that the oil price was $50/bbl instead of $20/bbl. The basic shapes of the curves are the same at the two oil prices—just the magnitude of the relative profit rises in proportion to the oil price.

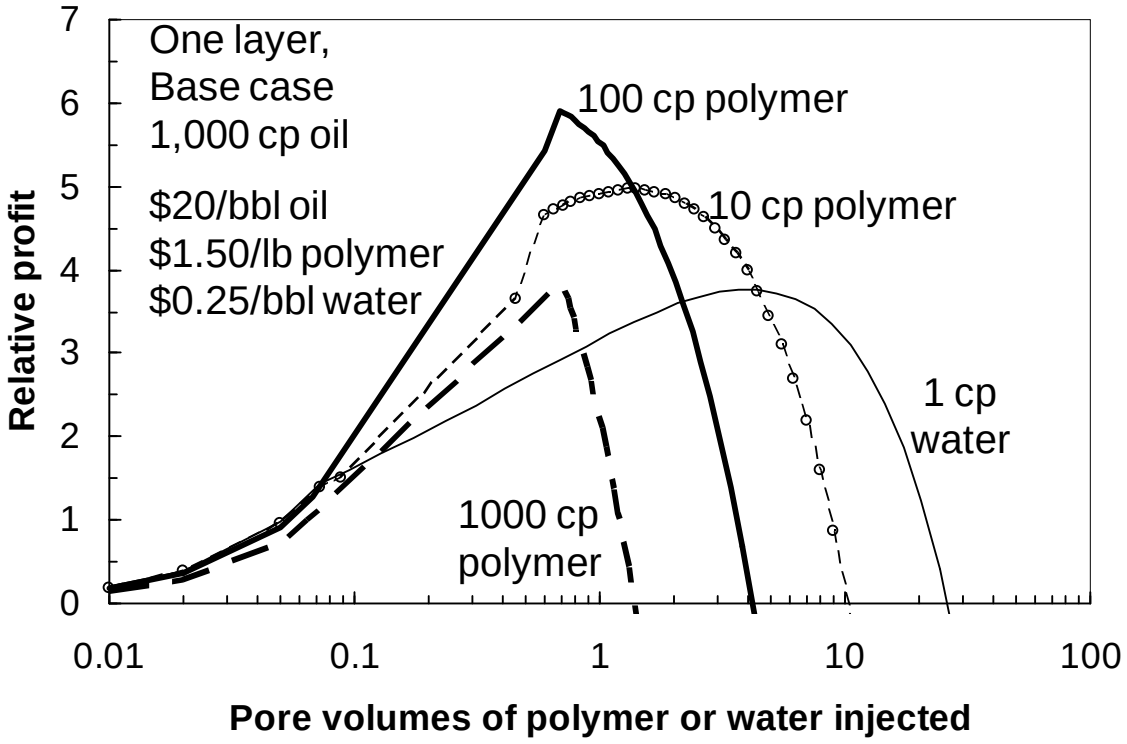

Fig. 15—Base case, one homogeneous layer 1,000-cp $20/bbl oil.

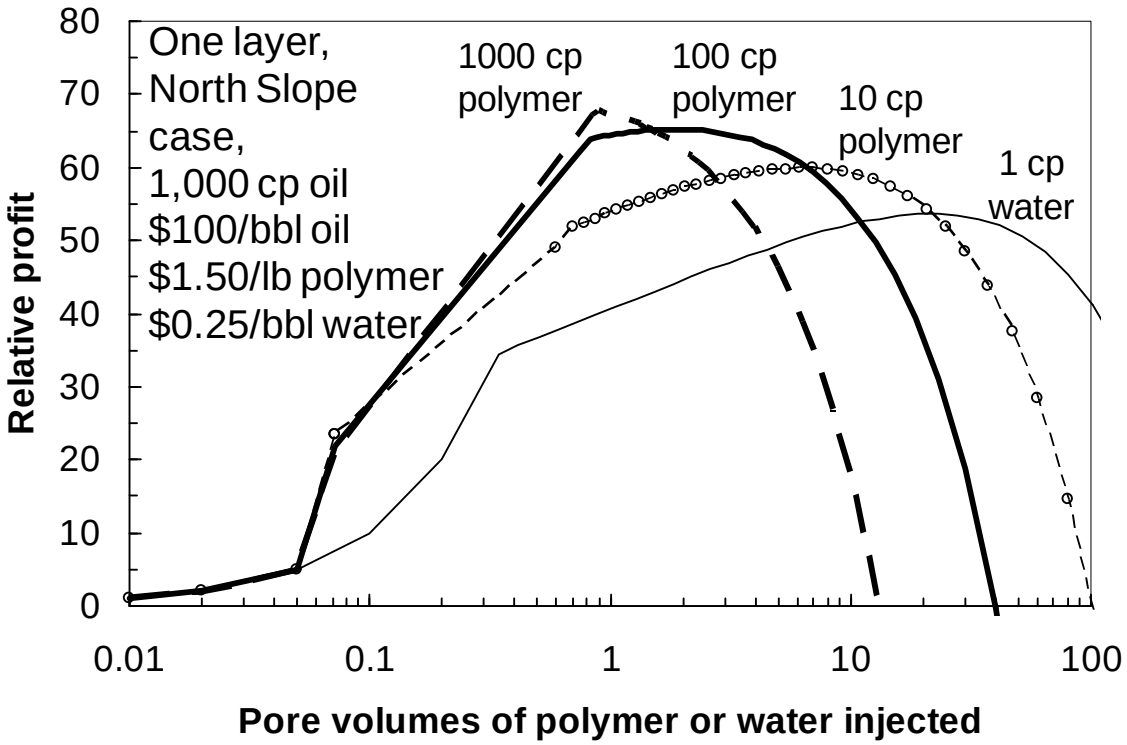

Fig. 16—North Slope case, one homogeneous layer 1,000-cp $20/bbl oil.

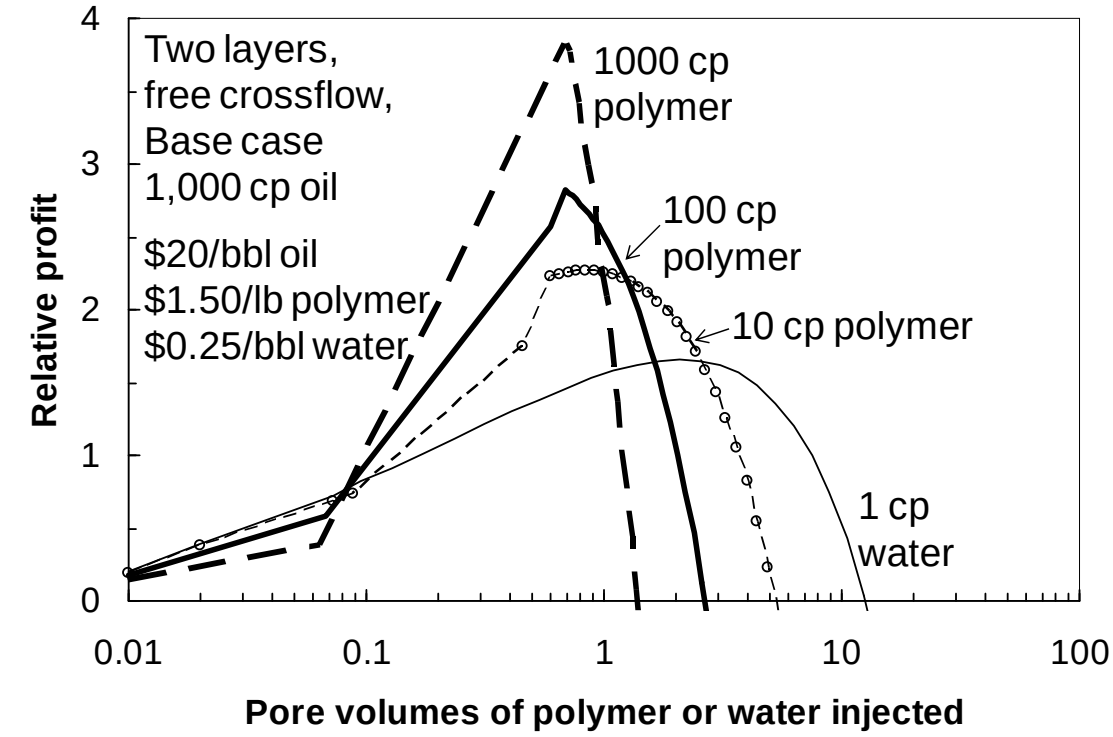

Fig. 17—Base case, two-layers, free crossflow, k_1=10k_2, 1,000-cp $20/bbl oil.

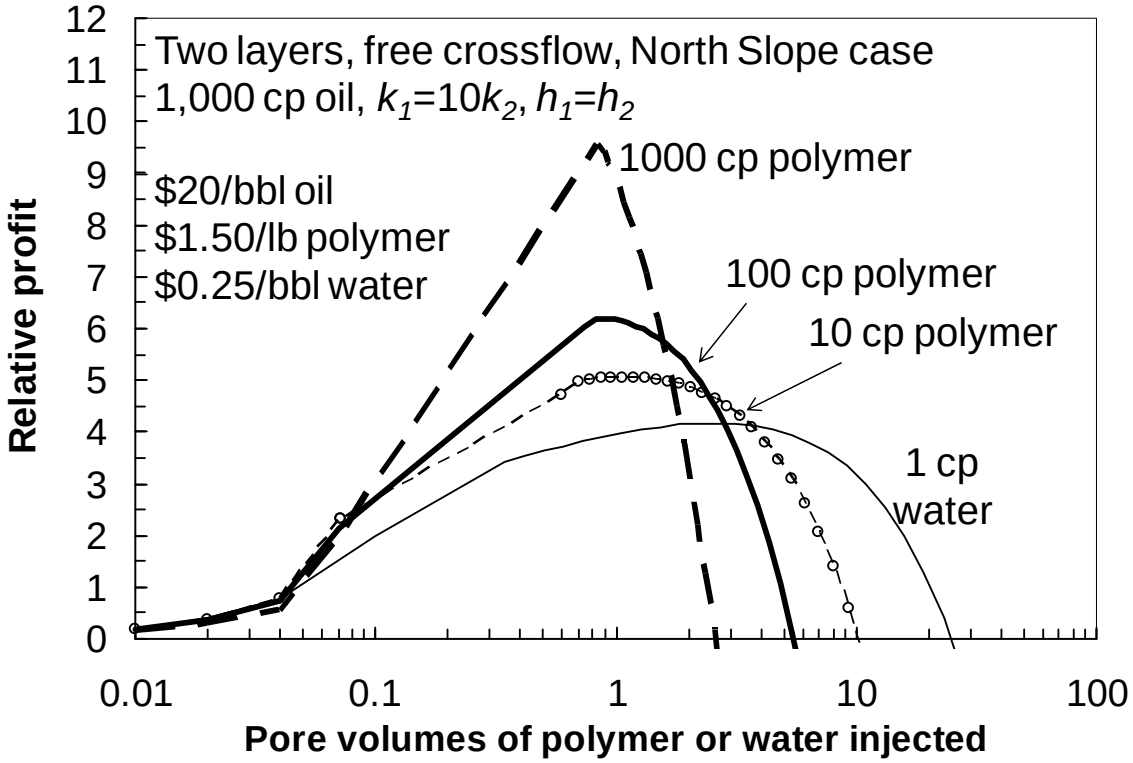

Fig. 18—North Slope case, two-layers, free crossflow, k_1=10k_2, 1,000-cp $20/bbl oil.

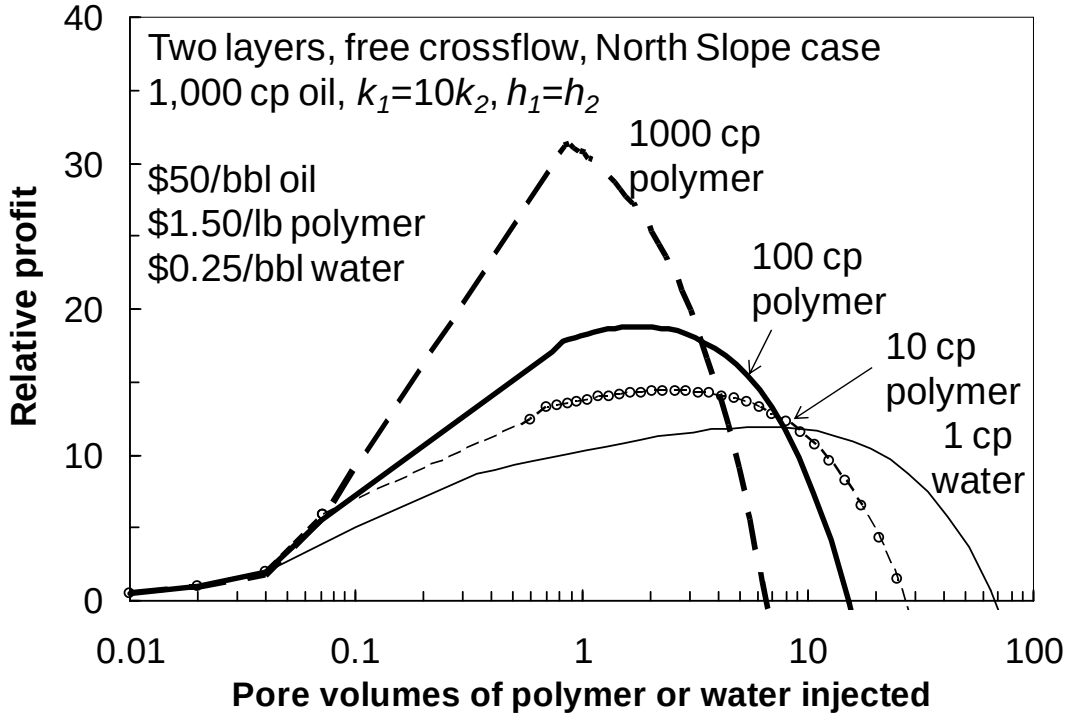

Fig. 19—North Slope case, two-layers, free crossflow, k_1=10k_2. 1,000-cp $50/bbl oil.

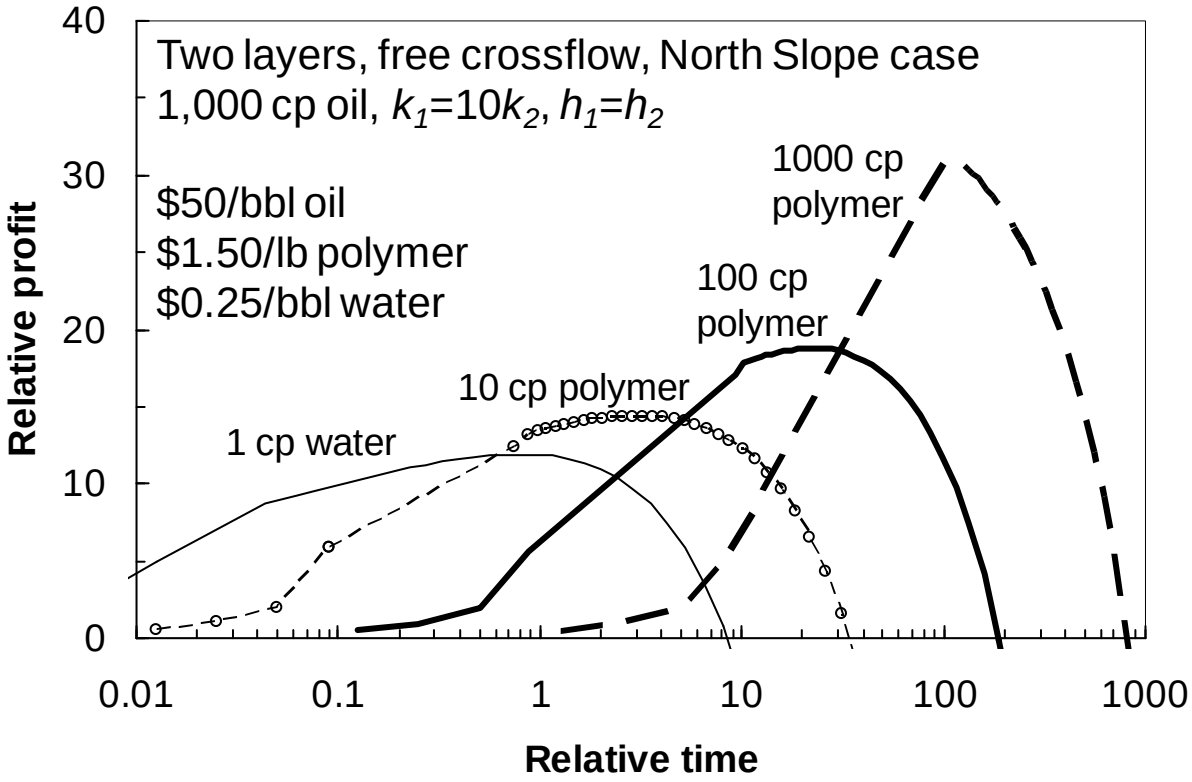

Fig. 20—Assuming that injectivity varies inversely with injection viscosity.

Increasing the injected polymer viscosity decreases the PV at which the peak profitability is observed (Figs. 15-19). However, that observation does not necessarily mean that polymer flooding will accelerate profits. If injectivity is assumed to be inversely proportional to polymer viscosity, Fig. 19 can be re-plotted as Fig. 20, which shows profit versus relative time. This figure suggests that injecting a 10-cp polymer solution may be economically attractive over waterflooding, but the benefits from injecting 100-cp or 1,000-cp polymer solutions may be delayed for unacceptably long times. Our simple economic analysis to this point did not include present value concepts.

The results emphasize that maximizing injectivity of polymer solutions is a critical need. Use of horizontal wells or fractures to maximize injectivity and accelerate oil production may be key to implementation of polymer flooding for recovery of viscous oils.

Effect of Formation Height

For the displacement calculations to date using two layers, the layers both had the same thickness ($h_1=h_2$). Using the North Slope relative permeability parameters, we investigated (using fractional flow calculations) the effect of formation height on oil recovery during polymer flooding of 1,000-cp oil in a two-layer reservoir where Zone 1 was 10 times more permeable than Zone 2. For 1,000-cp oil with free crossflow between layers, Fig. 21 plots mobile oil recovered at 1 PV of polymer injection for various zone height ratios (h_1/h_2) between 0.1 and 10. Fig. 22 presents the analogous plots for cases with no crossflow between layers. Gravity and capillary effects were not included in these calculations.

Examination of Figs. 12, 14, 21, and 22 reveals several important observations. First, as expected, both with and without crossflow, for 1 PV of polymer injection, recovery values increase with increasing ratio of h_1/h_2—i.e., as the more-permeable layer becomes thicker relative to the less-permeable layer (Figs. 21 and 22). Second, with free crossflow, nearly 100% recovery can be achieved by injecting 1 PV if the polymer is sufficiently viscous (1,000-cp curve in Figs. 14 and 21). This observation is consistent with our previous analysis,[21] showing that near 100% vertical sweep can be achieved with free crossflow if the reciprocal of the mobility ratio is greater than or equal to the permeability contrast (k_1/k_2). Third, without crossflow, large PV throughputs are needed to achieve high recovery values, even when injecting viscous polymer solutions (see Fig. 12).

Without crossflow, if one PV of polymer solution is injected, most of the recovery benefit is achieved using only a 10-cp polymer solution (Fig. 12). In contrast with free crossflow, injection of more viscous polymer solutions are needed to achieve high recovery values (Figs. 14 and 21). In one North Slope reservoir, the operator indicated that three distinct thick zones are present. One of these zones (100 ft thick) might be a target for polymer flooding to recover viscous oil. Within that particular zone, several sub-zones are present, but free crossflow is expected. Consequently, the free crossflow case may be of most interest for our future considerations.

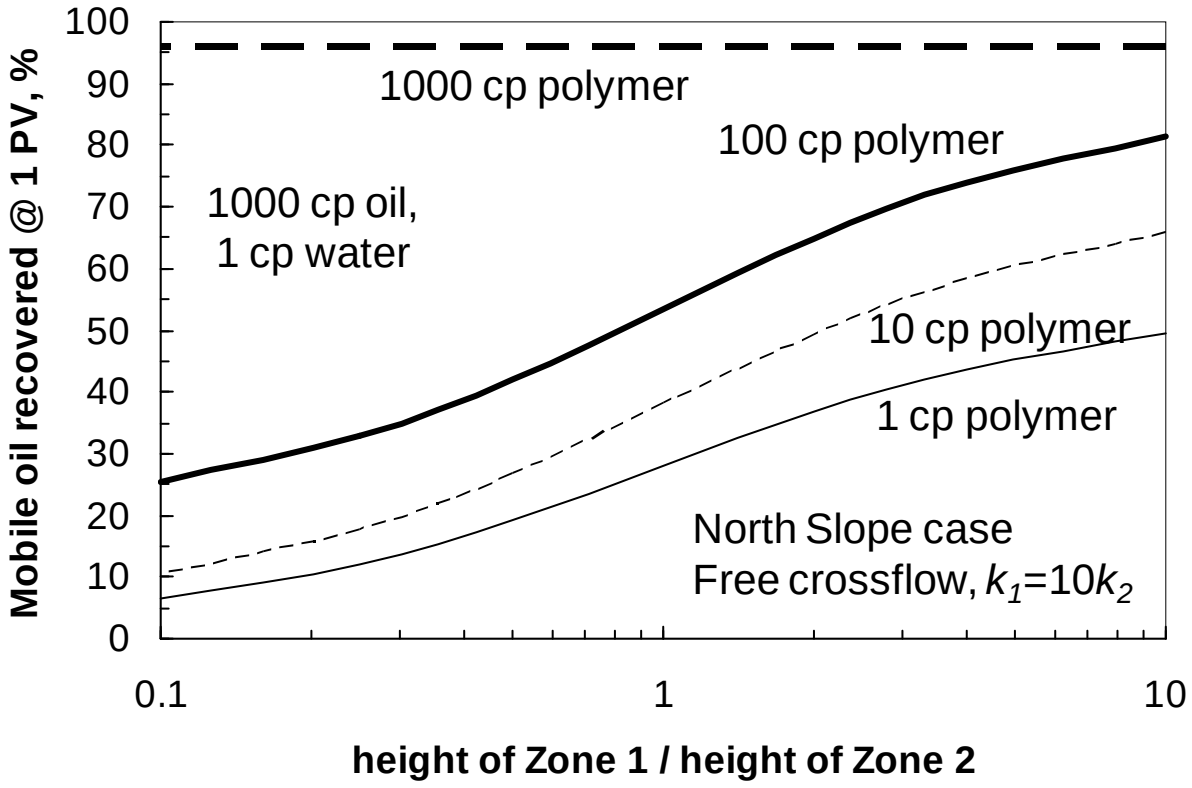

Fig. 21—Oil recovery after injecting 1 PV of polymer, free crossflow, various heights.

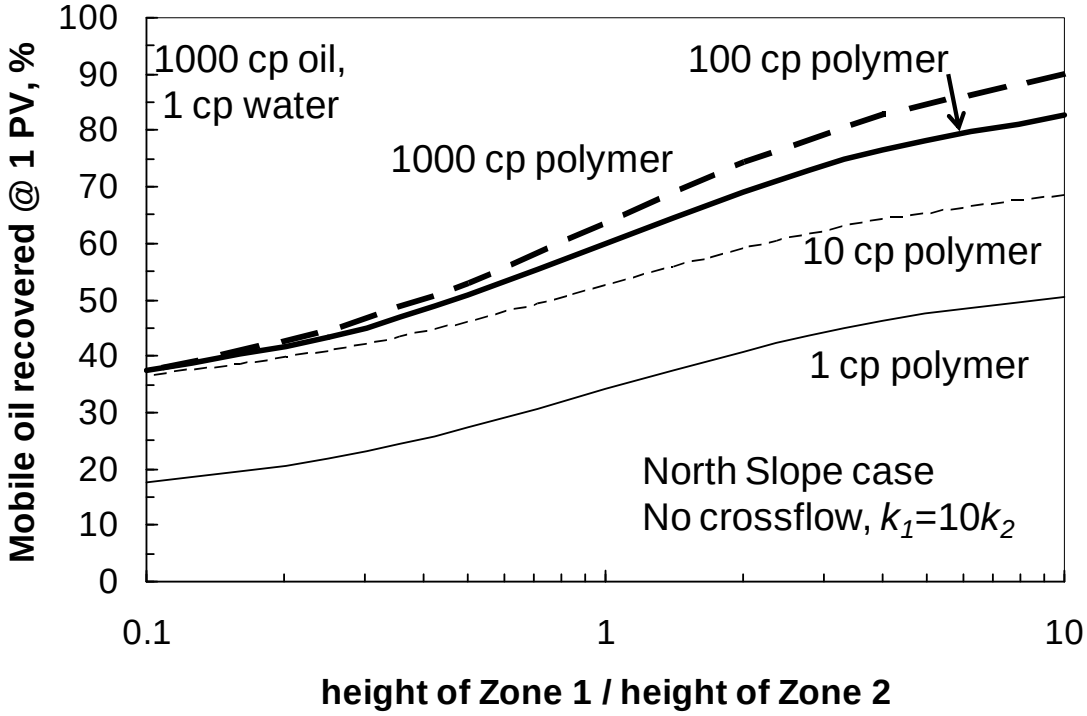

Fig. 22—Oil recovery after injecting 1 PV of polymer, no crossflow, various heights.

Figs. 23-30 plot recovery versus pore volume of polymer injected for many values of h_1/h_2 between 0.01 and 100 and for polymer solution viscosities ranging from 1 to 1,000. Figs. 23-26 apply to the cases with free crossflow, while Figs. 27-30 apply to the no-crossflow cases. For the crossflow cases, the curves associated with the various height ratios compress to become more similar as the injectant viscosity increases, especially for 1,000-cp polymer (Figs. 23-26). For the no-crossflow cases with greater than 10 PV throughput, the curves appears to converge as the injectant viscosity increases (Figs. 27-30). However, in the vicinity of 1 PV throughput, these curves become increasingly divergent as injectant viscosity increases.

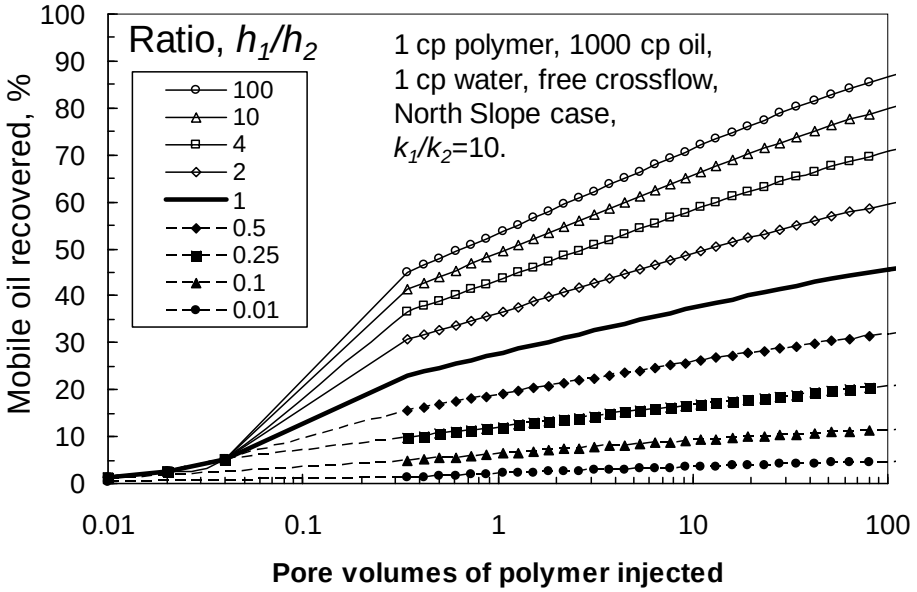

Fig. 23—Oil recovery versus PV and height, free crossflow, 1-cp polymer.

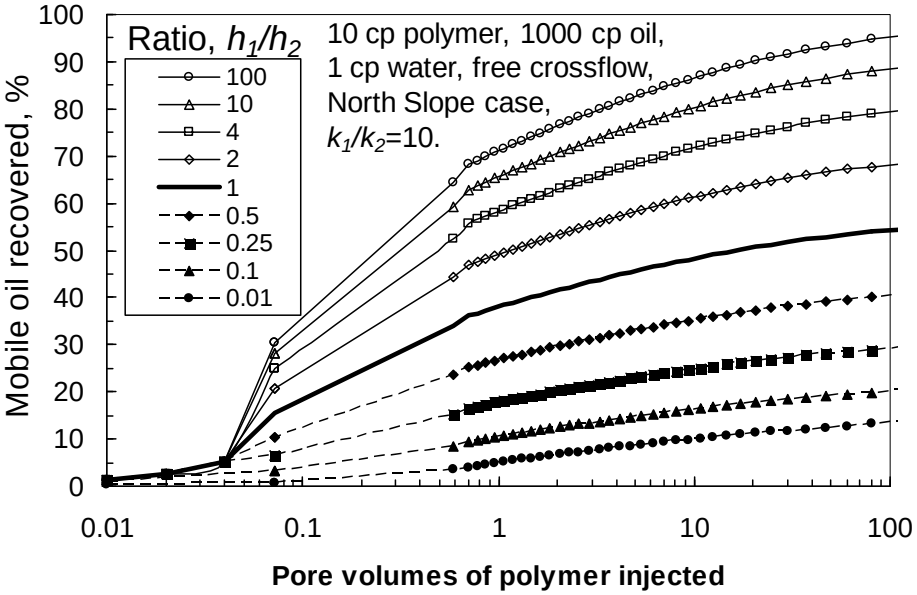

Fig. 24—Oil recovery versus PV and height, free crossflow, 10-cp polymer.

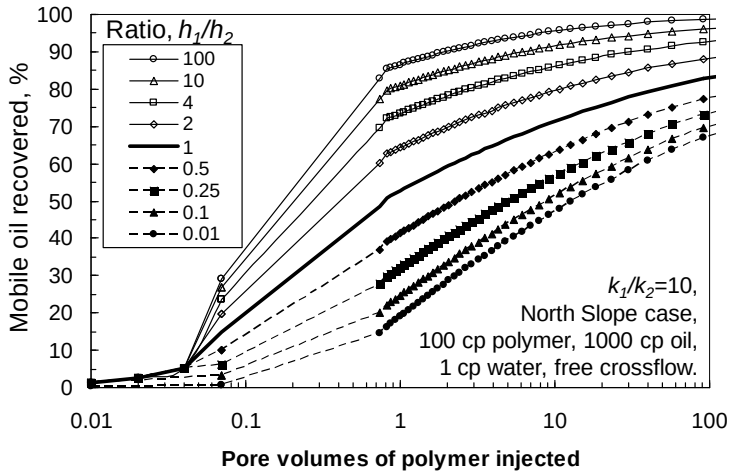

Fig. 25—Oil recovery versus PV and height, free crossflow, 100-cp polymer.

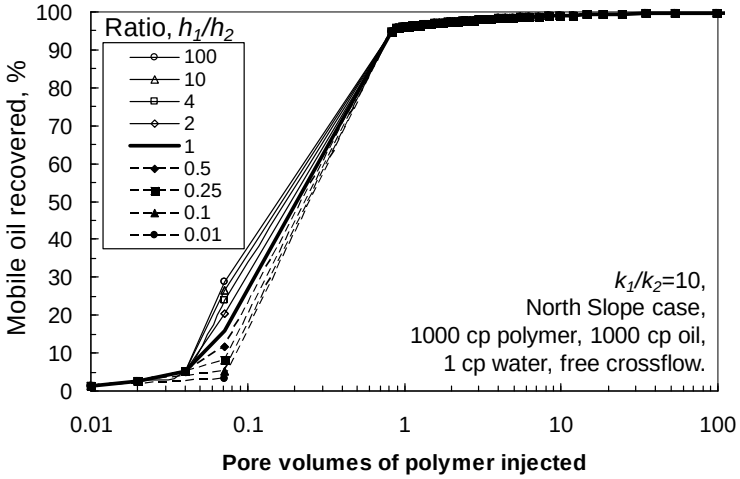

Fig. 26—Oil recovery versus PV and height, free crossflow, 1,000-cp polymer.

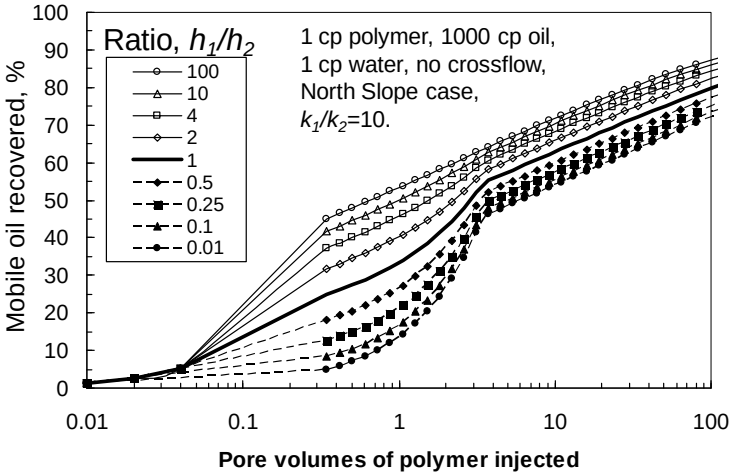

Fig. 27—Oil recovery versus PV and height, no crossflow, 1-cp polymer.

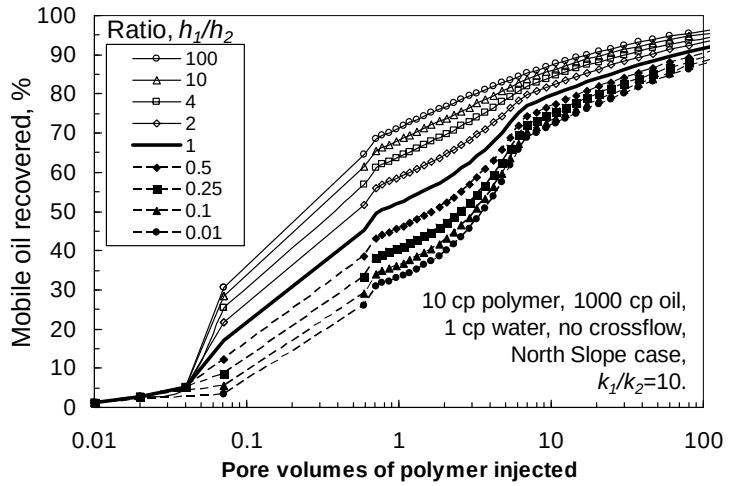

Fig. 28—Oil recovery versus PV and height, no crossflow, 10-cp polymer.

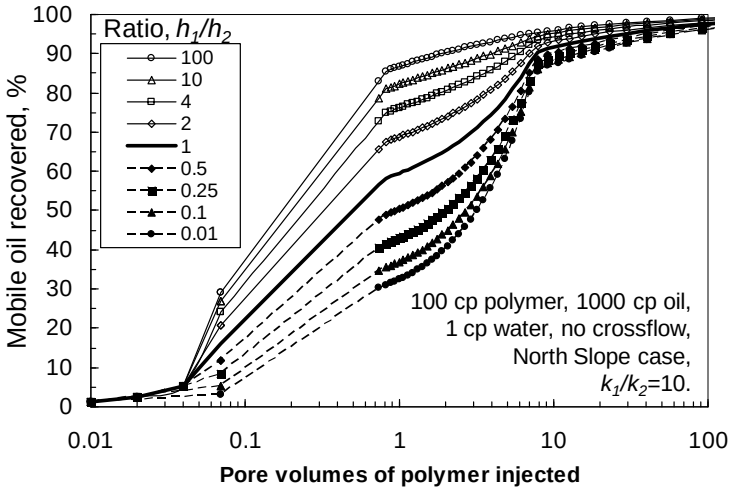

Fig. 29—Oil recovery versus PV and height, no crossflow, 100-cp polymer.

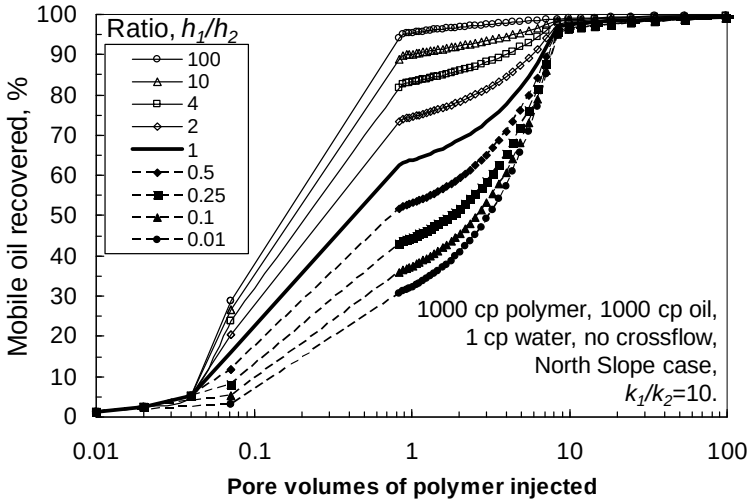

Fig. 30—Oil recovery versus PV and height, no crossflow, 1,000-cp polymer.

Effect of Gravity

In the analysis to this point, gravity effects were not considered. Will gravity have a significant effect on displacement efficiency for polymer flooding of viscous oil reservoirs? For these viscous crudes, the density difference ($\Delta\rho$) between water and oil is relatively small (12-23° API, 0.986 to 0.916 g/cm^3 density, with perhaps $\Delta\rho$=0.05 g/cm^3 being typical). An estimate of the vertical flux (u_z, in cm/s) of a polymer front can be made using the gravity portion of the Darcy equation:

$$u_z = - k \Delta\rho g / [1013300 \mu] \quad \text{.....(3)}$$

where k is permeability in darcys, $\Delta\rho$ is the density difference between the aqueous solution and oil in g/cm^3, g is the acceleration due to gravity (980 cm/s^2), and μ is the viscosity of the polymer solution in cp. Figs. 31 and 32 were generated using Eq. 3. Assuming a density difference of 0.05 g/cm^3, Fig. 31 plots the vertical component of velocity associated with a given viscosity and rock permeability, while Fig. 32 plots the vertical distance travelled by the polymer front in one year (due to gravity effects). The important message from these figures is that gravity effects may not usually have a strong influence on displacement during polymer flooding of viscous North Slope reservoirs. In one target reservoir, permeability averages about 50 md and the formation thickness totals about 70 ft. If a 10-cp polymer solution is injected, the vertical migration of the polymer front due to gravity will only be about 3 inches per year (from Eq. 3 and Fig. 32).

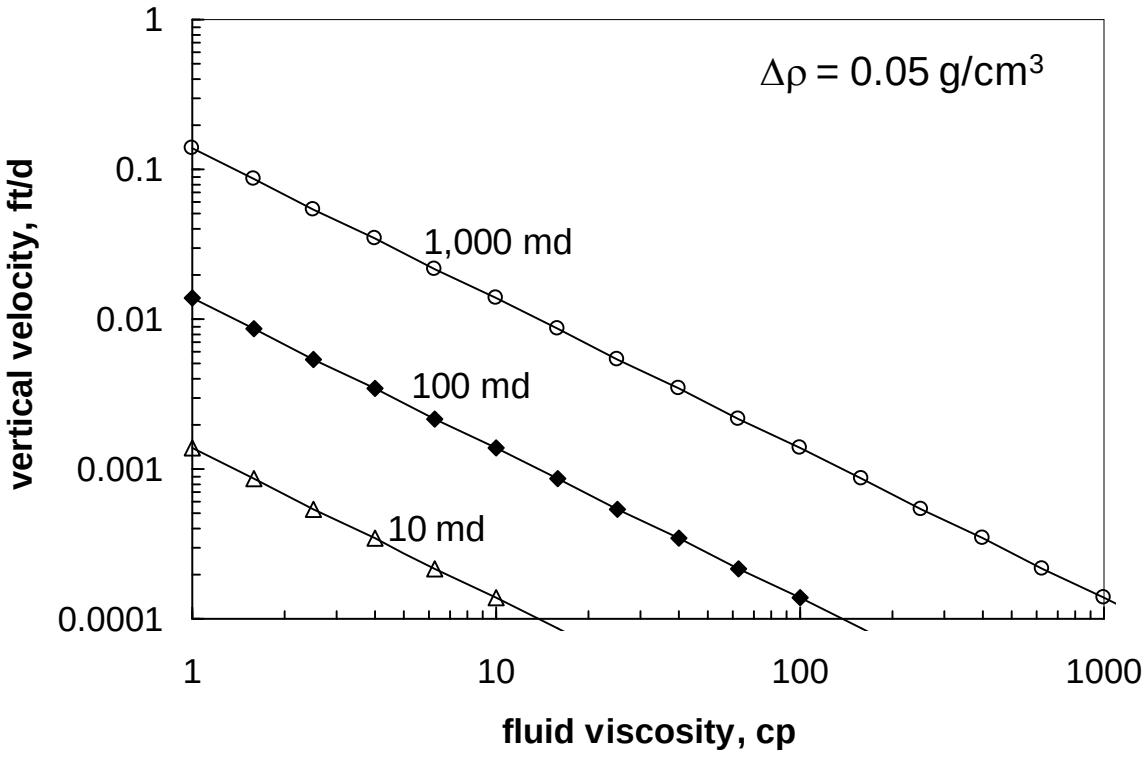

Fig. 31—Vertical velocity induced by gravity.

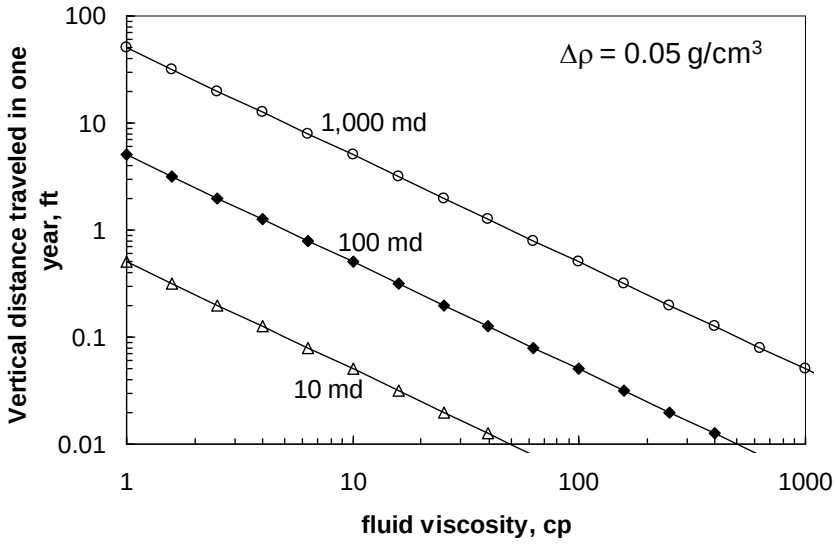

Fig. 32—Vertical distance travelled by the aqueous bank in one year (due to gravity).

Conclusions

1. We performed a number of base case simulations to establish confidence in the predictions of various reservoir simulators, including ECLIPSE, VIP, and POLYMER (a variant of UTCHEM). In the first case, we simulated simple one-dimensional displacement of oil (with various viscosities ranging from 1 to 100,000 cp) when injecting 1-cp water. For all three simulators, the results matched predictions from fractional flow calculations reasonably well. However, when two layers were present with different permeabilities, the simulations did not yield credible results. In particular, they predicted that, regardless of mobility ratio, recovery efficiency for cases with crossflow between the layers should be similar to those with no crossflow. Ultimately, we learned the proper formatting of the ECLIPSE simulator to obtain a reasonable match of recovery predictions with those from fractional flow calculations, notably for the free crossflow cases.
2. We performed fractional flow calculations where a polymer flood was implemented to displace 1,000-cp oil. Using these recovery results, a simple economic analysis was performed to make a preliminary assessment of the potential for polymer flooding in reservoirs with viscous oils. The analysis indicated that over a significant range of throughput values, polymer flooding provides a higher relative profit than waterflooding.
3. The results emphasize that maximizing injectivity of polymer solutions may be key to economic implementation of polymer flooding for recovery of viscous oils.
4. Both with and without crossflow, for 1 PV of polymer injection, oil recovery values increase as the more-permeable layers become thicker relative to the less-permeable layer. With crossflow, nearly 100% recovery can be achieved by injecting 1 PV if the polymer is sufficiently viscous (i.e., the reciprocal of the mobility ratio is greater than or equal to the permeability ratio, k_1/k_2). Without crossflow, large PV throughputs are needed to achieve high recovery values, even when injecting viscous polymer solutions.
5. Without crossflow, if one PV of polymer solution is injected, most of the recovery benefit is achieved using only a 10-cp polymer solution. (Even so, the total recovery benefit will at one PV will be low if the oil is viscous with no crossflow.) In contrast with free crossflow,

injection of more viscous polymer solutions is needed to achieve high recovery values. The free crossflow case may be of most interest for our future considerations.

6. For the permeabilities and viscosities that are likely to be experienced in our target North Slope reservoirs, gravity effects on the positions of polymer fronts will probably not be particularly important.

3. MEASUREMENT OF VISCOSITY VERSUS POLYMER CONCENTRATION

In assessing the viability of polymer flooding, a major issue is the cost-effectiveness of the polymer—i.e., how much viscosity the polymer provides versus the cost of the polymer. For a given polymer concentration, xanthan polysaccharides provide significantly greater viscosity than partially hydrolyzed polyacrylamides (HPAM). However, xanthan costs 2 to 4 times more than HPAM polymers. HPAM currently costs around $1.50/lb. For a given HPAM and HPAM concentration, the viscosity depends strongly on salinity. High molecular weight (Mw) HPAM polymers cost about the same as low Mw HPAM polymers. A given viscosity level can be achieved using a lower concentration of high Mw HPAM than for a low Mw HPAM—thus giving high Mw HPAM an economic edge. However, high Mw polymers have difficulty penetrating into small pores (low permeability rock). If the polymer cannot penetrate into the rock, it cannot displace oil from that rock. Consequently, trade-offs exist when trying to identify the most cost-effective polymer for a given application.

Brines

As a first step toward assessing the viability of polymer flooding in viscous North Slope reservoirs, we examined viscosity versus polymer concentration for many commercially available water soluble polymers in a number of brines. Our measurements were made at room temperature, consistent with the low temperatures of our target reservoirs (West Sak has an average temperature of 25°C). Our viscosity measurements were also made at a shear rate of 7.3 s^{-1}, consistent with the low flow velocity/shear rate expected deep in a reservoir. As summarized in Table 4, we used five different brines, ranging from 1% to 8% total dissolved solids (TDS). All brines were prepared by dissolving salts in distilled water and then filtering the brines through 0.45 μm Millipore filters.

Table 4—Brine compositions.

Name	%TDS	Composition
Quarter seawater	1.05	1.05% ASTM D-1141-52 sea salt
Half seawater	2.1	2.1% ASTM D-1141-52 sea salt
Seawater	4.195	4.195% ASTM D-1141-52 sea salt
2.52% TDS	2.52	2.3% NaCl, 0.22% $NaHCO_3$
8% TDS	8	6.48% NaCl, 0.1% KCl, 0.8% $CaCl_2$, 0.62% $MgCl_2$

Seawater is readily available for waterflooding on Alaska's North Slope. However, depending on the time of the year, the total salinity of arctic seawater may be noticeably less than that of seawater in other parts of the world. Consequently, based on input from the literature and industry, we decided to include brines with "seawater", "half seawater", and "quarter seawater". Table 5 provides the composition of ASTM D-1141-52 sea salt. Based on input from ConocoPhilips for the Kuparuk field, we also chose the 2.52% TDS brine, which contained no divalent cations (in contrast to the other four brines). As a fifth choice, we selected the 8% TDS brine, which has the greatest concentration of divalent ions as well as being the most saline. The first four brines can be argued to be of direct relevance to North Slope fields. The fifth brine is included simply to consider the high end of possible salinities.

Table 5—Composition of ASTM D-1141-52 sea salt.

Chemical	% of total salt
NaCl	58.490
$MgCl_2\ 6H_2O$	26.460
Na_2SO_4	9.750
$CaCl_2$	2.765
KCl	1.645
$NaHCO_3$	0.477
KBr	0.238
H_3BO_3	0.071
$SrCl_2\ 6H_2O$	0.095
NaF	0.007

Polymers

We examined several polymers from a number of commercial sources. The xanthan polymers were thought to have a Mw between 2 and 2.5 million daltons. Table 6 lists estimated molecular weights and degrees of hydrolysis for many of the HPAM polymers.

Table 6—Properties of several HPAM polymers. (Data from SNF)

Flopaam	Estimated Mw, million daltons	Degree of hydrolysis, mole, %	type
3230	6-8	30	copolymerized
3330	8-10	30	copolymerized
3430	10-12	30	copolymerized
3530	15	30	copolymerized
3630	18	30	copolymerized
3830	18-20	40	copolymerized
6030	20-22	40	post-hydrolyzed

Viscosity versus Polymer Concentration

Viscosity versus polymer concentration is shown in Figs. 33-37 and in Tables 7-12. For each polymer and brine, we determined viscosity at 7.3 s^{-1} and room temperature from 200 to 15,000 ppm polymer. For polymer solution viscosities above 10 cp, viscosity (μ) versus polymer concentration (C) fit quite well using the relation:

$$\mu = A\ C^B \quad \text{.....(4)}$$

The exponent in this equation, B, provides the slope of the log-log plots in Figs. 33-37. The third column of Tables 7-12 lists B values for the various polymers. These B values typically range from 1.6 to 2.5. This behavior is an advantage when using polymer solutions to displace viscous oils. To explain, most previous conventional polymer floods (directed at oil viscosities less than 50 cp) used relatively low polymer concentrations (1,000 ppm or less). In this range, the relation between viscosity and polymer concentration is nearly linear, so viscosity and polymer solution cost is directly proportional to polymer concentration. In this regime, if a doubling of viscosity is desired, a doubling of polymer solution cost may be needed. For more viscous oils, higher

polymer solution viscosities may be needed for efficient oil displacement. For these more concentrated polymer solutions, a *B* value of two means that doubling the solution viscosity can be achieved by increasing polymer concentration and cost by only 40%.

The last five columns of Tables 7-12 list polymer concentrations required to achieve various solution viscosities between 10 and 1,000 cp. Within a given table, the listings generally go from low to high on polymer requirement, so the most efficient polymers are listed first. Detailed examination of Tables 7-12 and Figs. 33-37 reveals several facts that are consistent with previous expectations. First, in the brines examined, polysaccharides (such as xanthan) provided a given viscosity level with much less polymer than for HPAM polymers (compare Tables 7 and 8). (Of course, the biopolymers cost noticeably more than the HPAMs.) Second, high Mw HPAMs provided a given viscosity level with less polymer than low Mw HPAMs. (For SNF HPAM polymers, Mw generally increased with increased product number. See Table 6.) Third, for a given HPAM, the polymer requirements to achieve a given viscosity increased with increased salinity (see Tables 9-11). Fourth, for a given xanthan, the polymer requirements to achieve a given viscosity were insensitive to salinity (compare XC HV, K9D236, or Fufeng in Table 8 at 2.52% TDS versus Table 12 at 8%TDS). Fifth, for a given HPAM, the polymer requirements to achieve a given viscosity increased with increased divalent cation content (compare Tables 7 and 10).

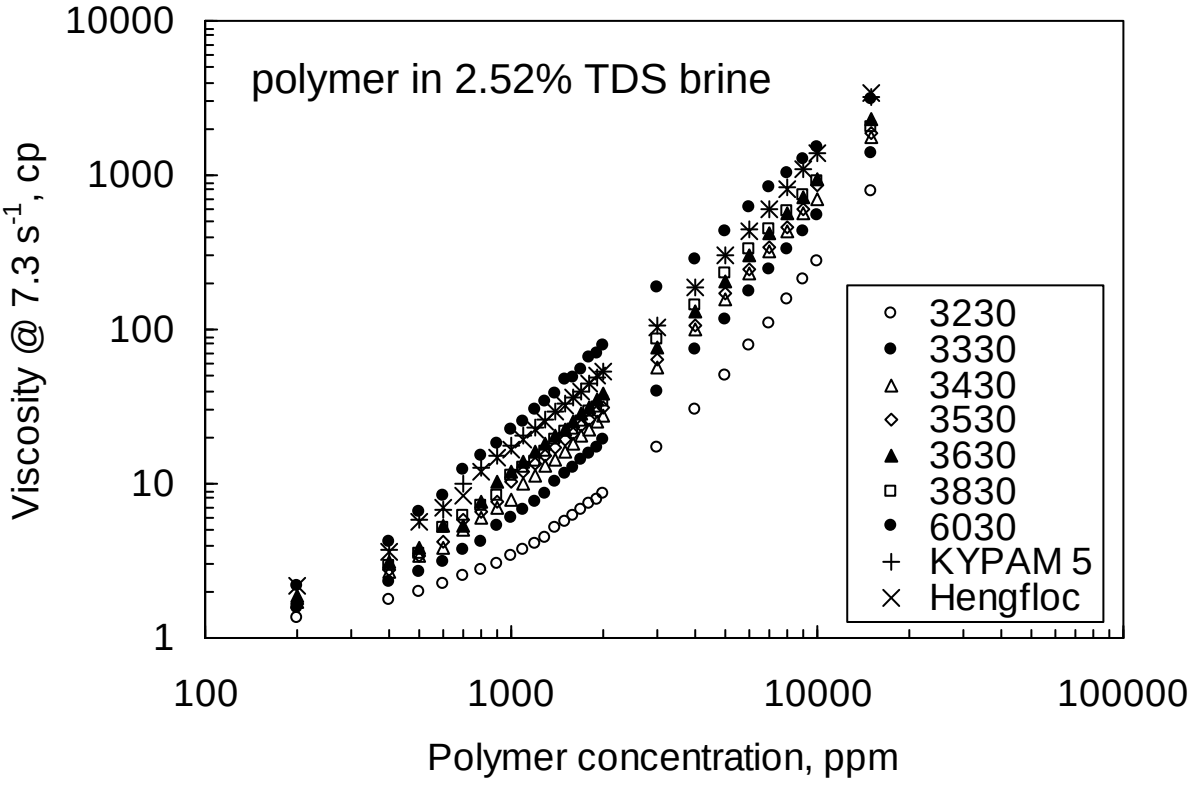

Fig. 33—Viscosity versus HPAM concentration in 2.52% TDS brine.

Table 7—HPAM in 2.52% TDS brine (2.3% NaCl + 0.22% $NaHCO_3$).
HPAM ppm (C) needed to achieve given cp (μ): $\mu = A\ C^{B}$

HPAM polymer	*A*	*B*	10 cp	25 cp	60 cp	100 cp	1000 cp
SNF 6030S	6.17×10^{-5}	1.85	654	1074	1724	2272	7886
Hengju KYPAM 5	3.86×10^{-5}	1.87	772	1258	2006	2635	8998
Hengju Hengfloc 63022	2.99×10^{-5}	1.90	795	1287	2038	2665	8926
SNF 3630S	2.17×10^{-5}	1.90	959	1553	2462	3222	10828
SNF 3830S	1.2×10^{-5}	1.97	1020	1625	2535	3286	10585
SNF 3530S	1.64×10^{-5}	1.91	1066	1721	2721	3555	11861
SNF 3430S	9.47×10^{-6}	1.96	1174	1872	2925	3794	12267
SNF 3330S	3.3×10^{-6}	2.05	1448	2263	3469	4450	13678
SNF 3230S	2.38×10^{-7}	2.26	2346	3517	5179	6492	17964

However, a few subtle surprises were seen in the measurements. For example, the relative positions of the SNF HPAMs changed, depending on the brine composition.

For the various xanthan polymers examined, some viscosity differences were seen between 500 and 5,000 ppm (Fig. 34). However, the variations in viscosity were noticeably less than for the range of HPAM polymers (Fig. 33). For a given polymer concentration, diutan provided the highest viscosity of any polymer tested (Fig. 34).

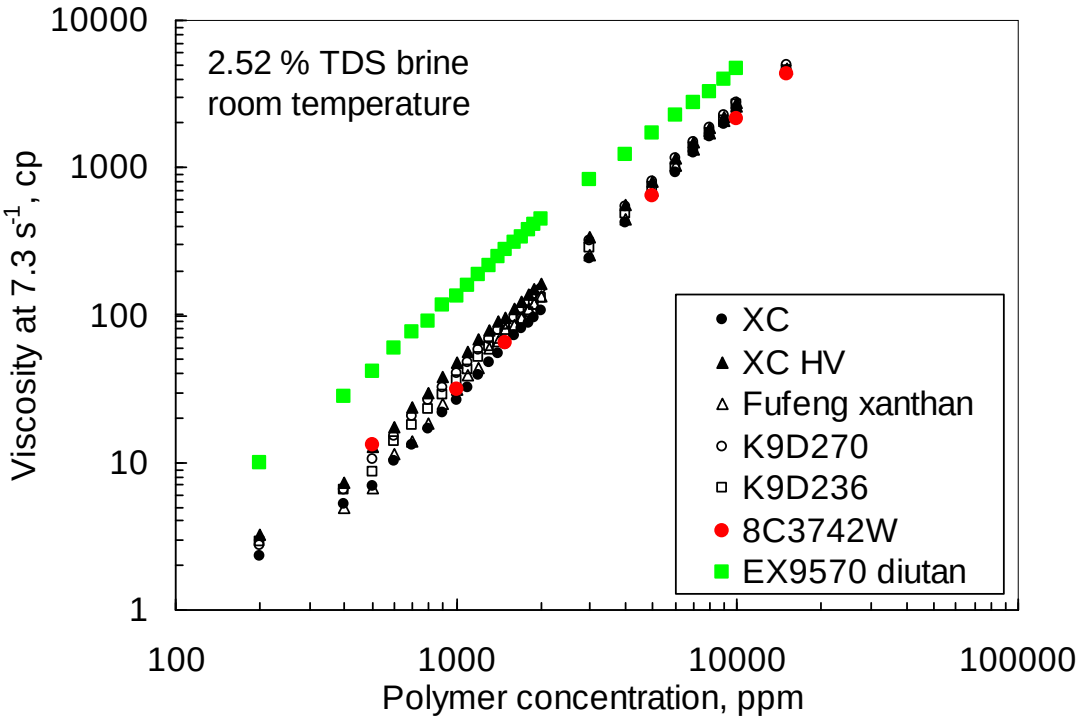

Fig. 34—Viscosity versus biopolymer concentration in 2.52% TDS brine.

Table 8—Biopolymer in 2.52% TDS brine (2.3% NaCl + 0.22% $NaHCO_3$).
Biopolymer ppm (C) needed to achieve given cp (μ): $\mu = A\,C^{B}$

Biopolymer	***A***	***B***	**10 cp**	**25 cp**	**60 cp**	**100 cp**	**1000 cp**
CP Kelco EX9570 diutan	$2.46\text{x}10^{-3}$	1.58	192	343	597	825	3540
CP Kelco XC HV xanthan	$2.38\text{x}10^{-4}$	1.76	417	700	1150	1536	5664
CP Kelco K9D270 xanthan	$1.25\text{x}10^{-4}$	1.84	466	768	1236	1632	5712
CP Kelco K9D236 xanthan	$1.15\text{x}10^{-4}$	1.83	497	819	1322	1747	6141
Shandong Fufeng xanthan	$6.24\text{x}10^{-5}$	1.91	539	871	1379	1803	6035
CP Kelco XC xanthan	$2.56\text{x}10^{-5}$	2.01	607	957	1480	1908	6003
CP Kelco 8C3742W xanthan	$5.32\text{x}10^{-5}$	1.90	593	960	1522	1991	6681

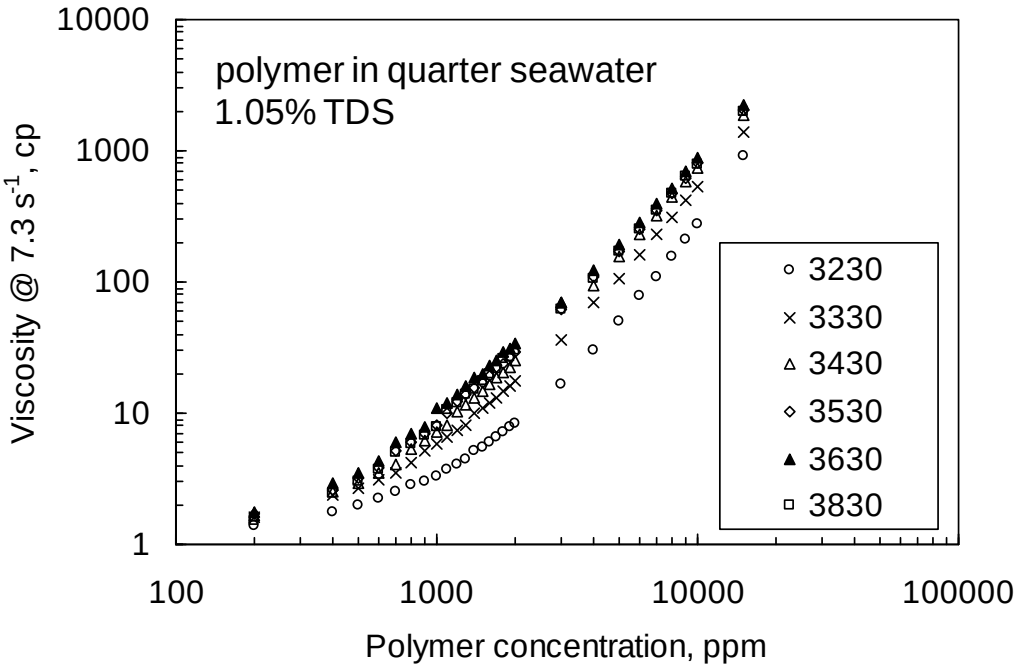

Fig. 35—Viscosity versus HPAM concentration in quarter seawater.

Table 9—HPAM in 1.05% TDS brine (quarter seawater).
Polymer ppm (C) needed to achieve given cp (μ): $\mu = A\,C^{B}$

HPAM polymer	***A***	***B***	**10 cp**	**25 cp**	**60 cp**	**100 cp**	**1000 cp**
SNF 3630S	$1.33\text{x}10^{-5}$	1.95	1035	1656	2595	3373	10989
SNF 3530S	$8.09\text{x}10^{-6}$	1.99	1141	1807	2804	3624	11508
SNF 3830S	$6.67\text{x}10^{-6}$	2.01	1165	1836	2835	3654	11461
SNF 3430S	$4.75\text{x}10^{-6}$	2.04	1243	1947	2988	3837	11839
SNF 3330S	$2.80\text{x}10^{-6}$	2.06	1495	2330	3561	4561	13915
SNF 3230S	$3.65\text{x}10^{-8}$	2.47	2574	3729	5312	6530	16564

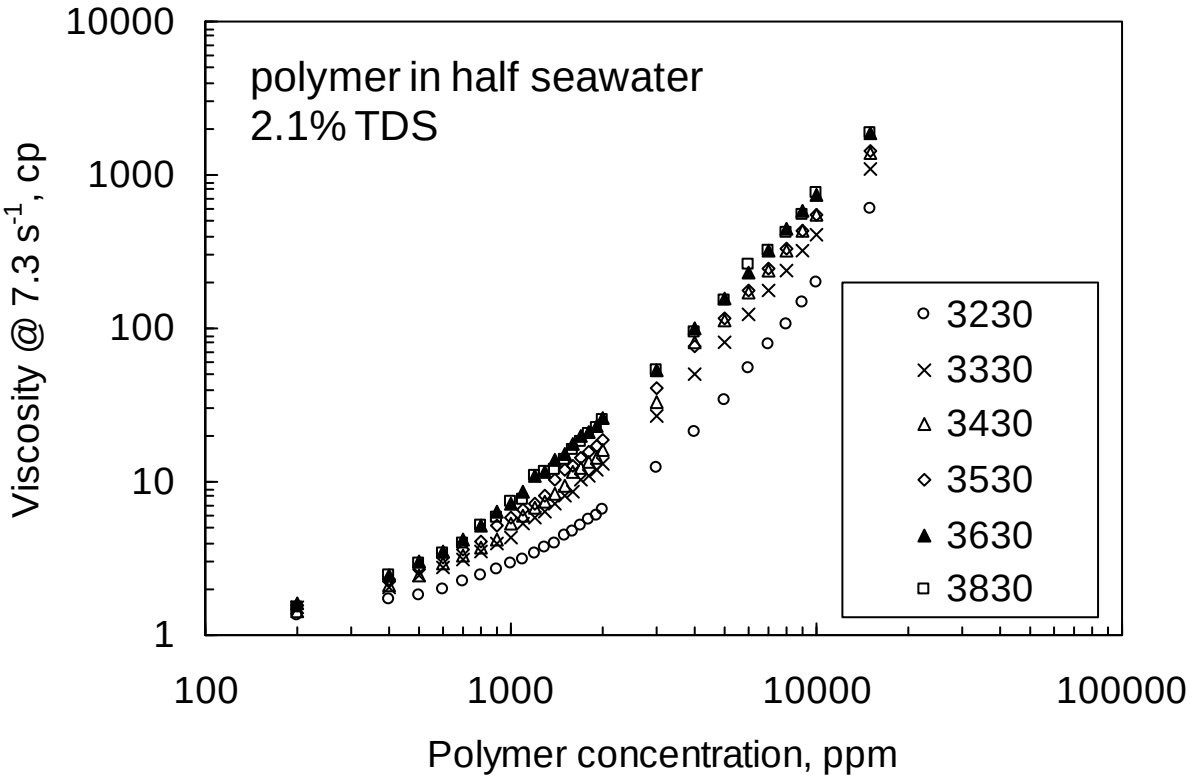

Fig. 36—Viscosity versus HPAM concentration in half seawater.

Table 10—HPAM in 2.1% TDS brine (half seawater).
Polymer ppm (C) needed to achieve given cp (μ): $\mu = A\,C^{B}$

HPAM polymer	***A***	***B***	**10 cp**	**25 cp**	**60 cp**	**100 cp**	**1000 cp**
SNF 3630S	$6.00\text{x}10^{-6}$	2.02	1219	1920	2963	3818	11961
SNF 3830S	$3.09\text{x}10^{-6}$	2.09	1298	2012	3058	3904	11742
SNF 3530S	$3.67\text{x}10^{-6}$	2.04	1428	2239	3438	4417	13658
SNF 3430S	$1.73\text{x}10^{-6}$	2.12	1543	2376	3591	4569	13533
SNF 3330S	$1.75\text{x}10^{-6}$	2.09	1734	2689	4092	5227	15760
SNF 3230S	$4.04\text{x}10^{-8}$	2.42	2914	4254	6105	7538	19500

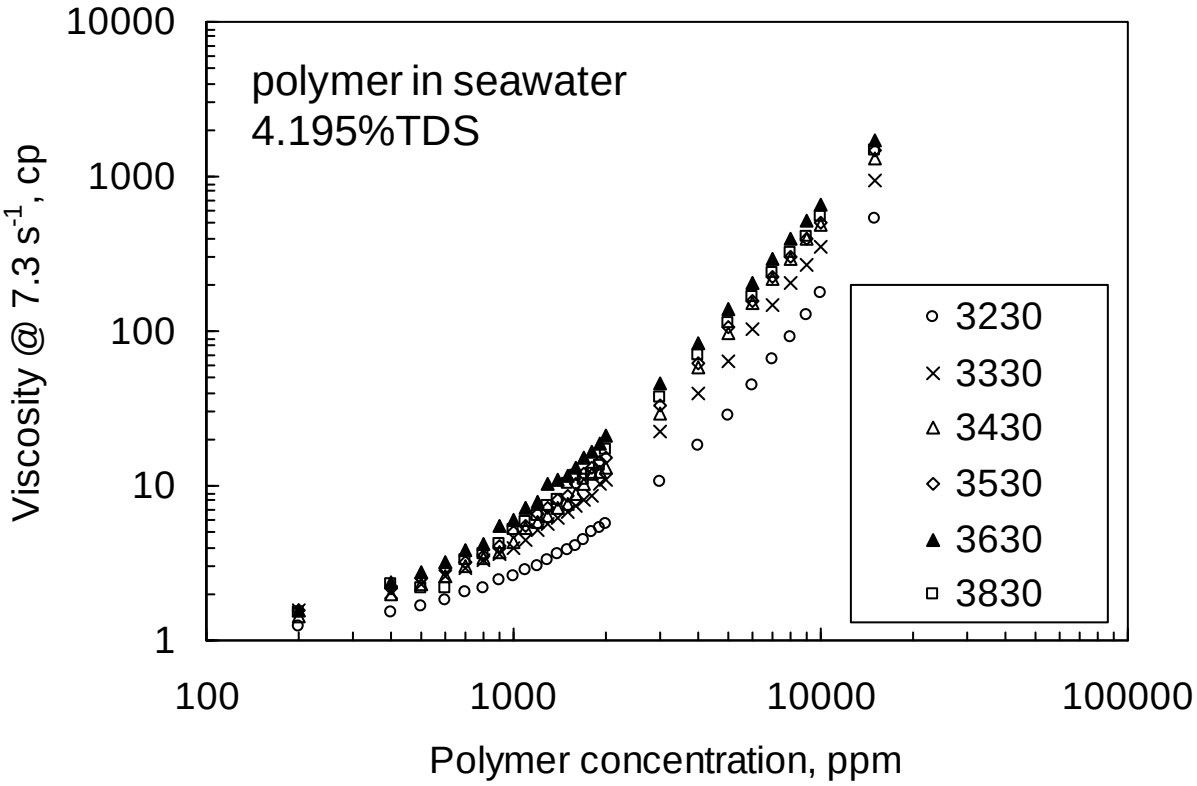

Fig. 37—Viscosity versus HPAM concentration in seawater.

Table 11—HPAM in seawater (4.195% TDS).
Polymer ppm (C) needed to achieve given cp (μ): $\mu = A\ C^{B}$

HPAM polymer	***A***	***B***	**10 cp**	**25 cp**	**60 cp**	**100 cp**	**1000 cp**
SNF 3630S	3.16×10^{-6}	2.07	1360	2116	3227	4128	12528
SNF 3830S	1.15×10^{-6}	2.17	1595	2435	3647	4617	13366
SNF 3530S	1.90×10^{-6}	2.10	1571	2428	3682	4694	14029
SNF 3430S	1.06×10^{-6}	2.16	1680	2566	3847	4873	14133
SNF 3330S	1.36×10^{-6}	2.09	1900	2943	4470	5705	17130
SNF 3230S	2.79×10^{-8}	2.45	3142	4570	6537	8055	20650

Table 12—Polymer in 8% TDS brine.
Polymer ppm (C) needed to achieve given cp (μ): $\mu = A\ C^{B}$

Polymer	A	B	10 cp	25 cp	60 cp	100 cp	1000 cp
CP Kelco XC HV xanthan	2.69×10^{-4}	1.75	409	690	1138	1524	5678
CP Kelco K9D236 xanthan	1.18×10^{-4}	1.83	495	817	1319	1744	6144
Shandong Fufeng xanthan	5.28×10^{-5}	1.94	517	829	1300	1690	5522
Hengju KYPAM 5 HPAM	6.69×10^{-7}	2.27	1430	2139	3144	3936	10834
Hengju Hengfloc 63022 HPAM	6.66×10^{-8}	2.47	2030	2940	4189	5151	13073
SNF 3530S HPAM	4.62×10^{-7}	2.22	2010	3036	4503	5668	15985
SNF 3830S HPAM	5.93×10^{-8}	2.44	2339	3404	4872	6006	15420
SNF 3330S HPAM	1.04×10^{-7}	2.34	2564	3792	5511	6854	18321
SNF 3230S HPAM	6.59×10^{-9}	2.58	3661	5225	7339	8948	21871
SNF 3430S HPAM	3.78×10^{-9}	2.60	4229	6017	8428	10259	24886

These viscosity results will be used as input for our future modeling studies.

Conclusions

We determined viscosity (at 7.3 s^{-1}, room temperature) versus polymer concentration for many commercially available water soluble polymers in a number of brines. For polymer solution viscosities above 10 cp, viscosity (μ) versus polymer concentration (C) fit quite well using the relation, $\mu = AC^{B}$. B values typically ranged from 1.6 to 2.5. This behavior provides a cost advantage when using polymer solutions to displace viscous oils.

Several observations were consistent with previous expectations. First, in the brines examined, polysaccharides (such as xanthan) provided a given viscosity level with much less polymer than for HPAM polymers. (Of course, the biopolymers cost noticeably more than the HPAMs.) Second, high Mw HPAMs provided a given viscosity level with less polymer than low Mw HPAMs. Third, for a given HPAM, the polymer requirements to achieve a given viscosity increased with increased salinity. Fourth, for a given xanthan, the polymer requirements to achieve a given viscosity were insensitive to salinity. Fifth, for a given HPAM, the polymer requirements to achieve a given viscosity increased with increased divalent cation content.

For the various xanthan polymers examined, some viscosity differences were seen between 500 and 5,000 ppm. However, the variations in viscosity were noticeably less than for the range of HPAM polymers. For a given polymer concentration, diutan provided the highest viscosity of any polymer tested. These viscosity results will be used as input for our future modeling studies.

4. POLYMER RESISTANCE FACTORS VERSUS PERMEABILITY

An important goal of our work is to determine the rheology in porous media for existing EOR polymers for the range of permeabilities anticipated in North Slope viscous oil reservoirs that might be candidates for polymer flooding. In general, we are trying to determine the most cost-effective polymer (most viscosity for the least cost) that will efficiently enter and flow through North Slope rock. The highest molecular weight (Mw) polymers generally provide the highest viscosity for a given polymer concentration. However, if the polymer Mw is too high, it may not effectively enter or flow through porous rock.[25-27] Consequently, in less-permeable rock, a polymer with a lower Mw (and lower cost-effectiveness) may be required.

We characterized the performance in 55-md and 269-md Berea sandstone for nine commercially available EOR polymers, including one xanthan, one diutan, and seven partially hydrolyzed polyacrylamides (HPAM). The HPAM polymers had molecular weights ranging from 6 to 22 million daltons. The 55-md Berea sandstone core was 14.35 cm long, with a square cross-section of 11.34 cm^2. Porosity was 17% and the pore volume was 27.7 cm^3. Two internal pressure taps divided the core into three sections with lengths of 2.2 cm, 10.15 cm, and 2 cm, respectively. The 269-md Berea sandstone core was 12.78 cm long, also with a square cross-section of 11.34 cm^2. Porosity was 21.2% and the pore volume was 30.8 cm^3. Two internal pressure taps divided the core into three sections with lengths of 2.39 cm, 8.75 cm, and 1.64 cm, respectively.

We performed a similar characterization in a 5,120-md porous polyethylene core, with dimensions and conditions similar to those for the two Berea cores. Our previous research[28] demonstrated that the pore structure of porous polyethylene was quite similar to that for Berea sandstone, although the porosity was considerably higher (35% versus 17% and 21.2% for the two Berea cores) The polyethylene core was 15.27 cm long, with a square cross-section of 11.64 cm^2. The pore volume was 62.8 cm^3. Two internal pressure taps divided the core into three sections with lengths of 2.54 cm, 10.3 cm, and 2.43 cm, respectively. As with the first two cores, the polyethylene core was initially saturated with 2.52% TDS (total dissolved solids) brine (2.3% NaCl+0.22% $NaHCO_3$). This filtered brine was also used to prepare all polymer solutions. All experiments were performed at room temperature.

Face-Plugging. Table 13 lists the polymer compositions, volumes, and throughputs (Σ, in cm^3/cm^2) for the three sets of experiments. Substantial numbers of pore volumes (PV) and throughputs were associated with each stage of polymer injection. Because each core had internal pressure taps, we could assess the level of face plugging by monitoring how the resistance factor in the first core section (F_{r1}) changed relative to that in the second core section (F_{r2}). (Resistance factor is the effective viscosity of the polymer solution in porous media, relative to that of water.) Fig. 38 plots the ratio, F_{r1}/F_{r2}, versus throughput for the experiments in the 55-md and 269-md cores, while Fig. 39 plots this ratio in the 269-md and 5,120-md cores. In Fig. 38, the upper set of vertically oriented labels apply to the 55-md Berea core (solid circles), while the lower set applies to the 269-md Berea core (solid triangles). In Fig. 39, the upper set of labels apply to the 5,120-md porous polyethylene core (open squares), while the lower set applies to 269-md Berea core (solid triangles, same data as in Fig. 38). The key message from Figs. 38 and 39 is that none of the polymers exhibited severe face-plugging for the three cores for the range of throughputs tested. We recognize that since diutan was injected last in each of

these tests, it may unfairly appear that diutan showed a greater degree of face plugging than the other polymers.

Table 13—Sequence and amounts of polymer solutions injected.

	55-md core		269-md core		5,120-md core	
Polymer	PV	Σ cm^3/cm^2	PV	Σ cm^3/cm^2	PV	Σ cm^3/cm^2
600 ppm CP Kelco K9D236 xanthan	20.5	50	58.4	159	31.4	169
2500 ppm SNF 3230S HPAM	19.0	97	19.5	212	43.4	403
1350 ppm SNF 3330S HPAM	19.6	144	19.5	265	28.6	557
2900 ppm SNF 3430S HPAM	14.8	180	17.9	313	19.5	662
1700 ppm SNF 3530S HPAM	14.8	216	17.5	361	22.1	781
970 ppm SNF 3630S HPAM	16.8	258	21.1	418	23.5	908
900 ppm SNF 3830S HPAM	19.3	305	19.5	471	21.4	1024
700 ppm SNF 6030S HPAM	16.5	346	42.2	586	23.1	1149
2500 ppm SNF 3230S HPAM (2^{nd})	26.8	410	90.9	832	49.2	1415
200 ppm CP Kelco EX9570 diutan	47.5	526	71.4	1026	36.5	1612

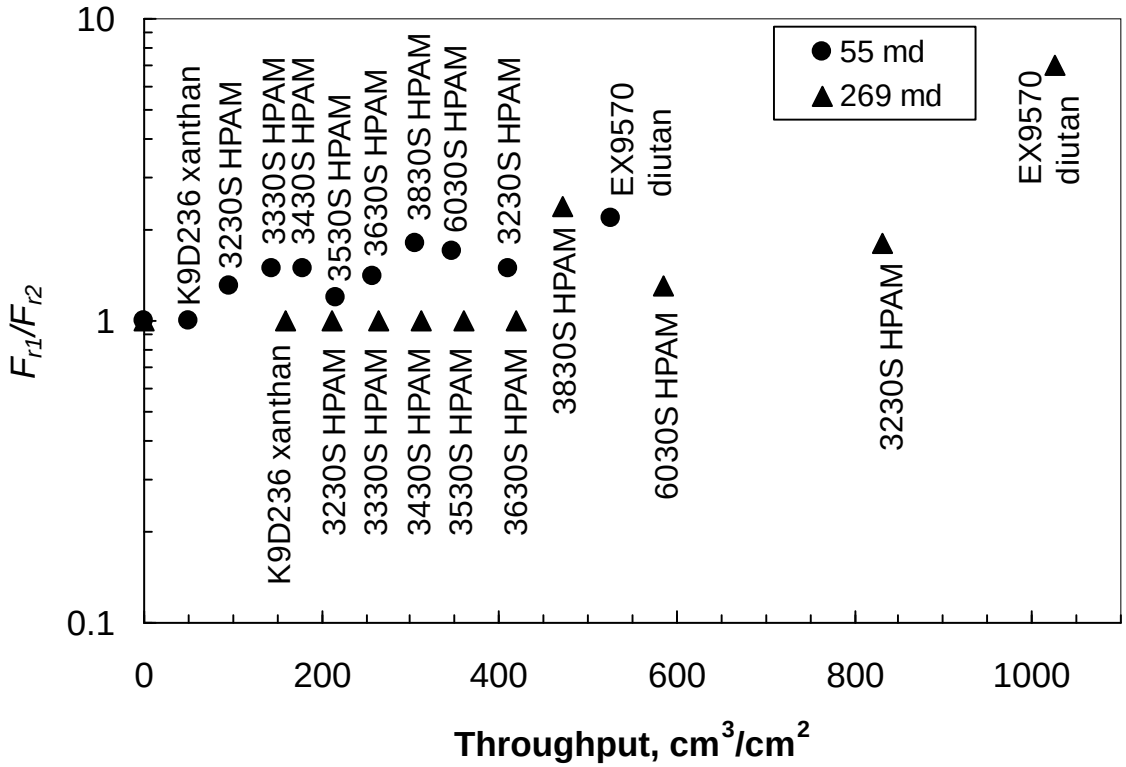

Fig. 38—F_{r1}/F_{r2} versus throughput in 55-md and 269-md Berea sandstone.

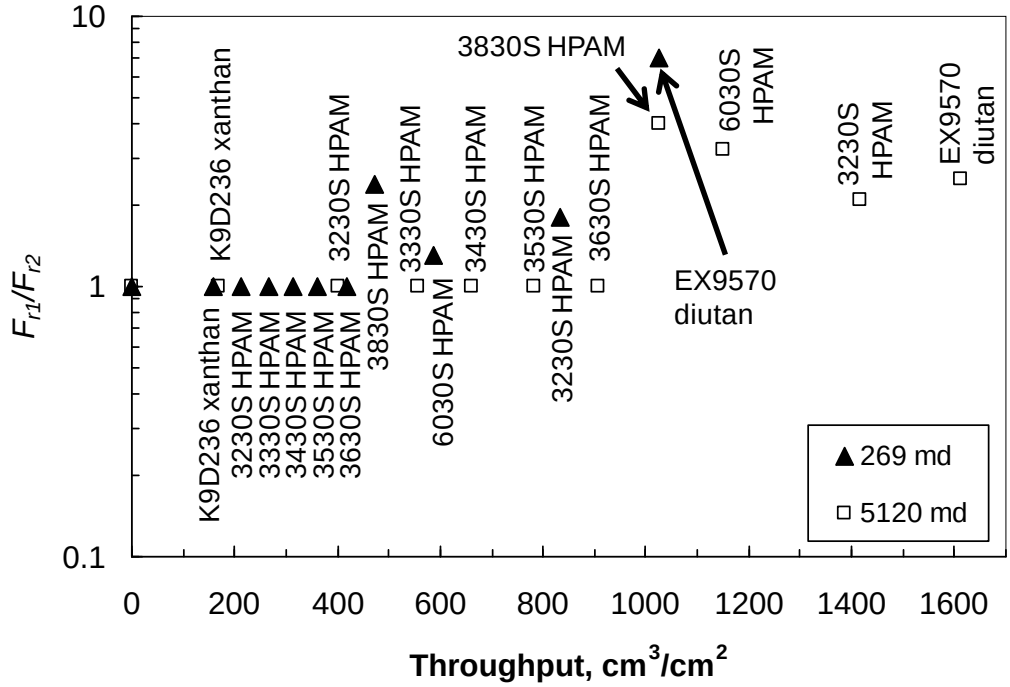

Fig. 39—F_{r1}/F_{r2} versus throughput in 269-md Berea sandstone and 5,120-md polyethylene.

Permeability Dependence of Rheology. Resistance factors can depend on permeability simply because the effective shear rate varies with pore size. A given rheological curve is expected to shift to higher velocities in proportion to the square root of the permeability ratio.[29,30] For our three cores, we found that resistance factor correlated quite well using the parameter $u(1-\phi)/(\phi k)^{0.5}$, where u is flux (in ft/d), ϕ is porosity, and k is permeability (in md). This observation can be confirmed in Figs. 40-48. With an original basis in a capillary bundle model of porous media, many previous researchers have used the correlating parameter, $u/(\phi k)^{0.5}$, or a modification thereof.[29-36]

Consistent with previous literature,[35,36] Fig. 40 confirms that xanthan solutions show shear-thinning or pseudoplastic behavior in porous media. The solid curve in Fig. 40 shows that the viscosity data parallels the resistance factor in the shear-thinning region. To make this match, shear rates (in s^{-1}, associated with the viscosity data) were divided by 310 when plotted on the x-axis. (This value of 310 was strictly an empirical factor that was needed to make the shear-thinning portions of the curves match.)

Also consistent with previous literature,[16,25,32] Figs. 41-48 confirm that HPAM resistance factors increase with increased flux at moderate to high flux values. This behavior was attributed to the viscoelastic character of HPAM and the elongational flow field in porous rock. The solid curves in each of these figures shows viscosity data, again with shear rate divided by 310 plotted on the x-axis. In each of these HPAM figures, the onset of pseudodilatant (viscoelastic) resistance factors correlates closely with the transition from Newtonian to shear-thinning viscosity behavior.

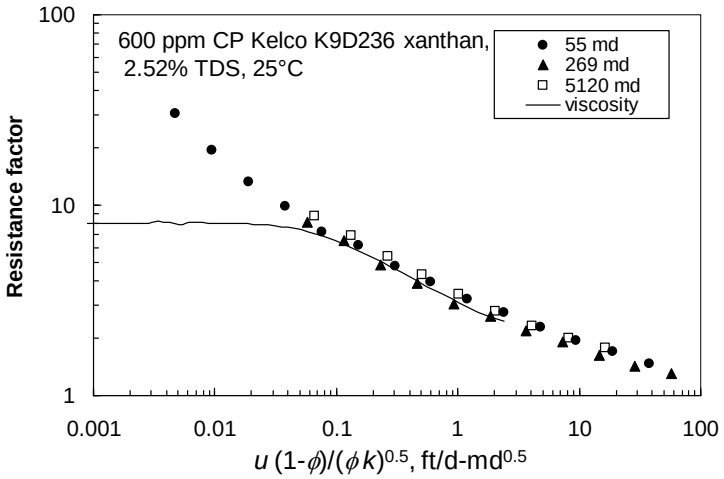

Fig. 40—Correlated resistance factors for 600-ppm CP Kelco K9D236 xanthan.

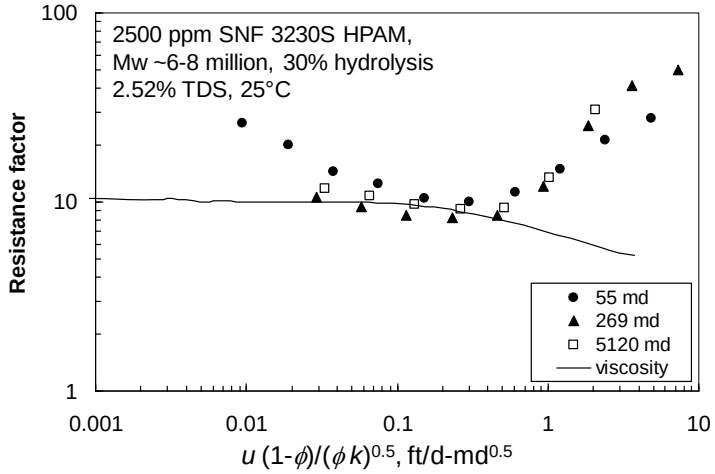

Fig. 41—Correlated resistance factors for 2500-ppm SNF 3230S HPAM (1st run).

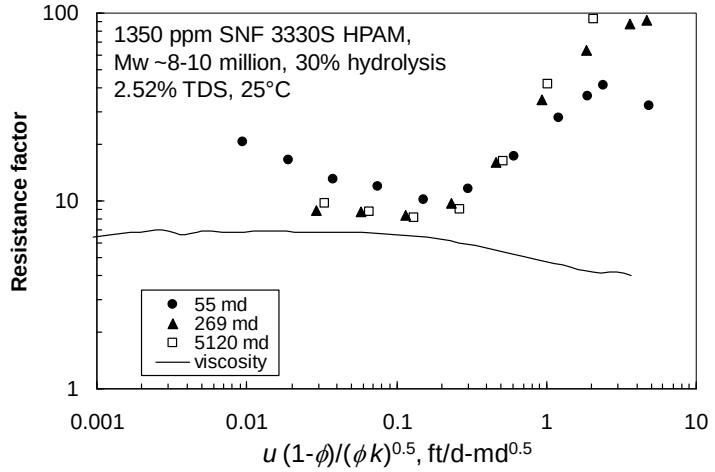

Fig. 42—Correlated resistance factors for 1350-ppm SNF 3330S HPAM.

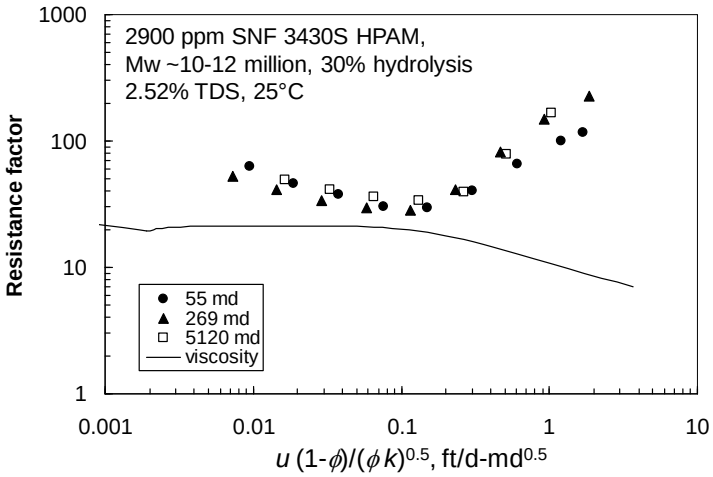

Fig. 43—Correlated resistance factors for 2900-ppm SNF 3430S HPAM.

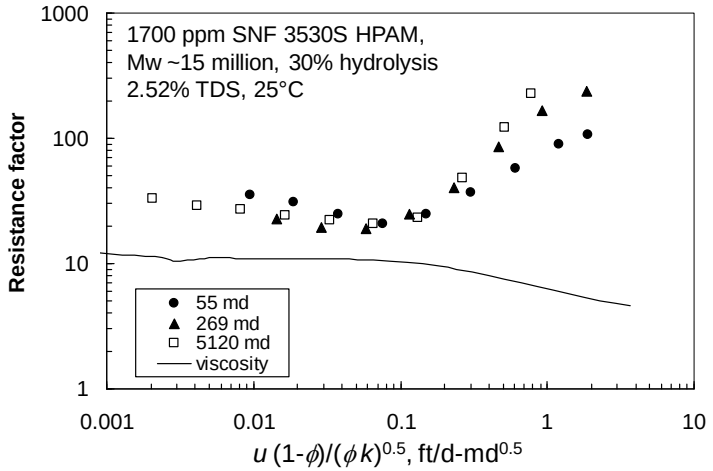

Fig. 44—Correlated resistance factors for 1700-ppm SNF 3530S HPAM.

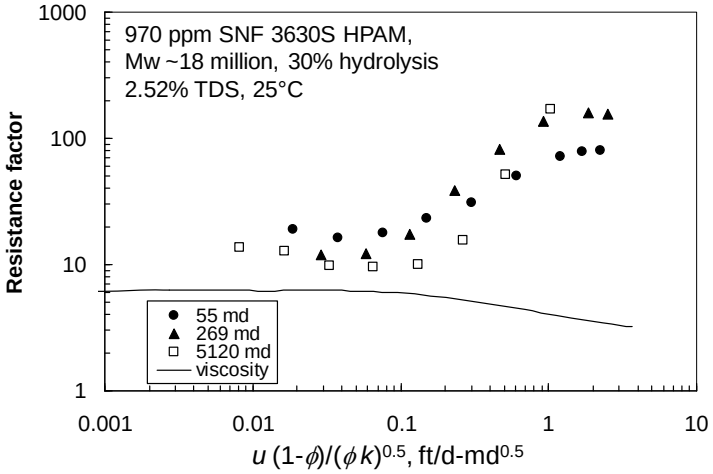

Fig. 45—Correlated resistance factors for 970-ppm SNF 3630S HPAM.

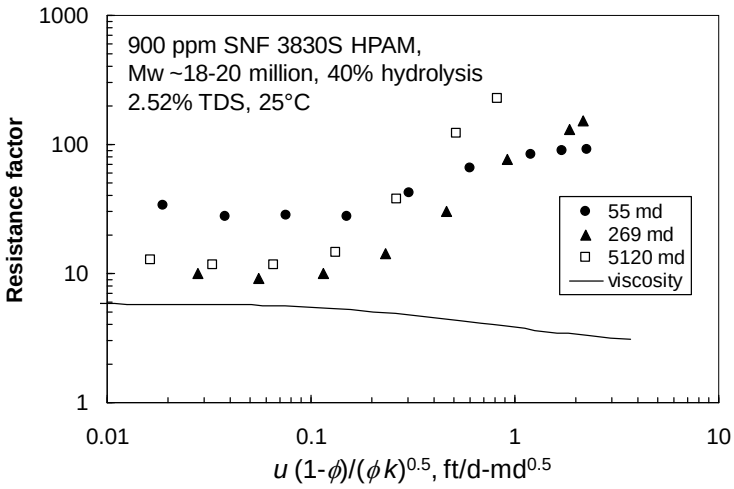

Fig. 46—Correlated resistance factors for 900-ppm SNF 3830S HPAM.

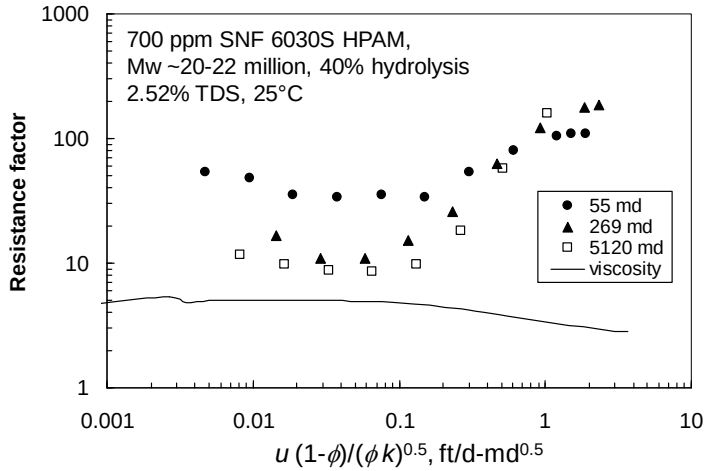

Fig. 47—Correlated resistance factors for 700-ppm SNF 6030S HPAM.

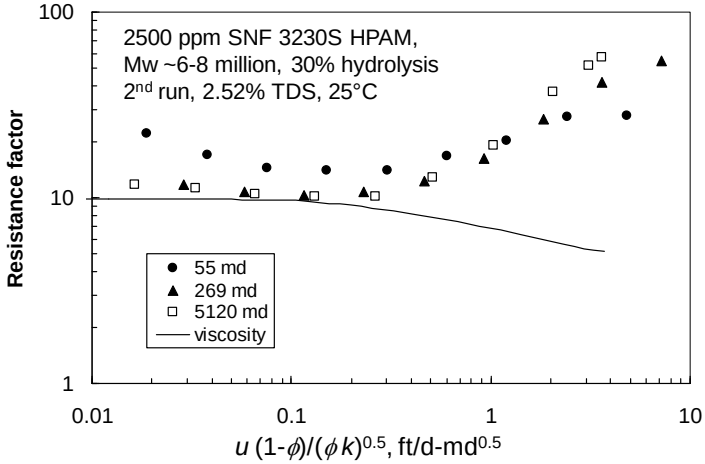

Fig. 48—Correlated resistance factors for 2500-ppm SNF 3230S HPAM (2nd run).

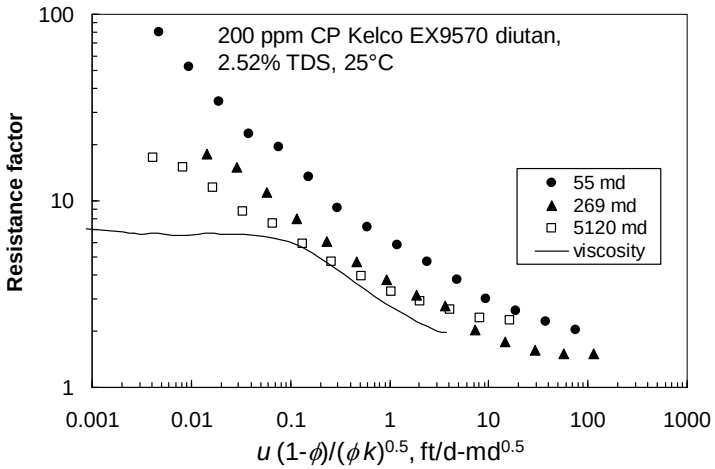

Fig. 49—Correlated resistance factors for 200-ppm CP Kelco EX9570 diutan.

The behavior of 200-ppm diutan (Fig. 49) in 269-md Berea and 5,120-md polyethylene followed that for 600-ppm xanthan (Fig. 40) reasonably closely, although the diutan showed greater variability. In 55-md Berea, the diutan curve was shifted significantly to the right of the other two curves (Fig. 49)—suggesting increased resistance to flow (e.g., internal filter cake formation, increased permeability reduction). The large throughput of various polymers prior to diutan injection also contributed to the relative mismatch for the 55-md diutan curve.

Unexpectedly High Resistance Factors at Low Fluxes. For the xanthan solution, the viscosity at low shear rates exhibited a plateau value of 8 (i.e., 8 cp or flow resistance 8 times greater than water, solid curve in Fig. 40). In contrast, in 55-md Berea sandstone, resistance factors at low flux reached as high as 30 (solid circles in Fig. 40). This behavior was also reported for xanthan solutions by Cannella *et al.*[35] and Hejri *et al.*[36] In 269-md Berea and 5,120-md porous polyethylene, we did not achieve sufficiently low velocities to observe this phenomenon.

For HPAM solutions, a viscosity plateau occured at low shear rates, just as with xanthan solutions (solid curves in Figs. 41-48). Thus, we also expected resistance factors to approach a fixed value at low flux values. This expectation was met by most low-flux HPAM resistance factors in 269-md Berea and 5,120-md polyethylene (Figs. 41, 42, and 44-48). (Although, one might argue in favor of a mild shear thinning behavior in porous media for some cases.) However, in 55-md Berea, a significant shear thinning behavior was noted for several cases at low flux (solid circles in Figs. 41 and 42). We suspect that this behavior was caused by ultra-high molecular weight polymers or "microgels."[37] These high Mw species may become mechanically entrapped (especially in less-permeable rock) and consequently reduce permeability and make the resistance factor appear significantly greater that the values expected from viscosity measurements. An important question is: Will this behavior occur deep within a reservoir or is it simply a laboratory artifact associated with using relatively short cores? Our expectation is that these high molecular weight species cannot be expected to propagate very far into the porous rock of a reservoir. They will be either mechanically degraded into smaller species[38] or they will be retained by the rock fairly close to the injection rock face.[37] Additional work is in progress to examine this issue.

HPAM Pseudodilatant (Viscoelastic) Behavior and Mechanical Degradation. Figs. 41-48 confirm that HPAM solutions show pseudodilatant or viscoelastic behavior in porous media—the resistance factor increases with increased flux for moderate to high fluid velocities.[14,16,25,31,39-41] Consistent with earlier work,[32] the onset of the pseudodilatant (viscoelastic) behavior correlated well with the parameter, $u(1-\phi)/(\phi k)^{0.5}$. Also consistent with previous literature,[25] the start of the resistance factor increase began at lower flux values as the polymer molecular weight increased (see Figs. 41-48).

HPAM solutions are also susceptible to mechanical degradation.[14,16,42,43] The degree of mechanical degradation experienced by the polymer correlates with the applied pressure gradient.[14] This fact explains the differences in resistance factors at the highest velocities in Figs. 41-48. For example, consider Fig. 44 (1700-ppm 3530S). As the correlating parameter (x-axis) increases above 0.1, resistance factor increases most steeply for the 5,120-md data and least steeply for the 55-md data. For a given value of the correlating parameter in this region, pressure gradient varies inversely with the square root of permeability. Consequently for a given value of the correlating parameter, as permeability decreases, pressure gradient increases, the level of polymer mechanical degradation increases, and the observed resistance factor decreases.

Table 14—Viscosities (μ_{zs}) and resistance factors (F_r) for HPAM solutions injected.

	1st core, 55 md			2nd core, 269 md			3rd core, 5,120 md		
Polymer	μ_{zs}, cp	Min. F_r	F_r at lowest rate	μ_{zs}, cp	Min. F_r	F_r at lowest rate	μ_{zs}, cp	Min. F_r	F_r at lowest rate
3230S (1st)	10.3	10.0	26	9.6	8.3	10.6	10.5	9.1	11.7
3330S	7.4	10.2	20.7	6.7	8.4	8.9	7.4	8.2	9.7
3430S	25.2	29.7	62.5	24.0	28.6	53.2	28.0	33.4	49.6
3530S	12.3	20.7	35.6	10.0	19.2	22.9	13.3	20.9	32.7
3630S	6.4	16.4	19.0	5.8	11.9	11.9	7.0	9.5	13.6
3830S	6.1	27.5	53.0	5.4	9.2	10.0	6.6	11.7	16.4
6030S	5.3	33.5	54.3	4.8	11.0	16.5	5.6	8.5	11.7
3230S (2nd)	10.3	13.9	22.3	9.6	10.2	11.8	10.3	10.1	13.6

Permeability Reduction within the Cores. In Figs. 41-48, a minimum resistance factor was often observed at intermediate flux values (for the HPAM solutions). Table 14 compares the low-shear viscosity (μ_{zs}) with the minimum resistance factor (F_r) (first and second data columns for 55 md; fourth and fifth data columns for 269 md; seventh and eighth data columns for 5,120 md). For the first injection of 3230S HPAM, the minimum F_r value was actually slightly less than the low-shear viscosity, indicating little or no permeability reduction in all three cores. For 3330S and 3430S, a modest permeability reduction was seen in all cores, with the minimum F_r value being 11-38% greater than μ_{zs}. For the higher Mw HPAMs (3530S, 3630S, 3830S, and 6030S), the minimum F_r value averaged twice the μ_{zs} value in the 269-md core and 55% greater than the μ_{zs} value in the 5,120-md core. In the 55-md core, the level of permeability reduction increased significantly as HPAM molecular weight increased, with the ratio of minimum F_r value to μ_{zs} rising from 1.68 for 3530S to 6.32 for 6030S. Interestingly, the level of permeability reduction dropped dramatically when the final 3230S HPAM was injected—to 1.35 in 55-md Berea, 1.06 in 269-md Berea, and 1 in 5,120 polyethylene. Obviously, the permeability reduction

was reversible to some extent. After the last polymer solution was injected (diutan, Fig. 49), over 100 PV of brine were forced through the core, and residual resistance factors (for Sections 2 and 3) were measured at 2.2 in the 55-md core, 1.4 in the 269-md core, and 1.0 in the 5,120-md core.

Flooding in a Longer Core

In the previous section, we noted an apparent shear-thinning behavior at low flux values, especially in the 55-md Berea core (see the solid circles in Figs. 40 and 41). Based on viscosity (versus shear rate) data, we expected to see Newtonian (flow-rate-independent) behavior at low flux values. For the particular case of xanthan injection into the 55-md core, we observed resistance factors (in the second core section) up to 30, whereas we expected a maximum value of about 8 from viscosity data (Fig. 40).

We were concerned that this apparent shear-thinning behavior in our short cores might be an experimental artifact (associated with microgels or very high Mw polymer species) that could not be expected to propagate deep into a real reservoir. To test this idea, we performed an experiment in a 57-md Berea sandstone core that was 122-cm long, with four equally spaced internal pressure taps—which created five 24.4-cm sections within the core. The core porosity was 17%, and the core cross-section was 15.24 cm^2. The permeabilities of the five core sections were 53 md, 64 md, 65 md, 74 md, and 41 md, respectively—giving a composite permeability of 57 md. Using our standard procedure, the core was saturated with filtered 2.52% TDS brine (2.3% NaCl + 0.22% $NaHCO_3$), and our polymer solution contained 600-ppm CP Kelco K9D236 xanthan in this same brine. The experiment was performed at 25ºC.

We injected 2.5 PV of xanthan solution at 5.17 ft/d flux. (One PV was 321 cm^3.) At that time, we varied the polymer injection rate over a wide range (0.005 to 5 ft/d). The resistance factor was measured at each rate in each of the five core sections. Values for the second through fifth core sections are plotted in Fig. 50: open triangles for the second core section (24-48 cm from the core inlet); open diamonds for the third core section (48-73 cm); open squares for the fourth core section (73-98 cm); open circles for the fifth core section (98-122 cm). (The first core section of this long core was treated as a filter.) Two other data sets are included for comparison in Fig 50. First, the solid circles plot resistance factors from the center 10.2-cm section of the short (14.4-cm) 55-md Berea core in Fig. 40 (with the data obtained after injecting 20 PV of xanthan solution). Second, the solid curve plots viscosity data (versus adjusted shear rate) for the xanthan solution that was injected into the 122-cm core.

For flux values above 0.1 ft/d, the various data sets in Fig. 50 converged. However, they diverged as flux decreased below 0.1 ft/d. At the lowest fluxes, the resistance factors approached the zero-shear viscosity value as the distance progressed into the core. This result supports our original suspicion that the unexpectedly high low-flux xanthan resistance factors may not practically propagate deep into a porous medium (i.e., a reservoir).

A few calculations can be performed to appreciate and quantify the degree to which the high low-flux xanthan resistance factors will propagate into 50-60-md Berea. Injecting 2.5 PV of polymer solution into the 122-cm core translates to injecting 3.1 PV through to the fourth pressure tap, 4.2 PV through to the third tap, 6.2 PV through to the second tap, and 12.5 PV through to the first pressure tap. If a xanthan bank was injected into a horizontal well to reach

500 ft into the formation, the behavior seen in Core Section 5 of Fig. 50 (open circles, essentially the viscosity behavior) would occur out beyond 160 ft from the well. The behavior seen in Core Section 4 (open squares of Fig. 50) would occur from 120 to 160 ft from the well. The behavior seen in Core Section 3 (open diamonds of Fig. 50) would occur from 80 to 120 ft; and the behavior seen in Core Section 2 (open triangles of Fig. 50) would occur from 40 to 80 ft.

For vertical wells, where flow is radial, the positions farthest from the wellbore and away from the most direct well-to-well streamlines would see the lowest flux values, but would also experience the lowest polymer throughput values. Consequently, the high xanthan resistance factors associated with the low-flux solid-circle data points in Figs. 40 and 50 are unlikely to provide a practical benefit (over simply the xanthan viscosity behavior) in displacing oil from a reservoir. Future work will address this same issue for HPAM (and possibly diutan) polymers.

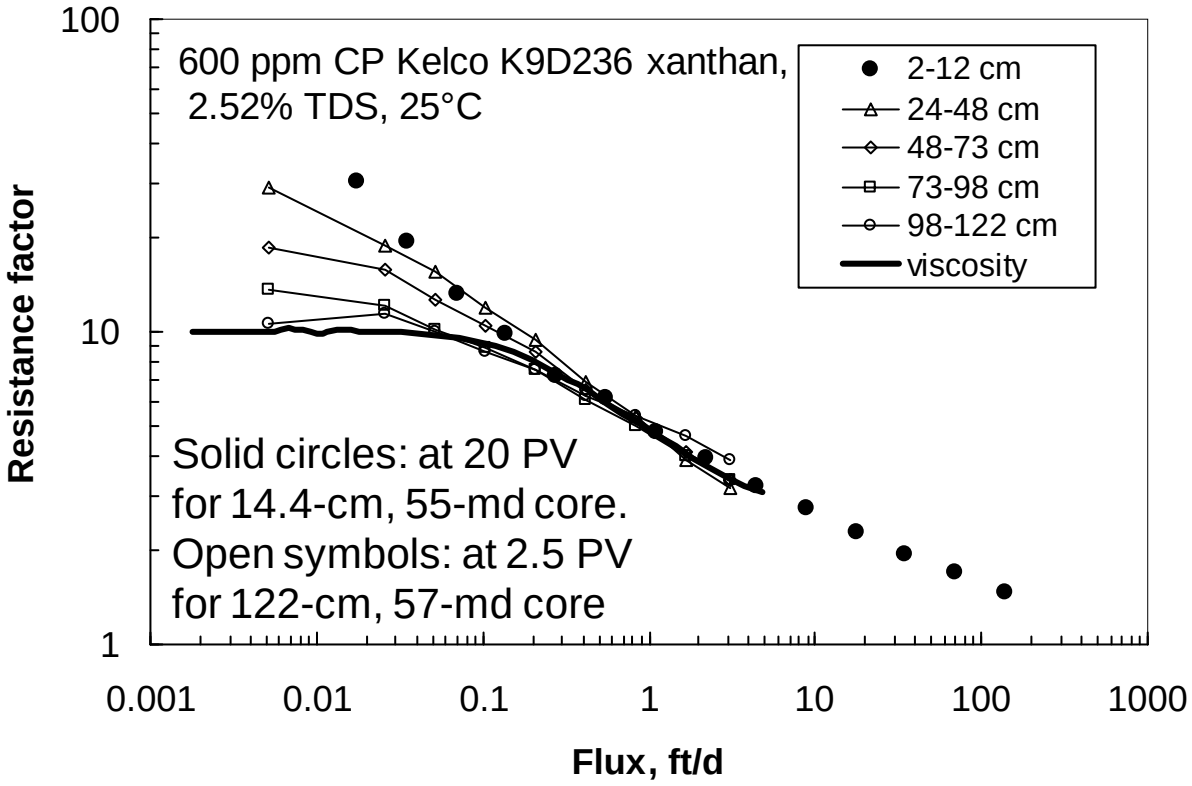

Fig. 50—Are high low-flux resistance factors able to propagate?

Effect of Mechanical Degradation

For the experiments reported to this point, the solutions were freshly prepared. In field applications, polymer solutions are likely to experience some level of mechanical degradation before penetrating deep into the reservoir. Most probably, the greatest level of mechanical degradation will occur as the polymer solutions first leave the wellbore and enter porous rock.[14,15,42,43] That is where the velocities are highest in the reservoir rock.[14] Our previous experience suggested that the high molecular weight species are responsible for HPAM causing permeability reductions and an unexpected shear thinning at low velocities in porous rock. These

species are especially susceptible to mechanical degradation.[38] To examine this issue further, we performed another set of experiments where HPAM solutions were first forced through a core at a high pressure gradient. Specifically, we forced the polymer solutions through a 13.3-cm long, 32-md Berea sandstone core using a pressure difference of 1,000 psi (2,292 psi/ft). This level of pressure gradient might be experienced by a polymer solution as it leaves a vertical wellbore to enter the formation rock. Table 15 lists the sequence and characteristics of the polymer solutions that were forced through the first core.

Table 15—Injection of polymer solutions at 2,292 psi/ft through a 32-md core.

Step	Polymer solution	PV injected	Flux, ft/d	F_{r1}	F_{r2}	F_{r3}
1	2500 ppm 3230S	41.6	12.5	35	45	34
2	1350 ppm 3330S	35.2	7.6	50	71	61
3	2900 ppm 3430S	30.1	3.8	97	141	132
4	1700 ppm 3530S	24.1	3.7	101	152	146
5	970 ppm 3630S	27.7	5.3	73	103	97
6	900 ppm 3830S	27.1	5.6	74	97	94
7	700 ppm 6030S	25.3	4.4	74	120	131
8	2500 ppm 3230S	45.2	11.6	30	46	48

The effluent from this core was re-injected into a second Berea core using a wide range of flux values to determine resistance versus flux for the mechanical degraded polymer solutions. This process imitates what happens to a polymer solution as it flows radially away from a wellbore. The second core (13.9 cm total length, 38-md composite permeability) had three sections with pressure taps located 2.2 cm from the inlet sand face and 1.9 cm from the outlet sand face. The second core section was 9.8 cm long and had a permeability of 46 md. The third core section (1.9 cm long) had a permeability of 17.5 md. (The first 2.2-cm core section, with a permeability of 48 md, was treated as a filter for the core.)

Fig. 51 plots resistance factor versus flux for the second (46-md) core section (solid circles) and for the third (17.5-md) core section (solid triangles) for the degraded SNF 3230S HPAM. The open symbols in Fig. 51 plot resistance factors for undegraded (fresh) polymer solutions from 55-md, 269-md, and 5,120-md cores (from Fig. 41). Fig. 52 plots the same resistance factors on the y-axis, but the x-axis plots the capillary-bundle parameter, $u(1-\phi)/(\phi k)^{0.5}$. The different curves in Fig. 52 correlated quite well using this parameter. The onset of shear-thickening or pseudodilatant behavior occurred at about the same x-axis value for all five cases. At low flux values, resistance factors for four of the five curves leveled out (i.e., approached Newtonian behavior) at a value consistent with the viscosity of the SNF 3230S polymer solution (10 cp). For the exception, fresh polymer injected into a 55-md core (open circles in Figs. 51 and 52), resistance factors increased from 10 to 26 as flux decreased from 1.1 to 0.035 ft/d. We suspect that this behavior was an artifact associated with high Mw polymer species that became trapped in the 55-md core. When the experiment was repeated with mechanically degraded SNF 3230S polymer in the 46-md and 17.5-md Berea core segments (solid symbols in Figs. 51 and 52), Newtonian behavior was seen at low flux values. This result confirms that mechanically degraded polymer did not contain the components that caused the apparent shear-thinning in the 55-md core.

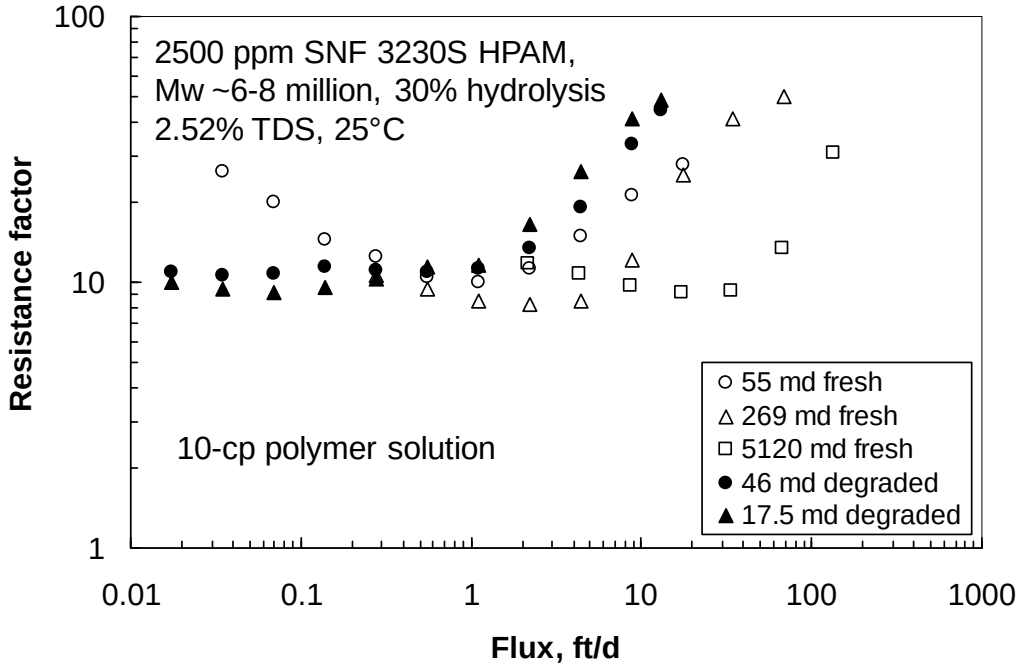

Fig. 51—Effect of mechanical degradation on SNF 3230S.

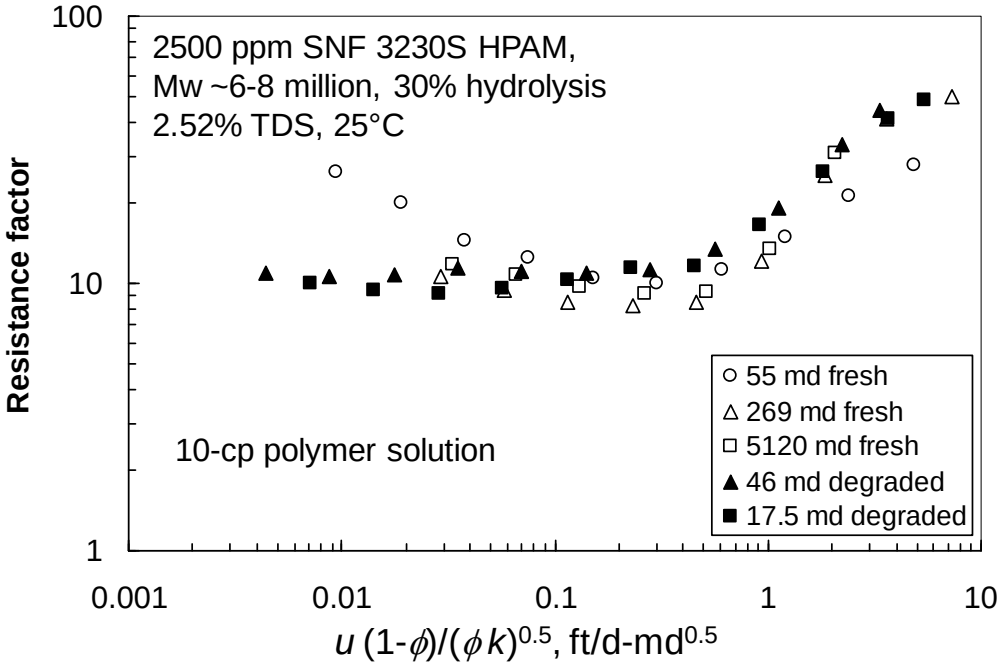

Fig. 52—Effect of mechanical degradation on SNF 3230S: capillary bundle correlation.

After the experiment with the mechanically degraded SNF 3230S, we successively performed similar tests with the other mechanically degraded polymers in the same core, using the sequence indicated by Table 15. For these polymers, Figs. 53-59 provide plots analogous to Fig. 52. Fig.

53 shows the results for SNF 3330S. Although the degraded SNF 3230S (6-8 million Mw as fresh polymer) propagated effectively through 46-md and 17.5-md Berea (Fig. 52), degraded SNF 3330S (8-10 million Mw as fresh polymer) exhibited high resistance factors (solid symbols in Fig. 53)—implying poor propagation. One might expect resistance factors for the degraded polymer in 46-md Berea (solid triangles in Fig. 53) would not be much greater than for the fresh polymer in 55-md Berea (open circles). Oddly, this expectation was not met. No explanation is evident. This high level for the resistance factors in the second and third core segments remained throughout the subsequent polymer injections (Figs. 54-59), thus clouding more detailed interpretation of the results. Nonetheless, the figures consistently show a defined shear-thickening behavior at moderate to high flux values and more or less Newtonian behavior at low flux values. The experiments associated with Figs. 53-59 may need to be repeated.

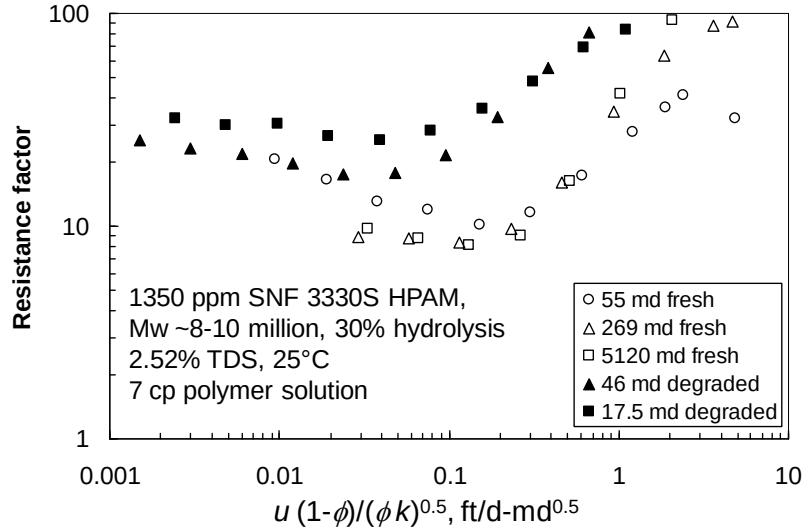

Fig. 53—Effect of mechanical degradation on SNF 3330S: capillary bundle correlation.

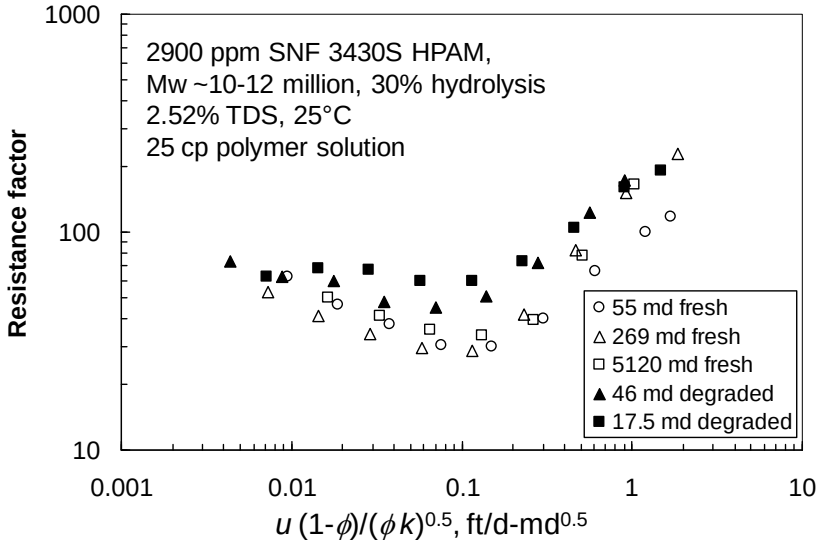

Fig. 54—Effect of mechanical degradation on SNF 3430S: capillary bundle correlation.

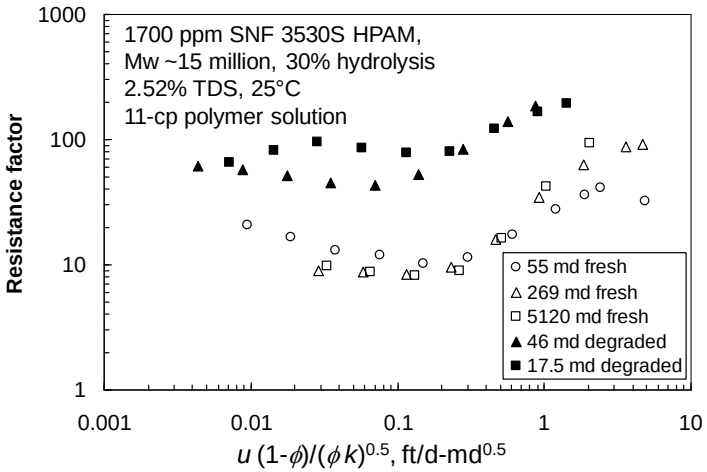

Fig. 55—Effect of mechanical degradation on SNF 3530S: capillary bundle correlation.

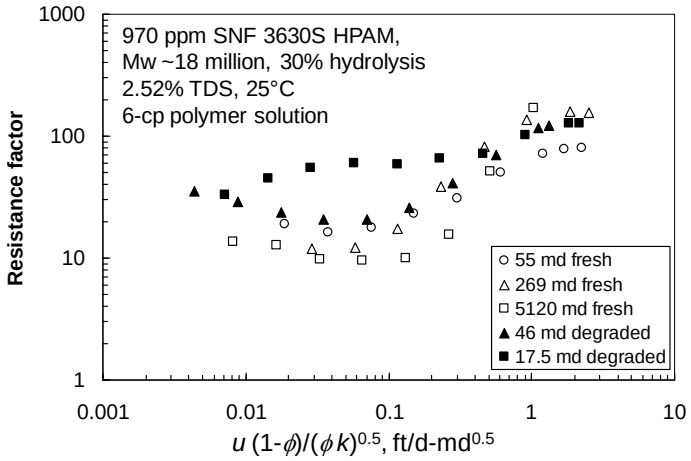

Fig. 56—Effect of mechanical degradation on SNF 3630S: capillary bundle correlation.

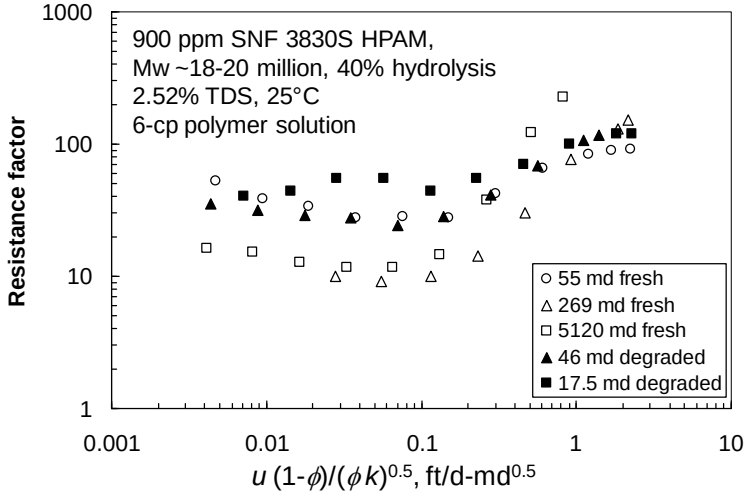

Fig. 57—Effect of mechanical degradation on SNF 3830S: capillary bundle correlation.

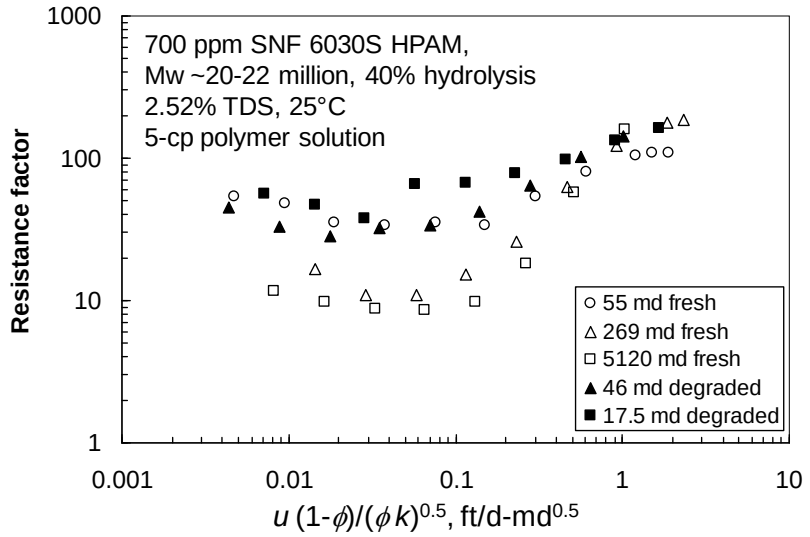

Fig. 58—Effect of mechanical degradation on SNF 6030S: capillary bundle correlation.

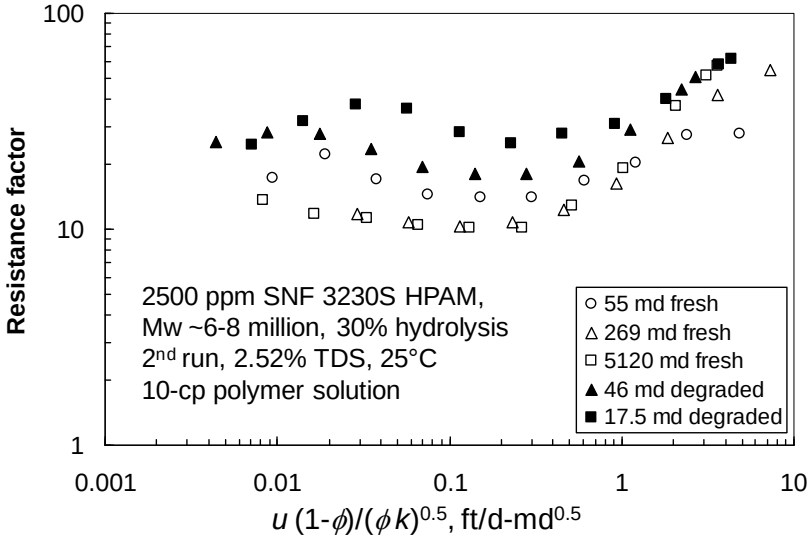

Fig. 59—Effect of mechanical degradation on SNF 3230S: last run.

Conclusions

1. We characterized the performance in 55-md, 269-md, and 5,120-md cores for nine commercially available EOR polymers, including one xanthan, one diutan, and seven partially hydrolyzed polyacrylamides (HPAM). None of the polymers exhibited severe face-plugging in any of the cores.
2. In cores with permeabilities from 55 to 5,120-md, xanthan and HPAM solution rheology in porous media correlated very well using the parameter: $u(1-\phi)/(\phi k)^{0.5}$, where u is flux, ϕ is porosity, and k is permeability. The onset of pseudodilatant (viscoelastic) resistance factors correlated closely with the transition from Newtonian to shear-thinning viscosity behavior.
3. At low flux values in a 14.4-cm-long, 55-md Berea sandstone core, both xanthan and HPAM can exhibit resistance factors that are much higher than expected and an apparent shear-

thinning behavior that deviates from expectations based on viscosity-versus-shear-rate data. Using xanthan injection into a 122-cm-long, 57-md Berea sandstone core, we showed that this behavior was an experimental artifact that is not expected to materialize and benefit oil recovery in field applications. We believe that the shear-thinning effect was also an experimental artifact for HPAM. In particular, for SNF 3230S HPAM, we showed that mechanically degraded polymer (resulting from flow through a core at 2,292 psi/ft pressure gradient), exhibited Newtonian behavior at low flux values in 46-md and 17.5-md Berea sandstone. Future tests will further examine this issue for HPAM solutions.

5. INJECTIVITY

Horizontal versus Vertical Wells. A key issue in any reservoir flooding process is whether fluid injectivity (injection rate divided by pressure drawdown) and oil productivity (production rate divided by pressure drawdown) will be sufficiently high to allow the oil to be produced at an economic rate. Injectivity and productivity are of particular concern in reservoirs with viscous oils, since production rate will be approximately inversely proportional to oil viscosity. Similarly, injectivity will be approximately inversely proportional to polymer solution viscosity during a polymer flood.

Horizontal wells provide an effective method to substantially improve injectivity/productivity over those associated with vertical wells. Eq. 5 (from Taber and Seright[12]) provides a means to estimate the injectivity for a horizontal well relative to a vertical well (in a 5-spot pattern).

$$q_{HW}/q_5 = \{\pi L / [\pi L + 4.6\, h\, log_{10}[h/(2r_w)]]\}\{2.93[log_{10}(W/r_w) - 0.42]\} \quad (5)$$

In this equation, L is the distance between parallel horizontal injection and production wells, W is the length of the horizontal wells, h is formation height, and r_w is wellbore radius (all in units of feet). In one viscous oil reservoir on the North Slope, L is about 1,250 ft, h is 77 ft, and W is about 6,000 ft. For these values (and a wellbore radius of 0.276 ft or 6 $^5/_8$" diameter), a horizontal well would provide 9.6 times the injectivity/productivity of a vertical well. (Both horizontal and vertical wells exist in North Slope viscous oil reservoirs.)

Polymer Throughputs, Velocities, and Injectivities. Horizontal wells generally have a substantially greater wellbore area open to flow than vertical wells. For a North Slope horizontal well with length of 6,000 ft and wellbore radius of 0.276 ft, the wellbore area is 10,400 ft^2. For comparison, for a North Slope vertical injector with radius of 0.328 ft (7 $^7/_8$" diameter) through 77 ft of pay, the wellbore area is 159 ft^2, or 65 times less than that of the horizontal well. Consequently, for a given injection volume, the throughput (cm^3 of injected volume per cm^2 of wellbore area) is 65 times less for a vertical well than a horizontal well. Thus, particulate matter in injected water or polymer solutions is 65 times more likely to plug a vertical well than a horizontal well (assuming that fractures do not open during the course of injection).

Because of the larger wellbore area, fluid velocities (fluxes) upon entering a formation from a horizontal well are much smaller than for a vertical well. For a vertical well injecting 300 BWPD (r_w=0.328 ft, h=77 ft), the flux as the fluid enters the formation is about 10 ft^3/ft^2/d (ft/d). For a horizontal well injecting 400 BWPD (r_w=0.276 ft, L=6,000 ft), the flux as the fluid enters the formation is 0.2 ft/d. As the fluid travels radially away from the well (for either horizontal or vertical wells), flux decreases. Deep within our target North Slope reservoirs (h=77 ft), flux is around 0.005 ft/d.

A flux of 10 ft/d is in the region of viscoelastic behavior for most of the HPAM polymers (Figs. 41-48) in 55-md or 269-md Berea sandstone. This viscoelastic behavior (and the associated high resistance factors at 10 ft/d) could lead to significantly reduced HPAM injectivity in vertical injection wells.[16] In contrast, in a horizontal well where the near-wellbore flux is 0.2 ft/d, HPAM

rheology is more or less Newtonian (Figs. 41-48), and injectivity reductions should occur in proportion to those expected for a Newtonian (flow-rate-independent) fluid.

The pseudoplastic (shear-thinning) xanthan and diutan solutions (Figs. 40 and 49) have an injectivity advantage over HPAM solutions in unfractured vertical wells. At 10 ft/d, they exhibit a relatively low resistance factor (and therefore relatively high injectivity), and resistance factors increase as the flux decreases and the polymer penetrates deeper into the formation. For horizontal wells, this advantage is diminished considerably.

Using the methods described by Seright *et al*.,[16] we estimated injectivities (relative to water) for the various polymer solutions described in Figs. 40-49. For the vertical injection well, the assumed conditions were: pressure drop from the wellbore to the external drainage radius was 1,025 psi, wellbore radius was 0.328 ft, formation height was 77 ft, and formation permeability was 100 md. For the horizontal injection well, the assumed conditions were: pressure drop from the wellbore to the external drainage radius was 725 psi, wellbore radius was 0.328 ft, formation height was 77 ft, formation permeability was 100 md, and well length was 6,000 ft. For both types of wells, polymer resistance factor behavior was taken from Figs. 40-49.

Table 16—Predicted polymer injectivities (relative to water).

Polymer	Vertical Well	Horizontal Well
600 ppm CP Kelco K9D236 xanthan	0.335	0.108
2500 ppm SNF 3230S HPAM	0.080	0.143
1350 ppm SNF 3330S HPAM	0.053	0.143
2900 ppm SNF 3430S HPAM	0.024	0.044
1700 ppm SNF 3530S HPAM	0.022	0.065
970 ppm SNF 3630S HPAM	0.030	0.129
900 ppm SNF 3830S HPAM	0.026	0.129
700 ppm SNF 6030S HPAM	0.026	0.143
200 ppm CP Kelco EX9570 diutan	0.335	0.108

Table 16 indicates that polymer solution injectivities (relative to water in our target North Slope wells) should typically be 2-8% for HPAM solutions in unfractured vertical wells, 33% for xanthan solutions in unfractured vertical wells, and 10-15% for most of our polymer solutions in unfractured horizontal wells.

Interestingly, our calculations indicate that flux values could typically be 0.01 ft/d or less deep within our target North Slope viscous oil reservoirs. These velocities are sufficiently low that we should further study and clarify polymer solution rheology in porous media at these low rates.

Injectivity after Water Breakthrough. If water is injected to displace viscous oil from a reservoir, it may quickly finger or channel through to a nearby injection well. Craig (1971) reported a relation between injectivity at water breakthrough (i_{wbt}), injectivity for a unit mobility displacement (i), areal sweep efficiency at water breakthrough (E_{Abt}), and mobility ratio (M).

$$i_{wbt} = i\, E_{Abt}\, M \quad (6)$$

Fig. 60 plots i_{wbt}/i as a function of E_{Abt} and M. For viscous oil reservoirs, this plot suggests that injectivity should be considerably higher after water breakthrough than before breakthrough. This fact may impact the decision for when a polymer flood should be implemented.

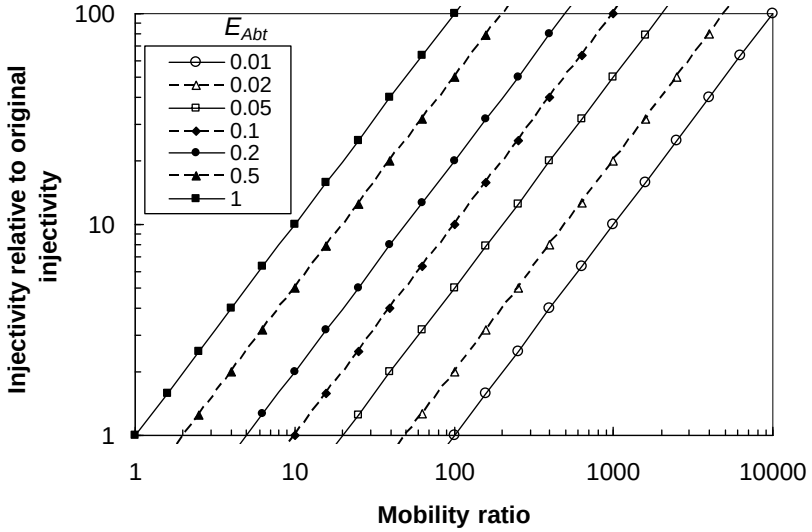

Fig. 60—Injectivity improvement upon breakthrough.

Effect of Fractures. Of course, great care must be exercised if injection occurs above the formation parting pressure. If the fractures are oriented improperly, they can cause severe channeling. If they extend out of zone, injected fluids may be lost and ineffective in displacing oil. However, if fractures are placed and oriented properly, they can improve injectivity, productivity, and sweep efficiency, especially for vertical wells.[15] Eq. 7 (from Taber and Seright[12]) estimates injectivity for linear flow (e.g., between parallel vertical fractures) relative to radial flow in a five-spot pattern.

$$q_L/q_5 = 2.93[log_{10}(W/r_w) - 0.42] \quad \ldots\ldots (7)$$

For the North Slope parameters discussed above, injectivity for linear flow would be 11.3 times greater than for the unfractured vertical well.

In contrast for a horizontal well, a single vertical fracture will not improve injectivity as much. For a vertical fracture that follows the length of a horizontal well, the improvement in injectivity is given by Eq. 8 (from Taber and Seright[12]).

$$q_L/q_{HW} = [\pi L + 4.6\ h\ log_{10}[h/(2r_w)]]/\pi L \quad \ldots\ldots (8)$$

For the North Slope parameters discussed above, injectivity for the parallel fractures would be only 1.19 times greater than for the unfractured horizontal well.

Relative to a single vertical fracture with a single orientation, in concept, injectivity could be enhanced by having two or more fractures emanating from the injector in different directions. Of

course, the danger with this approach is that fractures could extend most or all of the way between an injector-producer pair and cause severe channeling. We also recognize that the in situ stresses within the reservoir dictate fracture orientation, and a desirable arrangement of fractures may not be achievable. Nevertheless, part of our future work will consider injectivity enhancements from more than one fracture intersecting vertical and horizontal wells.

Conclusions

1. In one North Slope viscous oil reservoir, horizontal wells were calculated to provide injectivities and productivities that are 9-10 times those expected for vertical wells. Particulate matter in injected water or polymer solutions was 65 times more likely to plug a vertical well than a horizontal well (assuming that fractures do not open during the course of injection).
2. The viscoelastic behavior of HPAM polymers could lead to significantly reduced injectivity in unfractured vertical North Slope injection wells (2-8% that of water for the HPAM solutions investigated in this report). In contrast, in North Slope unfractured horizontal wells, injectivity reductions should be significantly less severe (with polymer injectivity 10-15% that of water for most of our cases).
3. The pseudoplastic (shear-thinning) xanthan and diutan solutions have an injectivity advantage over HPAM solutions in unfractured vertical wells, with estimated injectivity values around one-third that of water for the solutions that we examined. For horizontal wells, this advantage is diminished considerably.
4. For a horizontal well with a vertical fracture that perfectly follows the well and extends to the full formation height (i.e., true linear flow), water injectivity was estimated to be about 19% greater than for an unfractured horizontal injection well.
5. Flux values could typically be 0.01 ft/d or less deep within our target North Slope viscous oil reservoirs. These velocities are sufficiently low that we should further study and clarify polymer solution rheology in porous media at these low rates.

6. EVALUATION OF POLYMER MIXTURES FOR MOBILITY CONTROL

An important objective of our research project is to identify the most cost-effective polymers for use in our potential applications. To achieve this goal, improvements may be needed for conventional EOR polymers (HPAM and xanthan). We were aware that xanthan and guar gum could show a synergistic viscosity enhancement when mixed in a specific proportion. Although guar typically contains too much plugging debris to be useful for enhanced oil recovery, we wondered whether other polymer mixtures might show synergistic viscosity enhancements.

Polymers Examined

With the aim of joining the characteristic properties and advantages of synthetic polymers and biopolymers, a study was started using mixed solutions of the following commercial products: SNF Flopaam 3830S HPAM, CP Kelco XC HV xanthan, CP Kelco EX9570 diutan and alginic acid sodium salt (high viscosity; MP Biomedicals, LLC). Fig. 61 shows the chemical structures of the different polymers.

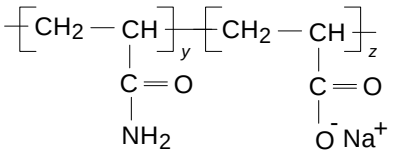

(a)

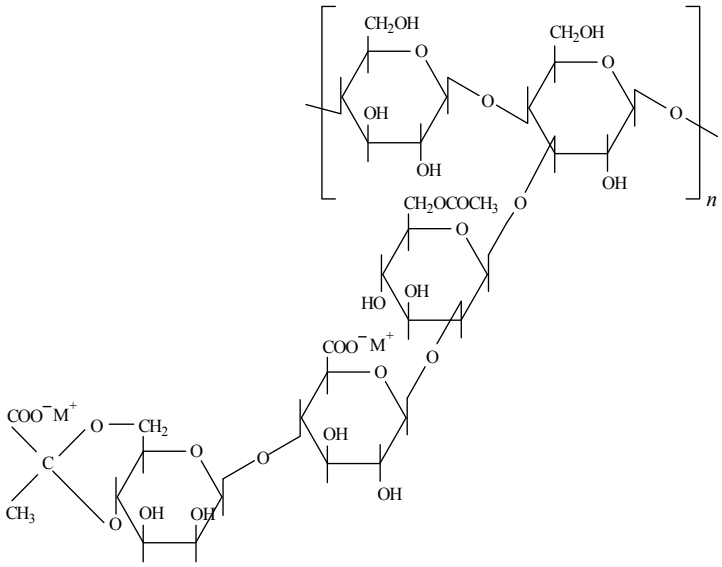

(b)

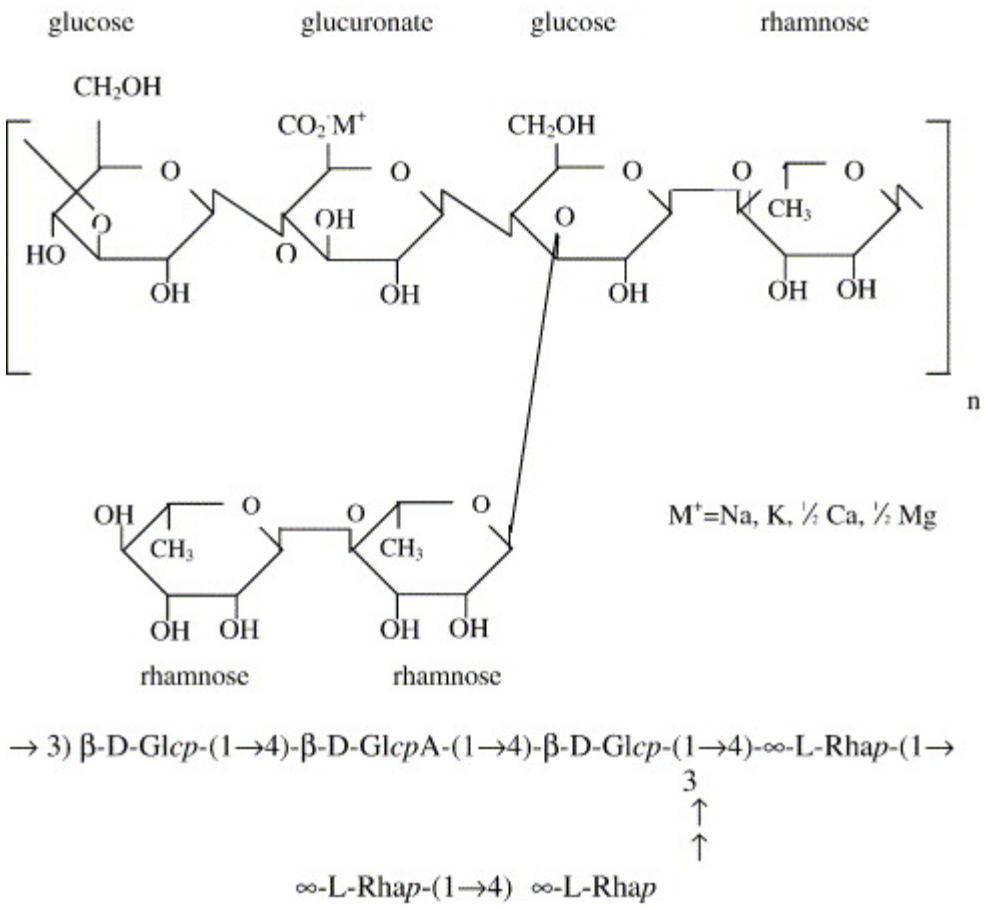

(c)

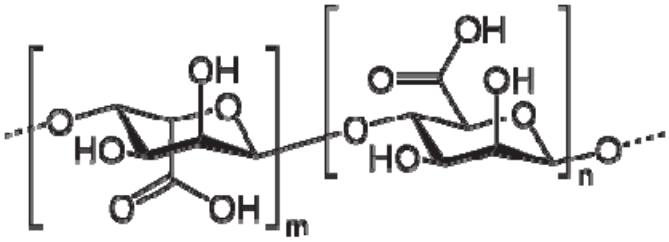

(d)

Fig. 61—Chemical structure of: (a) HPAM, (b) xanthan, (c) diutan, and (d) alginic acid.

The following binary mixtures were studied: HPAM/xanthan, HPAM/diutan, and HPAM/alginate (alginic acid sodium salt). All the mixed systems were evaluated in distilled water and brine. The polyacrylamide (HPAM) was dissolved overnight using a magnetic stirrer, while the biopolymers were dissolved in a blender (at medium speed) for 8 minutes. Stock solutions containing 2,000-ppm polymer were prepared first. Solutions with lower concentrations were prepared by dilution and mixing various weights of the stock solutions. Viscosities were measured at 25°C using a Physica MCR301 (Anton Paar) rheometer.

Brines

Three brines were used to evaluate the effect of ionic strength on viscosity of the polymers: (a) Brine 1: 2.3% NaCl, 0.22% $NaHCO_3$; 2.52% TDS (total dissolved solids); ionic strength 0.42. (b) Brine 2: 6.9% NaCl, 0.22% $NaHCO_3$; 7.12% TDS; ionic strength 1.21. (c) Brine 3: 5.8% NaCl, 0.8% $CaCl_2$; 6.6% TDS; ionic strength 1.21.

HPAM/Xanthan

Viscosity versus Concentration. Fig. 62 shows viscosity results for the HPAM in distilled water and in the three different brines. Basically, the same viscosity was observed in Brines 1 and 2, even though the ionic strength of Brine 2 was three times that of Brine 1. In the presence of $CaCl_2$ (i.e., Brine 3), the viscosity provided by HPAM was lower even though the ionic strength of Brine 3 was the same as Brine 2. The slopes of the log-log curves in Fig. 62 were 1.5 for Brines 1 and 2 and 1.2 for Brine 3. Relative to what happens in brines with only monovalent cations, HPAM hydrodynamic volume (and therefore viscosity) is reduced by intramolecular interactions that are accentuated in the presence of calcium. The flexible nature of the HPAM coil allows a greater degree of collapse for the polymer when divalent cations are present.

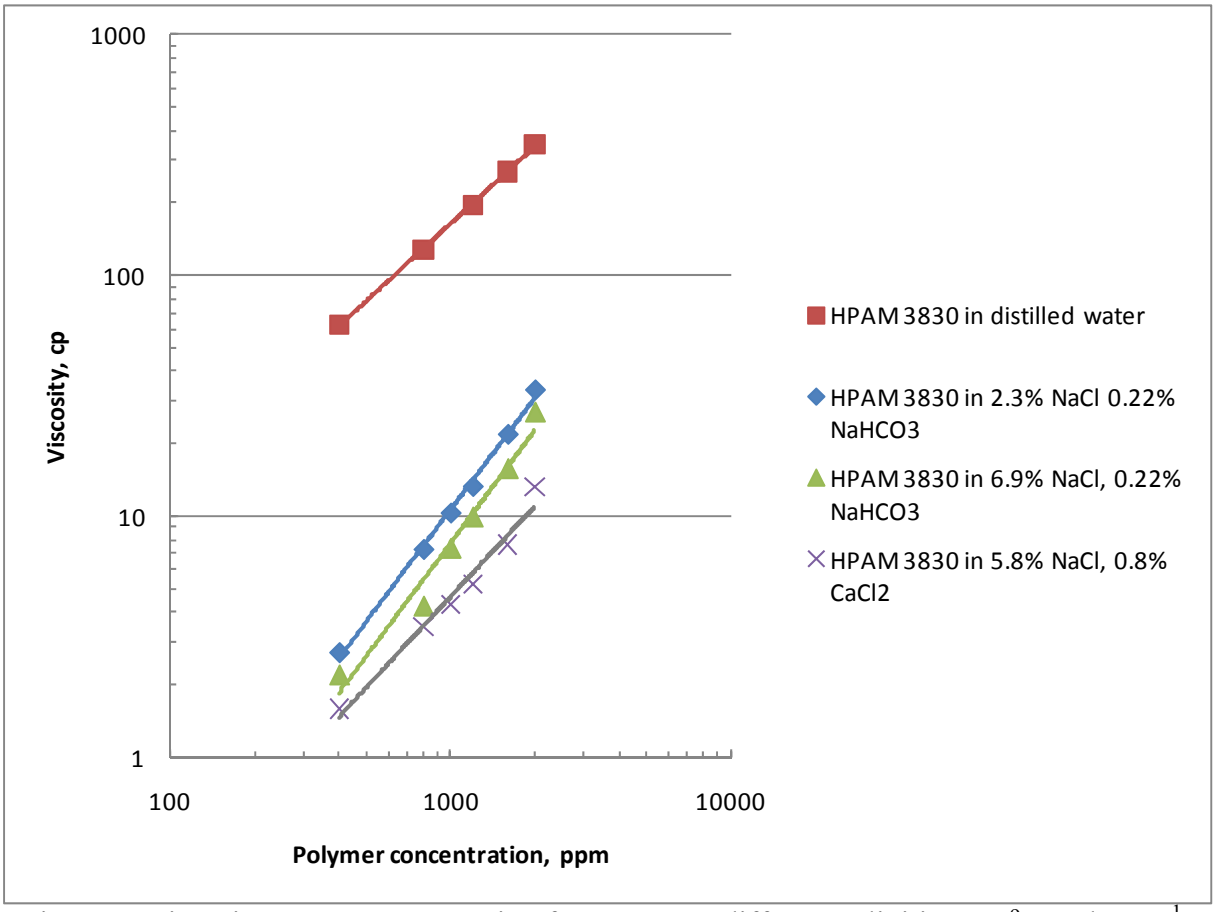

Fig. 62—Viscosity versus concentration for HPAM at different salinities. 25 ^{o}C and 7.3 s^{-1}.

When performing the same analysis with xanthan (CP Kelco XC HV, Fig. 63), xanthan shows the highest viscosity in distilled water. Xanthan viscosity in brines is lower than in distilled

water, but the viscosity reduction is much less dramatic than seen for HPAM (Fig. 62). Consistent with Chapter 3, xanthan viscosity behavior was virtually identical in the three brines (Fig. 63).

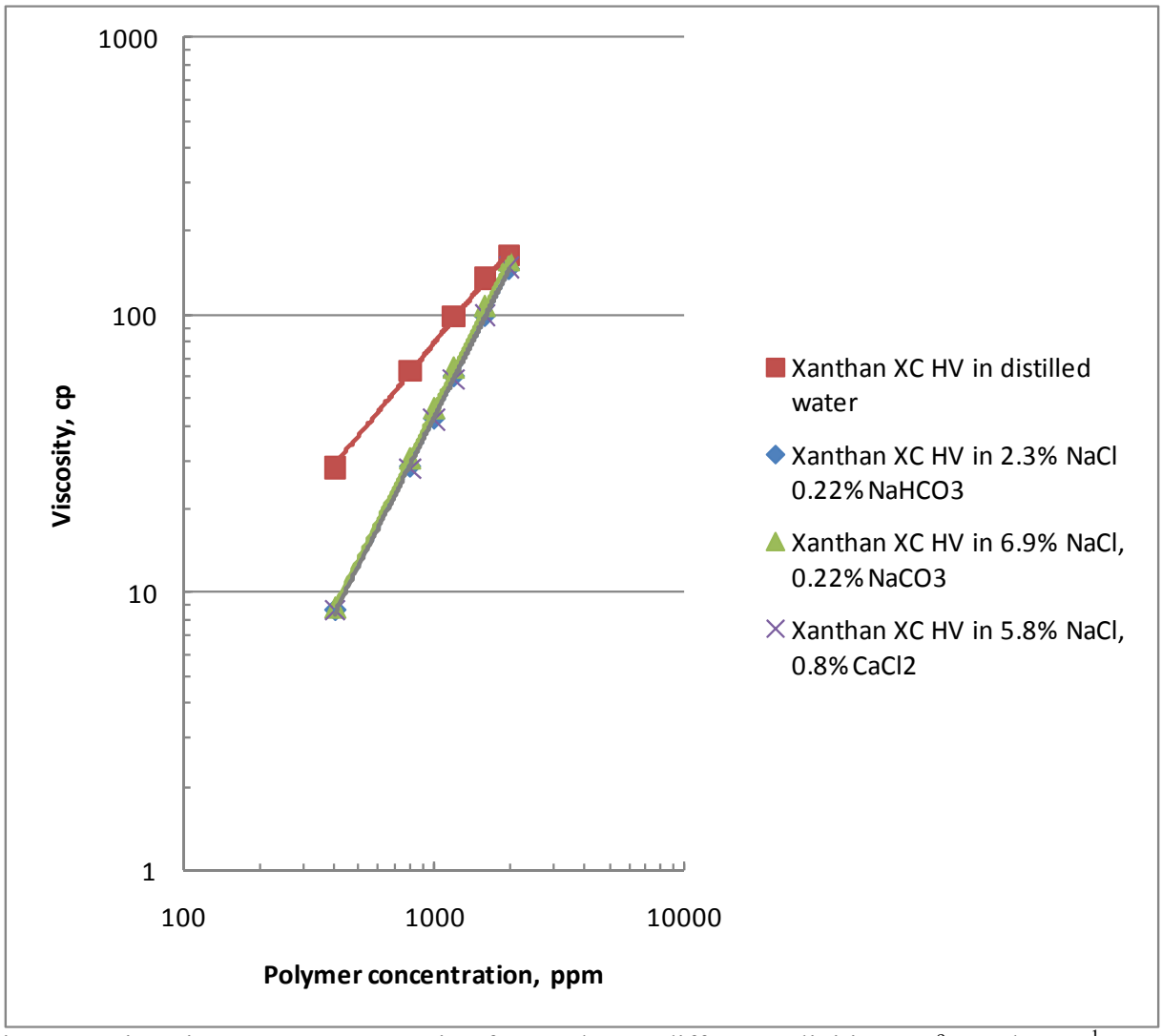

Fig. 63—Viscosity versus concentration for xanthan at different salinities. 25 °C and 7.3 s^{-1}.

For each curve of log(viscosity) versus log(concentration), a regression was performed using Eq. 4.

$$\mu = A\, C^{B} \quad \text{.....(4)}$$

Table 17 lists *A* and *B* parameters for various HPAM/xanthan mixtures. In distilled water, the *B* exponent was about 1.1 for all mixtures and pure polymers. In contrast, for the brines, the *B* exponent was 1.7 to 1.8 for all but the highest HPAM/xanthan ratios. In distilled water, both HPAM and xanthan are ionized, with negative charges distributed along the backbone. These charges enhance the solubility of polymers in water and expand the polymers to the maximum configuration due to electrostatic repulsion. Consequently, in the dilute or semi-dilute regimes,

the solution's dependence on polymer concentration is similar to that for an ideal solution, and the *B* exponent is close to 1. In brine, the charges are screened, and intramolecular and intermolecular attractions are increased. Therefore, the *B* exponent assumes higher values. The *B* exponents are greater for xanthan in brine than for HPAM in brine because xanthan's rod-like conformation more effectively promotes intermolecular interactions with increased polymer concentration.

Note in Table 17 that many polymer mixtures in brine show viscosity behavior that is virtually the same as for solutions with only xanthan. For example, in brine with 2.3% NaCl and 0.22% $NaHCO_3$, the mixture with 60% HPAM/40% xanthan has almost the same concentration parameters (and therefore the same viscosity behavior) as 100% xanthan (A=2x10^{-4}, B=1.70 versus 1.76). Since xanthan is considerably more expensive than HPAM, this observation suggests a significant economic value in using polymer mixtures instead of a single polymer.

Apparently, xanthan has an important role in expanding the HPAM backbone in the presence of brine. Considering that viscosity is directly proportional to the hydrodynamic volume of the polymer in solution, the presence of xanthan in a rod-like helix conformation contributes to a partial disentanglement of HPAM molecules.

Table 17—Concentration parameters for HPAM–xanthan mixtures.

Fraction of HPAM in polymer mixture	distilled water		2.3% NaCl, 0.22% $NaHCO_3$		6.9% NaCl, 0.22% $NaHCO_3$		5.8% NaCl, 0.8% $CaCl_2$	
	A	*B*	*A*	*B*	*A*	*B*	*A*	*B*
0.0 (100% xanthan)	4 x 10^{-2}	1.10	2 x 10^{-4}	1.76	2 x 10^{-4}	1.79	2 x 10^{-4}	1.77
0.2	5 x 10^{-2}	1.10	1 x 10^{-4}	1.80	2 x 10^{-4}	1.75	2 x 10^{-4}	1.76
0.4	5 x 10^{-2}	1.11	1 x 10^{-4}	1.76	1 x 10^{-4}	1.79	2 x 10^{-4}	1.71
0.5	5 x 10^{-2}	1.11	1 x 10^{-4}	1.74	2 x 10^{-4}	1.72	1 x 10^{-4}	1.73
0.6	7 x 10^{-2}	1.09	2 x 10^{-4}	1.70	9 x 10^{-5}	1.77	1 x 10^{-4}	1.71
0.8	8 x 10^{-2}	1.09	2 x 10^{-4}	1.64	2 x 10^{-4}	1.58	1 x 10^{-4}	1.62
1.0 (100% HPAM)	1 x 10^{-1}	1.07	3 x 10^{-4}	1.54	2 x 10^{-4}	1.56	8 x 10^{-4}	1.25

The main goal in investigating mixtures of HPAM and various biopolymers (especially xanthan) is to identify conditions where a mixture might be more cost-effective than HPAM alone. To achieve this goal, the polymer components in the mixture must be compatible, i.e., mix to form a single phase with no suspended material that would plug porous media. All mixtures investigated in this chapter met this requirement. A second requirement is that the cost-effectiveness of the mixture must be at least as attractive as that for a solution that contains only HPAM. Table 18 makes this determination for HPAM/xanthan mixtures to achieve 10 cp. The first column lists the fraction of the polymer in the mixture that is HPAM (the remainder is xanthan). Cases with four water salinities are included in the table. For each salinity listing, the first column gives the concentration of polymer (i.e., the sum of HPAM and xanthan concentrations, in parts per

million) required to achieve 10 cp. The second column within each salinity listing gives the maximum cost of xanthan (relative to the cost of SNF Flopaam 3830S HPAM) that allows the cost of the polymer mixture to match the cost of a 10-cp 3830S HPAM solution. For example, for a mixture with 60% HPAM/40% xanthan (581-ppm total polymer) in the second solvent (2.52% TDS), xanthan must cost no more than 2.22 times the cost of 3830S HPAM in order not to exceed the cost of a solution with 865-ppm 3830S HPAM in the same brine.

Tables 19 and 20 provide analogous information for achieving 50 cp and 100 cp, respectively. Xanthan is expected to cost 2-4 times more (per kg) than HPAM. Examination of Tables 18-20 reveals that xanthan would have to cost 50% less than 3830S HPAM to become feasible for use in distilled water (or in water with low salinity). Thus, as expected, HPAM alone is preferred for low-salinity applications. In contrast, for the high-salinity, high-hardness brine (5.8% NaCl, 0.8% $CaCl_2$), xanthan would be competitive if it cost 3.76 to 8.59 times the cost of 3830S HPAM (last columns of Tables 18-20), depending on the desired viscosity level. Thus, xanthan alone or a HPAM/xanthan mixture might be preferred in this brine.

Close examination of Tables 18-20 reveals certain compositions where a degree of synergy occurs between the polymers, and the concentration needed to achieve a given viscosity is less than expected. For example in Table 18 for the mixture with 60% HPAM in the brine with 2.3% NaCl, 0.22% $NaHCO_3$, only 581-ppm polymer was needed to achieve 10 cp, whereas more than 700 ppm was expected based on the trend in the remainder of the column. These anomalies will be investigated during our future work to identify the most beneficial compositions.

Table 18—Achieving 10 cp using HPAM/xanthan mixtures.
ppm lists the total (mixture) polymer concentration required to achieve 10 cp.
$X/H lists xanthan cost (relative to SNF 3830S HPAM) required to match the cost-effectiveness ($/cp) when only SNF 3830S HPAM is used (as given by the last row of the table).

Fraction of HPAM in polymer mixture	distilled water		2.3% NaCl, 0.22% $NaHCO_3$		6.9% NaCl, 0.22% $NaHCO_3$		5.8% NaCl, 0.8% $CaCl_2$	
	ppm	$X/H	ppm	$X/H	ppm	$X/H	ppm	$X/H
0.0 (100% xanthan)	151	0.49	468	1.85	422	2.44	452	4.20
0.2	124	0.50	600	1.55	484	2.40	468	4.81
0.4	118	0.38	693	1.41	621	2.09	560	4.98
0.5	118	0.25	747	1.31	540	2.81	777	3.88
0.6	95	0.45	581	2.22	709	2.13	839	4.14
0.8	84	0.41	733	1.90	942	1.46	1220	3.76
1.0 (100% HPAM)	74	--	865	--	1028	--	1895	--

In these tables, the brine that is most characteristic of North Slope brines contains 2.3% NaCl and 0.22% $NaHCO_3$. For this brine, the required xanthan cost ranges from 1.31 to 2.78 times the cost of 3830S HPAM. For xanthan only (i.e., no HPAM in the polymer mixture), xanthan must cost no more than 1.85 to 2.23 times the cost of 3830S HPAM. This range of price might be difficult for xanthan suppliers to achieve. However, before becoming too pessimistic about

xanthan's potential on the North Slope, the permeability dependence of HPAM performance may need to be considered. Flopaam 3830S has a high molecular weight (18-20 million daltons), and as such, experiences some difficulty when propagating through low-permeability rock (e.g., 50 md). A lower molecular weight HPAM, such as Flopaam 3530 (Mw ~15 million daltons) or Flopaam 3230S (Mw ~6-8 million daltons) may be needed. These lower Mw polymers cost roughly the same as 3830S but more polymer is needed to provide a given viscosity. Since xanthan can readily penetrate into the low-permeability rock, its cost-effectiveness improves relative to the lower Mw HPAMs.

Table 19—Achieving 50 cp using HPAM/xanthan mixtures.
ppm lists the total (mixture) polymer concentration required to achieve 50 cp.
$X/H lists xanthan cost (relative to SNF 3830S HPAM) required to match the cost-effectiveness ($/cp) when only SNF 3830S HPAM is used (as given by the last row of the table).

Fraction of HPAM in polymer mixture	distilled water		2.3% NaCl, 0.22% $NaHCO_3$		6.9% NaCl, 0.22% $NaHCO_3$		5.8% NaCl, 0.8% $CaCl_2$	
	ppm	$X/H	ppm	$X/H	ppm	$X/H	ppm	$X/H
0.0 (100% xanthan)	654	0.51	1167	2.11	1037	2.78	1121	6.12
0.2	534	0.53	1466	1.85	1215	2.72	1167	7.11
0.4	504	0.43	1730	1.70	1527	2.48	1434	7.31
0.5	504	0.32	1885	1.61	1375	3.20	1969	5.97
0.6	415	0.50	1497	2.61	1760	2.60	2151	6.48
0.8	367	0.53	1956	2.29	2609	1.53	3295	6.42
1.0 (100% HPAM)	333	--	2459	--	2885	--	6866	--

Table 20—Achieving 100 cp using HPAM/xanthan mixtures.
ppm lists the total (mixture) polymer concentration required to achieve 100 cp.
$X/H lists xanthan cost (relative to SNF 3830S HPAM) required to match the cost-effectiveness ($/cp) when only SNF 3830S HPAM is used (as given by the last row of the table).

Fraction of HPAM in polymer mixture	distilled water		2.3% NaCl, 0.22% $NaHCO_3$		6.9% NaCl, 0.22% $NaHCO_3$		5.8% NaCl, 0.8% $CaCl_2$	
	ppm	$X/H	ppm	$X/H	ppm	$X/H	ppm	$X/H
0.0 (100% xanthan)	1228	0.52	1730	2.23	1527	2.95	1659	7.21
0.2	1002	0.54	2154	1.99	1805	2.87	1730	8.39
0.4	942	0.46	2565	1.84	2249	2.67	2151	8.59
0.5	942	0.35	2807	1.75	2058	3.37	2939	7.13
0.6	784	0.53	2251	2.78	2604	2.82	3227	7.76
0.8	694	0.59	2985	2.46	4045	1.56	5055	7.82
1.0 (100% HPAM)	636	--	3857	--	4500	--	11954	--

Critical Concentration. Using viscosity measurements at low shear rate (1.22 s^{-1}), the intrinsic viscosity of SNF Flopaam 3830S HPAM was determined. The results obtained were: [η]=26.5 dL/g, using reduced viscosity data; and [η]=40.4 dL/g, using inherent viscosity data (from Fig. 64). In both cases, the C* (the concentration at which polymer behavior transitions from dilute to semi-dilute concentration regimes) was 208 ppm. (In the semi-dilute concentration regime, polymer chains are entangled with neighboring coils, but the chain segments between entanglements are sufficiently long that their conformation resembles that of an isolated polymer.) The critical reduced concentration (C*[η], Fig. 65) obtained was 0.55-0.84. Using the Fox-Flory equation, Graessley[44] predicted a critical reduced concentration (C*[η]) equal to 0.77 where the solution transitions to the semi-dilute regime. Thus, our result is consistent with the literature.

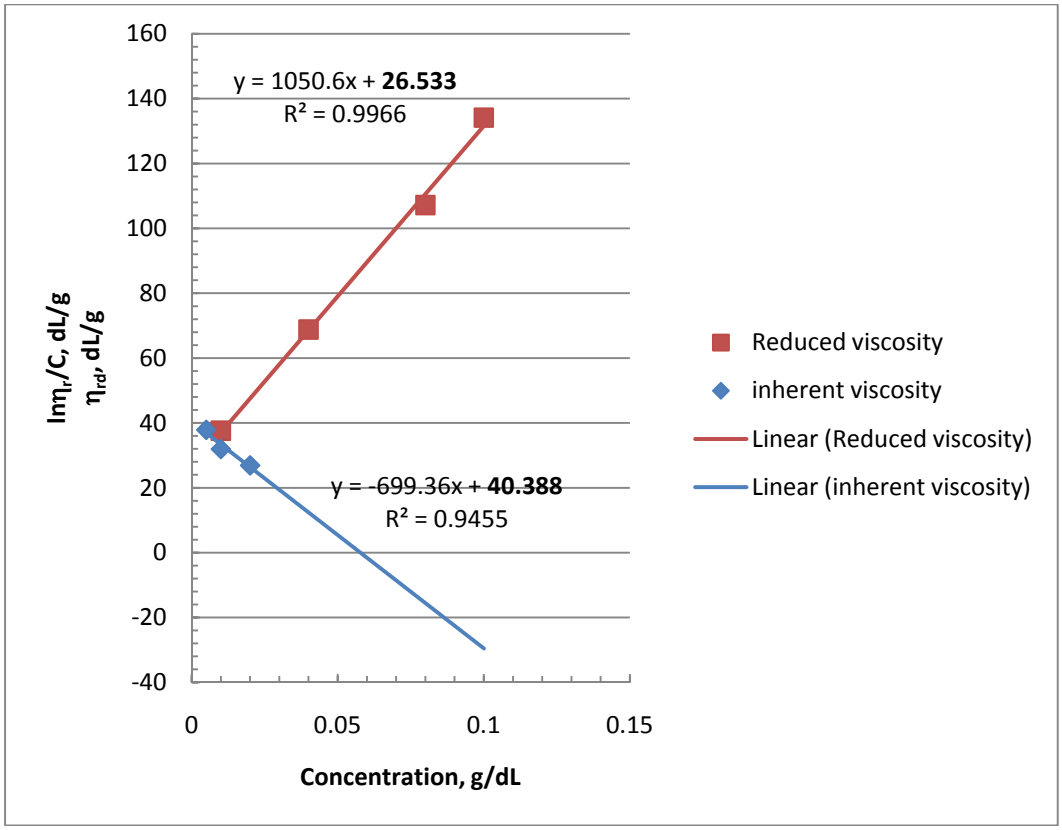

Fig. 64—Intrinsic viscosity of SNF 3830S HPAM.

Previous work indicated that constant slopes near 1.0, 2.0 and 3.3-3.75 should be expected for the curves in the dilute, semi-dilute, and concentrated regimes, respectively.[45-47] In addition, the critical reduced concentration (C**[η], Fig. 65) that delimits the semi-dilute and concentrated regimes should be around 4.0. The slopes that we observed for HPAM (Fig. 65) were 0.9 in Region 1 (dilute regime), 1.9 in Region 2 (semi-dilute regime), and 4.0 in Region 3 (concentrated regime). The intersection between the dilute and semi-dilute regimes occurred at C*[η]=0.55-0.84, C*=208 ppm. The intersection between the semi-dilute and concentrated regimes occurred at C**[η]=5.3, C**=2,000 ppm. These results are in relatively good agreement

with the literature. According to Colby,[48] for neutral polymer solutions (as would be the case for HPAM in brine), C**/C* ≅ 10.

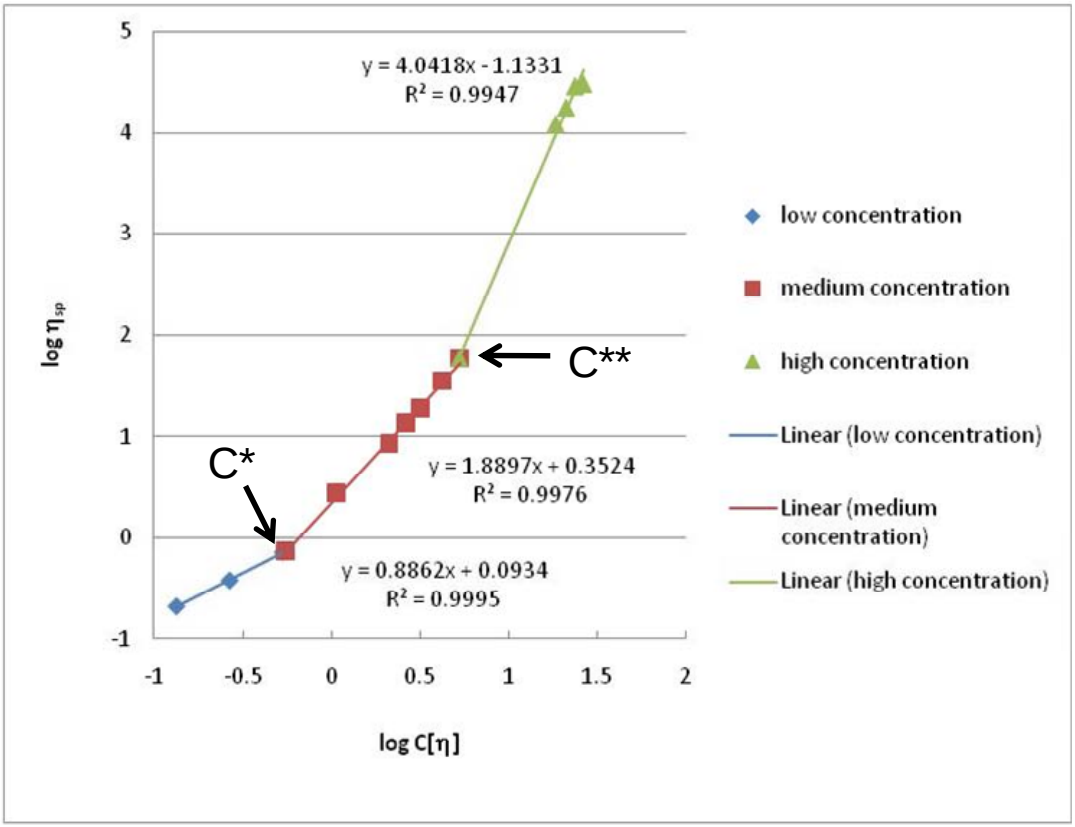

Fig. 65—log η_{sp} x log C[η] for HPAM 3830 in 2.3% NaCl, 0.22% $NaHCO_3$. [η]= 26.5 dL/g; C*[η]=0.55; C*=208 ppm; C**[η]=5.3; C**=2,000 ppm.

Corefloods. The behavior of the mixed polymer solutions was evaluated in a porous medium at room temperature (25°C) using a 15.27-cm long porous polyethylene core with a circular cross-section of 11.64 cm^2. Porosity was 35% and the pore volume was 62.8 cm^3. Two internal taps divided the core into three sections with lengths of 2.54 cm, 10.30 cm and 2.43 cm, respectively. The core was initially saturated with 2.52% TDS brine (2.3% NaCl, 0.22% $NaHCO_3$).

Fig. 66 plots resistance factor versus flux for two polymer solutions: (1) 400-ppm xanthan with 1,600-ppm HPAM and (2) 1600-ppm HPAM. In agreement with viscosity behavior, addition of 400-ppm xanthan significantly increased the low-flux resistance factor for a 1,600-ppm HPAM solution. However, it did not significantly change the flux at which the onset of viscoelastic (shear-thickening or pseudodilatant behavior) was observed (~10 ft/d in Fig. 66). In contrast, a different behavior was seen after adding 320-ppm xanthan to 480-ppm HPAM (Fig. 67). The beginning of pseudodilatant behavior was displaced from 10 ft/d to around 30 ft/d. Based on Fig. 65, 1,600-ppm HPAM was close to C** (transition concentration from semi-dilute to concentrated regime). At 480 ppm, the HPAM was in semi-dilute regime. In that case, the interactions with xanthan should be more noticeable, since no significant entanglements are expected between HPAM chains (in semi-dilute regime), and the molar volume for each polymer is similar.

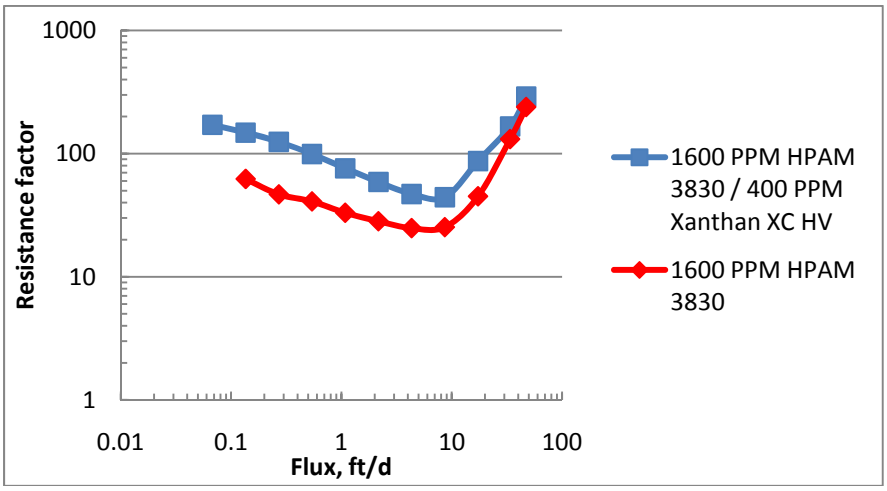

Fig. 66—Corefloods for 1,600-ppm HPAM versus 1,600-ppm HPAM/400-ppm xanthan. 2.52% TDS brine.

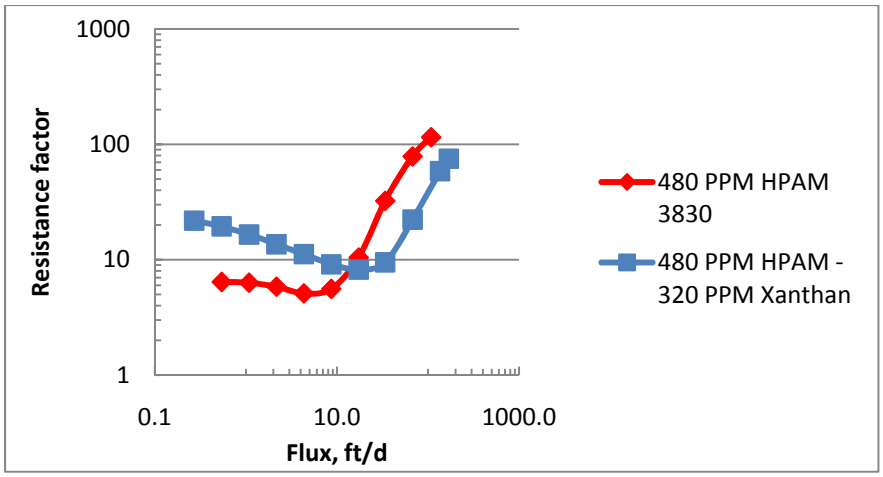

Fig. 67—Corefloods for 480-ppm HPAM/320-ppm xanthan. 2.52% TDS brine.

When distilled water was used as solvent, HPAM did not show a significant pseudodilatant (shear-thickening) behavior, even at high polymer concentrations (Figs. 68 and 69). Instead, at moderate to high fluxes, a region of near Newtonian behavior was observed. Considering that the HPAM viscosity (as well as the resistance factor) in distilled water was much higher than in brine, pseudodilatant behavior required more than simply a high hydrodynamic volume of the polymer. Similarly, even at high concentrations (5,000 ppm), xanthan solutions did not exhibit pseudodilatant behavior (Fig. 69). Presumably, pseudodilatancy occurs because coiled HPAM polymers must untangle to some extent when being forced through a pore throat. In saline brines, HPAM polymers are in a normal coil configuration, and significant energy is required to untangle the coil (i.e., expand and elongate the polymer molecule). This energy is seen in the form of high resistance factors (i.e., resistance factor increasing with increased flux). For xanthan or for HPAM in distilled water, the polymers are already in an expanded configuration, so much less additional energy is needed to force the molecule through a pore throat.

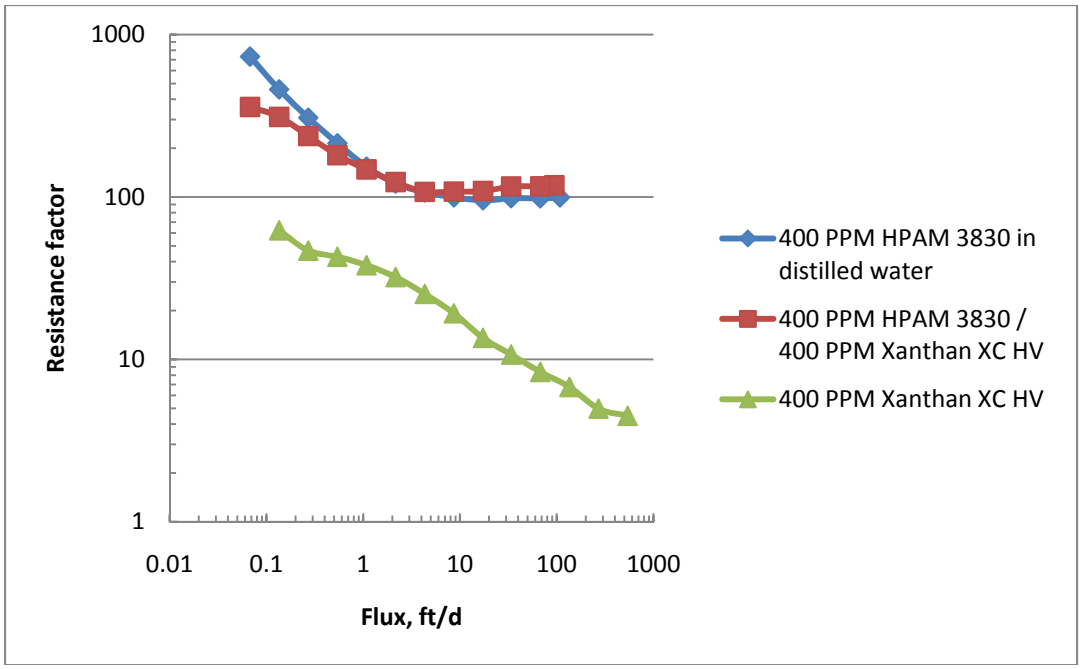

Fig. 68—Resistance factor versus flux for three solutions in distilled water.

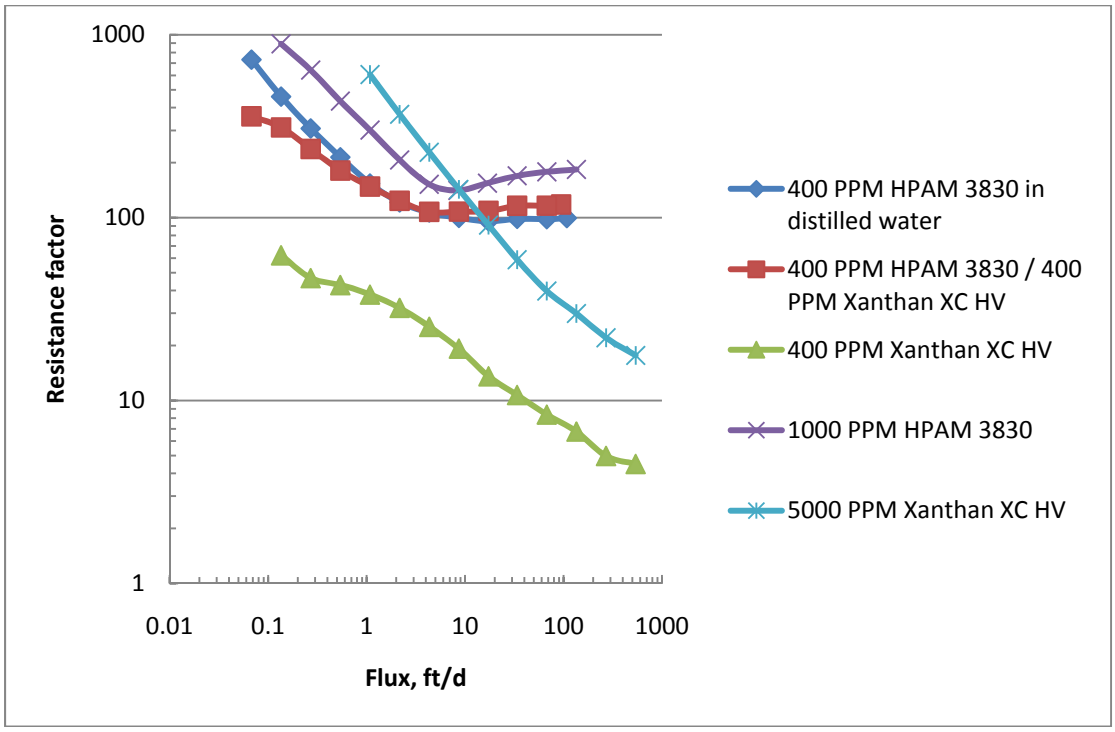

Fig. 69—Resistance factor versus flux for five solutions in distilled water.

Fig. 70 shows that the pseudodilatant behavior of HPAM in brine occurred even in the dilute regime (below 200 ppm)—at concentrations as low as 25 ppm. In brine, with an increase of HPAM concentration, the onset of pseudodilatant behavior was shifted to lower flux (Fig. 71). This effect was most pronounced for the lowest polymer concentrations (below 200 ppm).

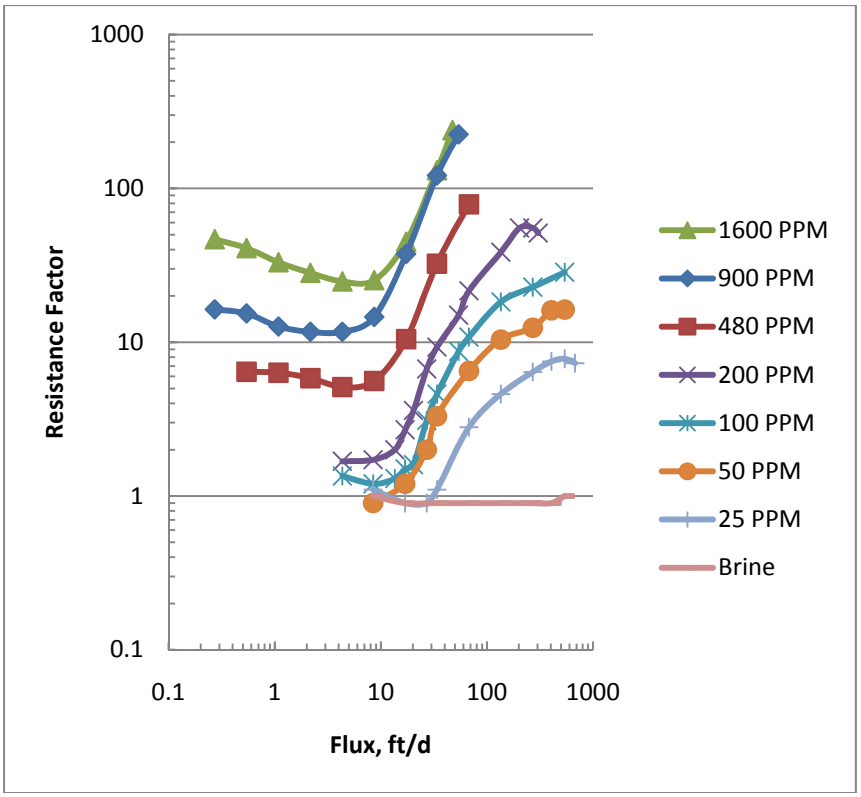

Fig. 70—HPAM pseudodilatancy at different concentrations. 2.52% TDS brine.

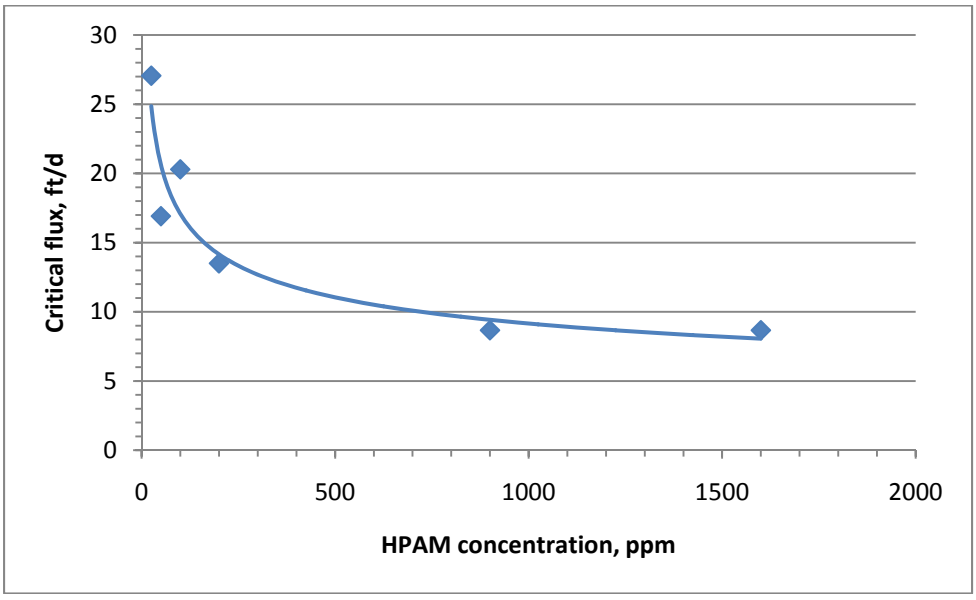

Fig. 71—Critical flux for onset of pseudodilatant behavior. HPAM in 2.52% TDS brine.

Comparing the curves for xanthan, HPAM, and HPAM/xanthan with the same viscosity (~14 cp, Fig. 72), resistance factors were basically the same at low flux (until around 8.4 ft/d), regardless of the polymer used. At higher flux values, xanthan shows pseudoplastic behavior, while the HPAM and HPAM/xanthan show pseudodilatant behavior. For the HPAM/xanthan solution, the flux for onset of pseudodilatancy shifted from ~10 ft/d to ~30 ft/d during our first experiment of this type (squares in Fig. 72). However, during a subsequent repetition, we observed the same behavior as for HPAM alone (triangles in Fig. 72). This experiment will be repeated later to clarify the discrepancy.

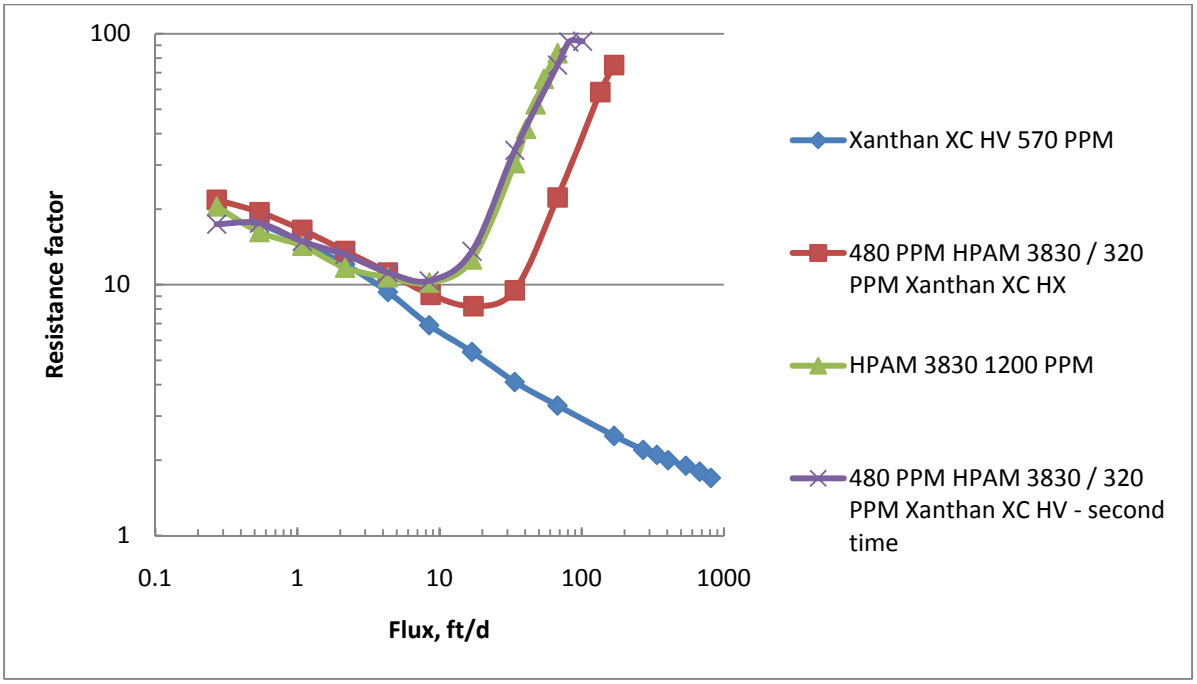

Fig. 72—Corefloods with 570-ppm xanthan, 480-ppm HPAM/320-ppm xanthan, and 1,200-ppm HPAM. 2.52% TDS brine.

The pseudodilatant (shear-thickening) behavior of HPAM in porous media was attributed to HPAM viscoelasticity and the flow-induced transition in polymer conformation from a random coil to a stretched state.[49,50] The shear-thickening behavior observed in porous media for flexible polymers, such as polyacrylamide and polyethylene oxide, and the shear-thinning behavior for more rigid molecules, such as xanthan and carboxymethylcellulose,[49] is well understood above C*. As was shown in Fig. 70, HPAM shows pseudodilatant behavior even at 25 ppm.

A random coil polymer chain in solution experiences a competition between entropic forces which expand the molecule and net attractive forces between the segments which favor collapse. Consequently, the average size and conformation of a single polymer chain in solution depends on both solvent and temperature.[51]

According to Colby,[48] stretching is a natural consequence of the conformational change of the Rouse chain in shear. The Rouse model[52] is the simplest model for flexible polymer dynamics. Only connected interactions of the monomers (i.e., covalently bonded units) are included in the Rouse model, by mapping the polymer chain onto a connected series of beads and springs

(harmonic oscillators). As such, the Rouse model only applies to unentangled polymer liquids. However, the Rouse model in shear flow, with the standard assumption that chains stretch along the flow direction but are unperturbed orthogonal to the flow direction, leads to the expectation of no shear thinning.

Real chains have finite extensibility, but shear thinning starts when the chain's conformation is first perturbed by the flow. In contrast, finite extensibility is not important until the chain is strongly stretched and is expected to gradually make shear thinning cease.

In Fig. 73, HPAM in distilled water shows pronounced shear thinning at low fluxes, but at higher fluxes near-Newtonian or a very mild shear-thickening (pseudodilatant) behavior is seen. In contrast, this polymer shows a pronounced shear thickening in brine. In distilled water, HPAM is in the maximum state of expansion, due to charge repulsion between carboxylate groups in the polymer backbone. With the increase of flux in a porous medium, the polymer suffers orthogonal distortion to align with the flow direction, showing shear-thinning behavior. In brine, the charges are screened, and the HPAM polymer collapses to approach a random coil configuration, decreasing the hydrodynamic volume of the polymer. With the increase of flux, these coils are stretched and disentangled, ultimately approaching the stretched configuration corresponding to the polymer in distilled water.

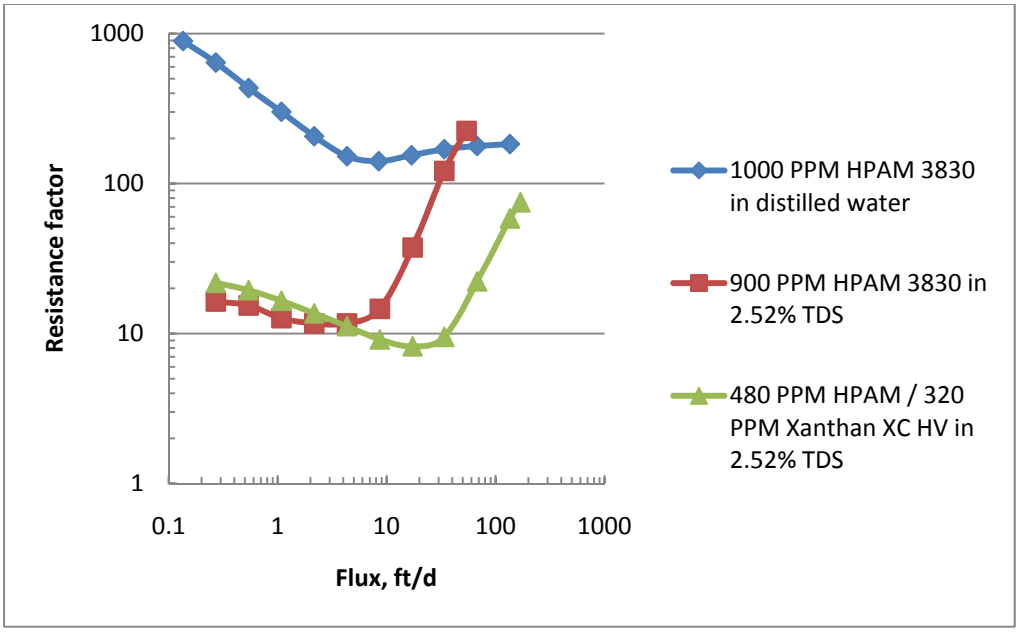

Fig. 73—Corefloods with 1,000-ppm HPAM in distilled water, 900-ppm HPAM in 2.52% TDS, and 480-ppm HPAM/320-ppm xanthan in 2.52% TDS.

The increased viscosity of HPAM-xanthan mixed solutions and the displacement of critical flux (for the onset of pseudodilatant behavior, shifting to higher flux values) could be explained by the elongation of the HPAM backbone. It is conceivable that quaternary structures form between xanthan and HPAM. Additional work is needed to investigate this idea.

HPAM/Diutan

Fig. 74 shows the effect of brine on HPAM and diutan solution viscosities. Diutan presented no sensitivity to salinity change. Compared to xanthan (Fig. 63), the salt insensitivity of diutan may be due to the presence of charges directly on the diutan backbone, whereas xanthan's backbone is neutral with charges on the side groups. Except at lower concentrations, the viscosity of diutan in brine was as high as the corresponding viscosity of HPAM in distilled water.

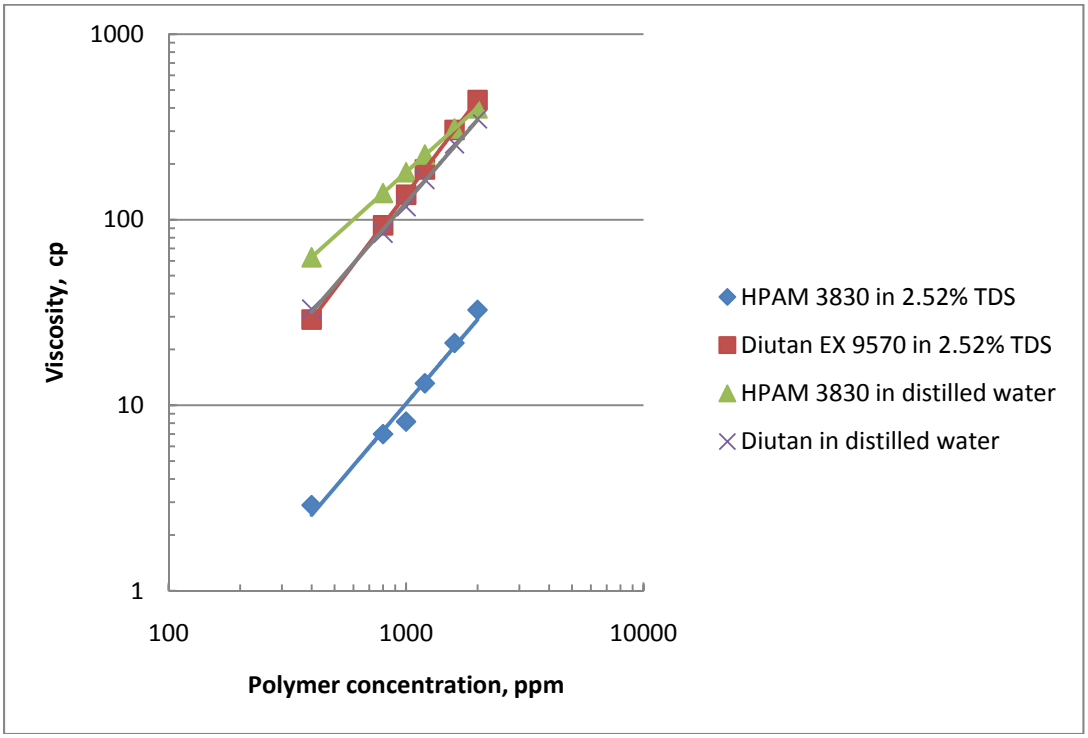

Fig. 74—Salinity effects for HPAM versus diutan. 25 °C and 7.3s^{-1}.

Table 21—Concentration parameters for HPAM–diutan mixtures. In distilled water and 2.52% TDS. Data fitted using Eq. 4.

Fraction of HPAM in polymer mixture	Distilled water		2.52% TDS	
	A	*B*	*A*	*B*
0.0 (100% diutan)	0.0044	1.4831	0.001	1.6954
0.2	0.0088	1.3935	0.0008	1.7080
0.4	0.0204	1.2815	0.0006	1.7037
0.5	0.029	1.237	0.0007	1.6541
0.6	0.0367	1.2092	0.0004	1.6975
0.8	0.0558	1.16	0.0003	1.6463
1.0 (100% HPAM)	0.0637	1.1507	0.0003	1.5067

For HPAM/diutan mixtures, Table 21 provides *A* and *B* parameters for the viscosity-concentration fit to Eq. 4, much like Table 17 provided for HPAM-xanthan mixtures. Table 22 summarizes an analysis for cost-effectiveness of the HPAM-diutan mixtures in 2.52% TDS brine, similar to those in Tables 18-20. Table 22 suggests that diutan could be competitive for use if it costs no more than 4.39 to 6.23 times that of 3830S HPAM.

Table 22—Achieving a given viscosity using HPAM/diutan mixtures. 2.52% TDS brine. ppm lists the total (mixture) polymer concentration required to achieve a given viscosity. $D/H lists diutan cost (relative to SNF 3830S HPAM) required to match the cost-effectiveness ($/cp) when only SNF 3830S HPAM is used (as given by the last row of the table).

Fraction of HPAM in polymer mixture	10 cp		50 cp		100 cp	
	ppm	$D/H	ppm	$D/H	ppm	$D/H
0.0 (100% diutan)	229	4.39	591	4.94	890	5.20
0.2	250	4.76	643	5.44	964	5.75
0.4	301	4.90	773	5.63	1161	5.98
0.5	325	5.18	860	5.80	1307	6.08
0.6	390	4.94	1006	5.76	1513	6.15
0.8	559	4.98	1485	5.84	2263	6.23
1.0 (100% HPAM)	1004	--	2922	--	4630	--

Fig. 75 shows that the *G'/G''* crossover for HPAM occurred at much lower frequencies than for diutan and decreased with increased polymer concentration. To appreciate this behavior, the responses in oscillatory experiments must be understood.[52] Small-amplitude oscillatory shear experiments involve measurement of the unsteady response of a sample that is contained between two parallel plates. The upper plate undergoes small-amplitude oscillations in its own plane with frequency, ω. For Newtonian fluids, the shear stress is in-phase with the shear rate, and there are no normal stresses. For polymeric materials, the shear stress oscillates with frequency, but is out of phase with the shear rate. Often, the data are presented in terms of the real and imaginary parts of the complex viscosity $\eta^*(\omega)$: $\eta^*=\eta' - i\eta''$. The real part, η', the dynamic viscosity, may be thought of as the viscous contribution, associated with energy dissipation. The imaginary part, η'', may be thought of as the elastic contribution, associated with energy storage. For Newtonian fluids, $\eta'=\mu$ and $\eta''=0$.

Other functions used by polymer rheologists are: $G^* = i\omega\eta^* = G' + iG''$, where $G'=\omega\eta''$ is known as the "storage modulus" and $G''=\omega\eta'$ is known as the "loss modulus". The dynamic viscosity, η', approaches the zero-shear-rate viscosity at low frequency. On the other hand, the out-of-phase part of the complex viscosity associated with energy storage approaches zero linearly with ω. Thus, there is a nonzero limiting value of η''/ω at low frequency. At intermediate frequencies, η' and η''/ω both show large power-law regions. Finally, at high frequencies, η' may approach a limiting value. For dilute solutions, this value is found to be slightly larger than

the solvent viscosity. Also at high frequencies, η''/ω may become proportional to $1/\omega^2$. Since this parameter corresponds to a storage modulus, *G'*, that is constant, the fluid acts like an elastic solid, which indicates that there is not sufficient time for molecular rearrangements at high frequencies.[52] This type of response increases with increased polymer concentration, due to the increase of entanglements and intermolecular interactions.

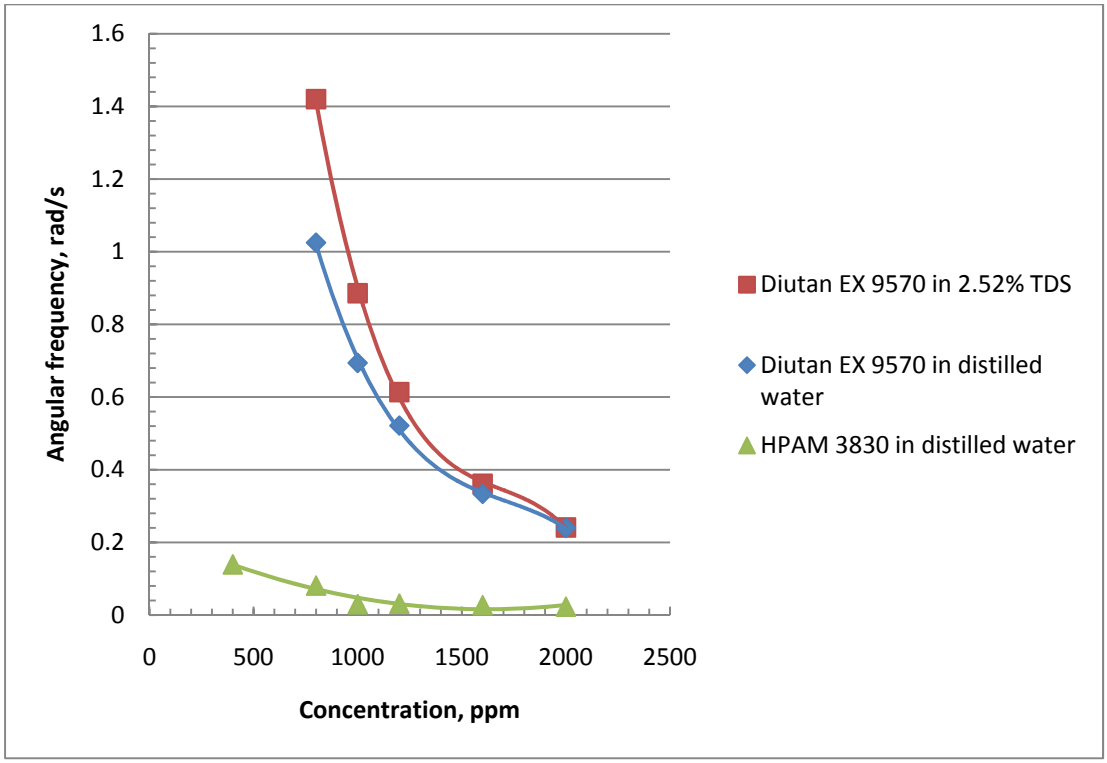

Fig. 75—Angular frequency at the *G'/G"* crossover point (from viscous to elastic behavior) versus concentration for HPAM and diutan. No *G'/G"* crossover point was observed for HPAM in brine.

In Fig. 75, the low frequency values for the HPAM *G'/G"* crossover mean that HPAM solutions assume elastic solid-like behavior quickly—much faster than diutan. This property of HPAM probably is due to its flexibility and is related to the pseudodilatant behavior in porous media. In brine, no crossover of *G'/G"* was observed for HPAM. The polymer showed more viscous than elastic behavior (*G">G'*). Diutan behavior in 2.52% TDS brine was similar to that in distilled water (squares and diamonds in Fig. 75).

Fig. 76 shows the frequency of the *G'/G"* crossover for HPAM/diutan mixtures in brine. As the HPAM content of the mixture increased in the 2.52% TDS brine, the *G'/G"* crossover was displaced to higher frequencies. In contrast, the opposite behavior was seen in distilled water (Fig. 77).

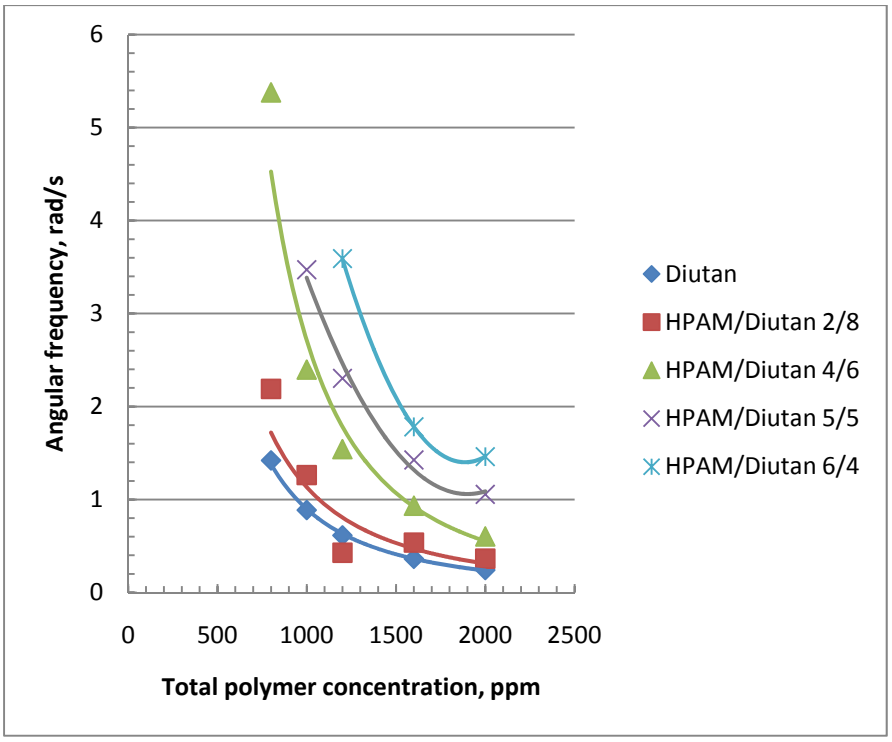

Fig. 76—Angular frequency at the *G'/G"* crossover point (from viscous to elastic behavior) versus concentration for HPAM/diutan mixtures in 2.52% TDS brine.

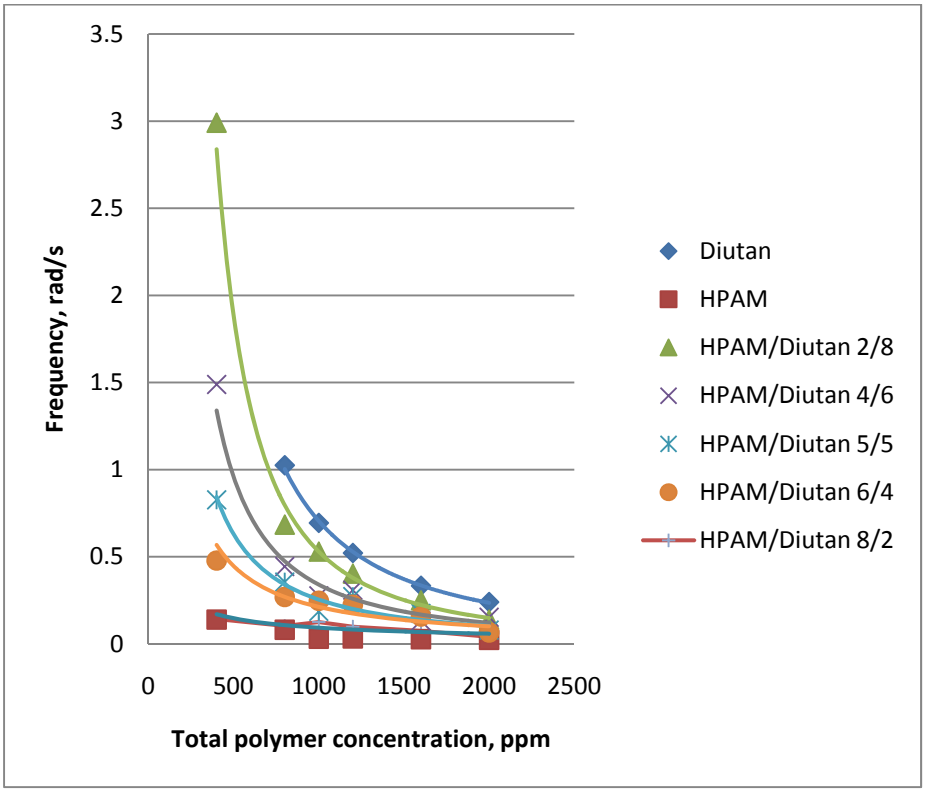

Fig. 77—Angular frequency at the *G'/G"* crossover point (from viscous to elastic behavior) versus concentration for HPAM/diutan mixtures in distilled water.

As shown above (Figs. 73 and 74), the rheological behavior of HPAM in solution is very dependent on salinity. This can be explained by its polyelectrolyte character and high flexibility. With increase in salinity, the charges on the HPAM backbone are screened and the macromolecular coil tends to collapse. In contrast, diutan has a much more rigid backbone, with no significant conformational changes upon screening of the charges. In distilled water, HPAM assumes its maximum hydrodynamic volume, provoking the highest resistance to flow. Even with diutan having a molecular weight and hydrodynamic volume on the same order as HPAM, the rigidity of diutan contributes to a slower frequency response, and the *G'/G"* crossover for diutan occurs at high frequencies (Fig. 75). In brine, the HPAM coil collapses, forming a more compact structure, less sensitive to the disturbance applied. Therefore, no *G'/G"* crossover is observed. When the two polymers are mixed in brine, the transition from viscous to solid-like behavior (*G'/G"* crossover) becomes less likely, compared to diutan, but more likely compared to HPAM. For example, in the case of HPAM/diutan with a concentration ratio of 6/4, the *G'/G"* crossover occurred at much higher frequency than diutan alone, indicating the presence of a polymeric structure less flexible than diutan. With a decrease of polymer concentration, the *G'/G"* crossover did not occur. Perhaps the *G'/G"* crossover for HPAM in brine was not observed because it occurs at a very high frequency. This result suggests the formation of HPAM/diutan mixed structures. In distilled water, this type of structure was minimized by electrostatic repulsions, and the *G'/G"* crossover occurred at frequencies between those observed for diutan and HPAM (Fig. 77).

HPAM/Alginate

Fig. 78 plots viscosity data as a function of polymer concentration for HPAM and alginate solutions. Alginate aqueous solutions provided much lower viscosities than HPAM, both in distilled water and brine. This result probably is related to the lower molecular weight (not given by the supplier) of alginate. Alginate is found in a wide variety of brown seaweeds and is a linear block copolymer of α-L-glucuronic acid (G) and β-D-mannuronic acid (M). The blocks vary in size. Alternating G and M segments as well as random blocks may also be present. The type of structure is influenced by the seaweed source as well as the growing conditions of the weed. The block structure ultimately dictates the properties of the alginate produced. Roughly speaking, the M to G ratio of the alginate largely controls functionality.

The *B* concentration exponent (Table 23) obtained for alginate was lower than for HPAM, both in distilled water and brine, indicating that alginate has a lower capacity of increasing the solution viscosity with the increase of polymer concentration. For all brines and polymer concentrations that we investigated, alginate and HPAM-alginate mixtures were not cost-effective viscosifiers. In the very best circumstances, the maximum allowable cost of alginate is less than one-quarter of the cost of 3830S HPAM.

No crossover of *G'/G"* was observed neither for alginate or HPAM/alginate solutions in distilled water or brine, indicating that alginate has more viscous than elastic behavior (*G">G'*). This observation is consistent with the low solution viscosities for this alginate polymer.

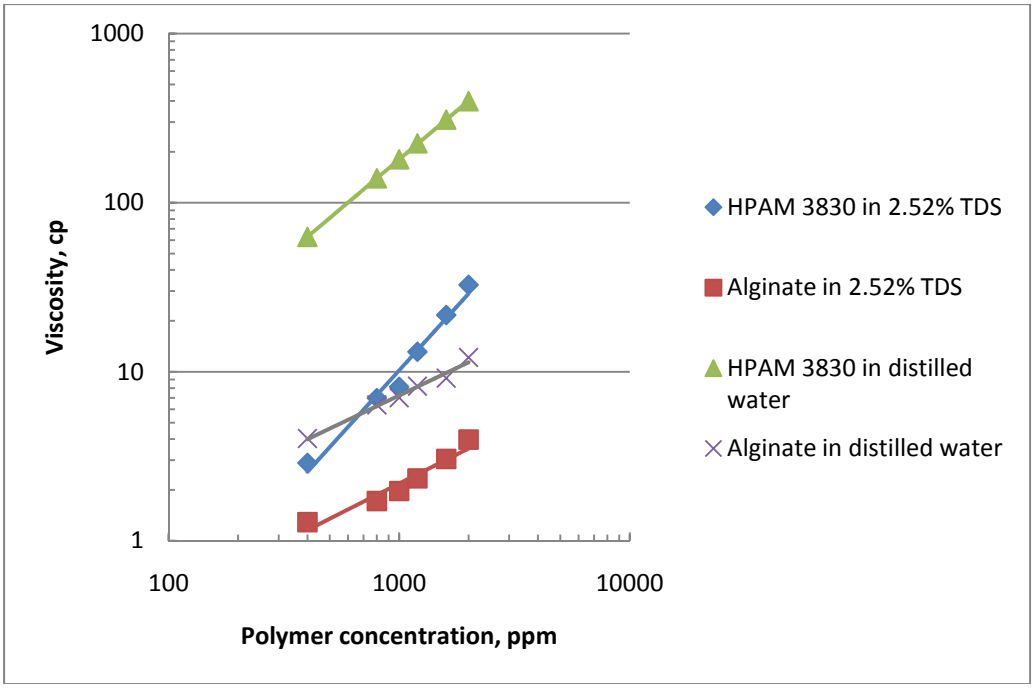

Fig. 78—Viscosity versus concentration for HPAM and alginate in distilled water and 2.52% TDS brine. 25 °C and 7.3 s^{-1}.

Table 23—Concentration parameters for HPAM–alginate mixtures in distilled water and 2.52% TDS. Data fitted using Eq. 4.

Fraction of HPAM in polymer mixture	Distilled water		2.52% TDS	
	A	*B*	*A*	*B*
0.0 (100% alginate)	0.0805	0.6514	0.0186	0.6896
0.2	0.0775	0.8521	0.0072	0.8847
0.4	0.0831	0.9443	0.0024	1.1005
0.5	0.0785	0.9911	0.0018	1.1594
0.6	0.0843	1.0106	0.0013	1.2255
0.8	0.0939	1.046	0.0007	1.3528
1.0 (100% HPAM)	0.0637	1.1507	0.0003	1.5067

Conclusions

With the aim of joining the characteristic properties and advantages of synthetic polymers and biopolymers, a study was started using mixed solutions of the following commercial products. The following binary mixtures were studied: HPAM/xanthan, HPAM/diutan, and HPAM/alginate. All the mixed systems were evaluated in distilled water and brine.

1. Many HPAM/xanthan mixtures in brine show viscosity behavior that is virtually the same as solutions with only xanthan. For example, in brine with 2.3% NaCl and 0.22% $NaHCO_3$, the mixture with 60% HPAM/40% xanthan has almost the same viscosity behavior as 100% xanthan. Since xanthan is considerably more expensive (per kg) than HPAM, this observation suggests a significant economic value in using polymer mixtures instead of a single polymer.
2. The main goal in investigating mixtures of HPAM and various biopolymers (especially xanthan) is to identify conditions where the use of the mixture might be more cost-effective than HPAM alone. To achieve this goal, the polymer components in the mixture must be compatible (i.e., mix to form a single phase with no suspended material that would plug porous media). All mixtures investigated in this chapter met this requirement.
3. A second requirement is that the cost-effectiveness of the mixture must be at least as attractive as that for a solution that contains only HPAM. Xanthan would have to cost 50% less than 3830S HPAM to become feasible for use in water with low salinity. Thus, as expected, HPAM alone is necessarily preferred for low-salinity applications.
4. In contrast, for the high-salinity, high-hardness brine (5.8% NaCl, 0.8% $CaCl_2$), xanthan would be competitive if it cost 3.76 to 8.59 times more than 3830S HPAM, depending on the desired viscosity level. Thus, xanthan alone or a HPAM/xanthan mixture might be preferred in this brine.
5. The brine that was most characteristic of North Slope brines contained 2.3% NaCl, 0.22% $NaHCO_3$. For this brine, the required xanthan cost ranges from 1.31 to 2.78 times the cost of 3830S HPAM. For xanthan only (i.e., no HPAM in the polymer mixture), xanthan must cost no more than 1.85 to 2.23 times the cost of 3830S HPAM. This range of price might be difficult for xanthan suppliers to achieve.
6. However, before becoming too pessimistic about xanthan's potential on the North Slope, the permeability dependence of HPAM performance may need to be considered. A lower molecular weight HPAM may be needed. These lower Mw polymers cost roughly the same as a high Mw HPAM, but more polymer is needed to provide a given viscosity. Since xanthan can readily penetrate into the low-permeability rock, its cost-effectiveness improves relative to the lower Mw HPAMs.
7. When distilled water is used as a solvent, HPAM does not show pseudodilatant (shear-thickening) behavior even at high polymer concentrations. Presumably, pseudodilatancy occurs because coiled HPAM polymers must untangle to some extent when being forced through a pore throat. In saline brines, HPAM polymers are in a normal coil configuration, and a significant energy is required to untangle the coil (i.e., expand and elongate the polymer molecule). This energy is seen in the form of high resistance factors (i.e., resistance factor increasing with increased flux). For xanthan or for HPAM in distilled water, the polymers are already in an expanded configuration, and much less additional energy is needed to force the molecule through a pore throat—thus, shear thickening is not seen.
8. Pseudodilatant behavior of HPAM in brine occurred at concentrations as low as 25 ppm.
9. A HPAM-xanthan mixture showed displacement of critical flux (for the onset of pseudodilatant behavior) to higher flux values. This behavior could be explained by the elongation of the HPAM backbone. It is conceivable that quaternary structures form between xanthan and HPAM.
10. Diutan could be competitive for use if it costs 4.39 to 6.23 times the cost of 3830S HPAM.
11. Alginate was generally ineffective as a viscosifier, compared with the other polymers.

NOMENCLATURE

A = constant in Eq. 4
API = American Petroleum Institute
B = exponent in Eq. 4
C = polymer concentration, parts per million [g/cm^3]
C^* = polymer concentration at the transition from dilute to semi-dilute behavior, parts per million [g/cm^3]
C^{**} = polymer concentration at the transition from semi-dilute to concentrated behavior, parts per million [g/cm^3]
dp/dl = pressure gradient, psi/ft [Pa/m]
E_{Abt} = areal sweep efficiency at water breakthrough
F_r = resistance factor
F_{r1} = resistance factor in Core Section 1
F_{r2} = resistance factor in Core Section 2
F_{r3} = resistance factor in Core Section 3
G' = storage modulus, Pa
G'' = loss modulus, Pa
G^* = complex modulus, Pa
G = α-L-glucuronic acid
g = acceleration due to gravity, 980 cm^2/s
HPAM = partially hydrolyzed polyacrylamide
h = formation height, ft [m]
h_1 = height of Zone 1, ft [m]
h_2 = height of Zone 2, ft [m]
i = In Eq. 6: injectivity for unit mobility displacement, BPD/psi [m^3/d-Pa]
i = square root of -1
i_{wbt} = injectivity at water breakthrough, BPD/psi [m^3/d-Pa]
k = permeability, darcys [μm^2]
k_{ro} = relative permeability to oil
k_{roo} = endpoint relative permeability to oil
k_{rw} = relative permeability to water
k_{rwo} = endpoint relative permeability to water
k_1 = permeability of Zone 1, darcys [μm^2]
k_2 = permeability of Zone 2, darcys [μm^2]
L = distance between horizontal injection and production wells, ft [m]
M = mobility ratio
M = β-D-mannuronic acid
M_w = molecular weight, daltons
no = oil saturation exponent in Eq. 2
nw = water saturation exponent in Eq. 1
Δp = pressure drop, psi [Pa]
PV = pore volumes of fluid injected
q = flow rate, BPD [m^3/d]
q_{HW} = injection rate for a horizontal well, BPD [m^3/d]
q_L = injection rate for pure linear flow, BPD [m^3/d]

q_5 = injection rate for a vertical well in a 5-spot pattern, BPD [m^3/d]
r_w = wellbore radius, ft [m]
S_{or} = residual oil saturation
S_{wr} = residual water saturation
TDS = total dissolved solids
u = flux, ft/d [m/d]
u_z = vertical flux, ft/d [m/d]
W = length of a horizontal well, ft [m]
$\dot{\gamma}$ = shear rate, s^{-1}
$[\eta]$ = intrinsic viscosity, dL/g [cm^3/g]
η_{sp} = specific viscosity, (viscosity minus solvent viscosity)/(solvent viscosity)
η^* = complex viscosity, cp [mPa-s]
η' = dynamic viscosity, cp [mPa-s]
η'' = imaginary viscosity, cp [mPa-s]
μ = viscosity, cp [mPa-s]
μ_w = water viscosity, cp [mPa-s]
μ_{zs} = zero-shear viscosity, cp [mPa-s]
$\Delta\rho$ = density difference, g/cm^3
Σ = throughput, cm^3/cm^2
ϕ = porosity
ϕ_1 = porosity in Zone 1
ϕ_2 = porosity in Zone 2
ω = angular frequency, Hz [s^{-1}]

REFERENCES

1. Stryker, A.R. , R. Watkins, D.K. Olsen, A. K. Sarkar, E. B. Ramzel, W.I. Johnson and J. Butz.: "Feasibility Study of Heavy Oil Recovery in the United States" NIPER/BDM-0225, September 1995.
2. Thomas, C.P., D.D. Faulder, T.C. Doughty, D.M. Hite and G.J. White: "Alaska North Slope Oil and Gas, A Promising Future or an Area in Decline" DOE/NETL-2007/1279, August 2007.
3. Taber, J.J., Martin, F.D., and Seright, R.S.: "EOR Screening Criteria Revisited - Part 1:," Introduction to Screening Criteria and Enhanced Recovery Field Projects," *SPE Reservoir Engineering* (Aug. 1997) 189-198.
4. Taber, J.J., Martin, F.D., and Seright, R.S.: "EOR Screening Criteria Revisited - Part 2: Applications and Impact of Oil Prices," *SPE Reservoir Engineering* (Aug. 1997) 199-205.
5. Nelms, R.L. and R.C. Burke.: "Evaluation of Oil Recovery Characteristics to Assess North Dakota Carbon Dioxide Miscible Flood Potential "12th Williston Basin Horizontal Well and Petroleum Conference, May 2-4, 2004, Minot, North Dakota.
6. http://www.netl.doe.gov/publications/press/2005/tl_heavy_oil.html.
7. Mohanty, K.K: "Development of Shallow Viscous Oil Reserves in North Slope," DOE Report DE-FC26-01BC15186, December 2004.
8. Manning, R.K. et al.: "A Technical Survey of Polymer Flooding Projects," DOE report DOE/BC/10327-19, U.S. DOE, (Sept. 1983).
9. Seright, R.S.: "Improved Techniques for Fluid Diversion in Oil Recovery," first annual report, DOE/BC/14880-5, U.S. DOE (Dec. 1993) 2-72.
10. Kumar, M., Hoang, V., Satik, C., and Rojas, D.: "High-Mobility-Ratio-Waterflood Performance Prediction: Challenges and New Insights," *SPEREE,* (Feb. 2008) 186-196.
11. Maitin, B.K.: "Performance Analysis of Several Polyacrylamide Floods in North German Oil Fields," paper SPE 24118 presented at the 1992 SPE/DOE Symposium on Improved Oil Recovery, Tulsa, April 22-24.
12. Taber, J.J. and Seright, R.S.: "Horizontal Injection and Production Wells for EOR," paper SPE 23952 presented at the 1992 SPE/DOE Symposium on Enhanced Oil Recovery, Tulsa, OK, April 22-24.
13. Van den Hoek, P.J. *et al*.: "Waterflooding Under Dynamic Induced Fractures: Reservoir Management and Optimization of Fractured Waterfloods," paper SPE 110379 presented at the 2008 SPE Improved Oil Recovery Symposium, Tulsa, OK, April 19-23.
14. Seright, R.S.: "The Effects of Mechanical Degradation and Viscoelastic Behavior on Injectivity of Polyacrylamide Solutions," Society of Petroleum Engineers J. (June 1983) 475-85.
15. Wang, D.M., Han, P., Shao, Z., Weihong, H., and Seright, R.S.: "Sweep Improvement Options for the Daqing Oil Field," *SPEREE* (Feb. 2008) 18-26.
16. Seright, R.S., Seheult, J.M., and Talashek, T.A. 2008: "Injectivity Characteristics of EOR Polymers," paper SPE 115142 presented at the SPE Annual Technical Conference and Exhibition, Denver, CO, 21-24 September.
17. Trantham, J.C., Threlkeld, C.B., and Patternson, H.L.: "Reservoir Description for a Surfactant/Polymer Pilot in a Fractured, Oil-Wet Reservoir—North Burbank Unit Tract 97," *JPT* (September 1980) 1647-1656.
18. Craig, F.F.: "The Reservoir Engineering Aspects of Waterflooding," SPE Monograph **3**, Society of Petroleum Engineers, Dallas (1971) 73-74.

19. Coats, K.H., Dempsey, J.R., and Henderson, J.H.: "The Use of Vertical Equilibrium in Two-Dimensional Simulation of Three-Dimensional Reservoir Performance," *SPEJ*, **11**(1), (March 1971) 63-71.
20. Zapata, V.J. and Lake, L.W.: "A Theoretical Analysis of Viscous Crossflow." Paper SPE 10111 presented at the 1981 SPE Annual Technical Conference and Exhibition, San Antonio, TX, Oct. 5-7.
21. Sorbie, K.S. and Seright, R.S.: "Gel Placement in Heterogeneous Systems with Crossflow," paper SPE 24192 presented at the 1992 SPE/DOE Symposium on Enhanced Oil Recovery, Tulsa, OK, April 22-24.
22. Wang, D. *et al*.: "Commercial Test of Polymer Flooding in Daqing Oil Field," SPE paper 29902 presented at the 1995 SPE International Meeting on Petroleum Engineering, Beijing, China, Nov. 14-17.
23. Wang, D.M., Seright, R.S., Shao, Z., Wang, J.: "Key Aspects of Project Design for Polymer Flooding at the Daqing Oil Field," *SPEREE* (December 2008) 1117-1124.
24. Wang, D.M., Dong, H., Lv, C., Fu, X., and Nie, J.: "Review of Practical Experience of Polymer Flooding at Daqing," *SPEREE* (June 2009) 470-476.
25. Jennings, R.R., Rogers, J.H., and West, T.J. 1971: "Factors Influencing Mobility Control by Polymer Solutions," *JPT* **23**(3): 391–50, SPE 2867-PA.
26. Vela, S., Peaceman, D.W. and Sandvik, E.I.: "Evaluation of Polymer Flooding in a Layered Reservoir with Crossflow, Retention, and Degradation," *SPEJ*, **16**(2), (April 1976) 82-96.
27. Zhang, G. and Seright, R.S.: "Conformance and Mobility Control: Foams versus Polymers," paper SPE 105907 presented at the 2007 SPE International Symposium on Oilfield Chemistry, Houston, TX, Feb. 28-Mar. 2.
28. Seright, R.S. Prodanovic, M., and Lindquist, W.B.: "X-Ray Computed Microtomography Studies of Fluid Partitioning in Drainage and Imbibition Before and After Gel Placement: Disproportionate Permeability Reduction," *SPEJ* (June 2006) 159-170.
29. Chauveteau, G.: "Rodlike Polymer Solution Flow through Fine Pores: Influence of Pore Size on Rheological Behavior," *J. Rheology* **26**(2), (1982), 111-142.
30. Seright, R.S.: "Effect of Rheology on Gel Placement," *SPERE* (May 991) 212-218.
31. Hirasaki, G.J., and Pope, G.A.: "Analysis of Factors Influencing Mobility and Adsorption in the Flow of Polymer Solution Through Porous Media. *SPEJ* **14**(4), (1974), 337–346.
32. Durst, F., Haas, R., and Interthal, W.: "Laminar and Turbulent Flows of Dilute Polymer Solutions: A Physical Model," *Rheologica Acta* **21**(4-5), (1982) 572-577.
33. Duda, J.L., Hong, S., and Klause, E.E.: "Flow of Polymer Solutions in Porous Media: Inadequacy of the Capillary Model," *Ind. & Eng. Chem. Fund*. **22**, (1983) 299-305.
34. Heemskerk, J. *et al*. 1984: "Quantification of Viscoelastic Effects of Polyacrylamide Solutions," paper SPE 12562 presented at the SPE/DOE Symposium on Enhanced Oil Recovery Symposium, Tulsa, OK, 15-18 April.
35. Cannella, W.J., Huh, C., and Seright, R.S. 1988: "Prediction of Xanthan Rheology in Porous Media," paper SPE 18089 presented at the SPE Annual Technical Conference and Exhibition, Houston, TX, 2-5 October.
36. Hejri, S, Willhite, G.P., and Green, D.W. 1988: "Development of Correlations to Predict Flocon 4800 Biopolymer Mobility in Porous Media," paper SPE 17396 presented at the SPE/DOE Symposium on Enhanced Oil Recovery Symposium, Tulsa, OK, 17-20 April.
37. Chauveteau, G. and Kohler, N. 1984. Influence of Microgels in Polysaccharide Solutions on Their Flow Behavior Through Porous Media, *SPEJ* **24**(3): 361-368.

38. Seright, R.S., Maerker, J.M., and Holzwarth G. 1981: "Mechanical Degradation of Polyacrylamides Induced by Flow Through Porous Media.," American Chemical Society *Polymer Preprints*, **22**(August): 30–33.
39. Pye, D.J. 1964: "Improved Secondary Recovery by Control of Water Mobility," *JPT* **16**(8): 911–916, SPE 845-PA.
40. Smith, F.W. 1970: "The Behavior of Partially Hydrolyzed Polyacrylamide Solutions in Porous Media," *JPT* **22**(2): 148–156. SPE 2422-PA.
41. Masuda, Y., Tang. K-C., Mlyazawa, M., and Tanaka, S. 1992: "1D Simulation of Polymer Flooding Including the Viscoelastic Effect of Polymer Solution," *SPERE* **7**(2): 247–252, SPE 9499-PA.
42. Maerker, J.M. 1975: "Shear Degradation of Partially Hydrolyzed Polyacrylamide Solutions," *SPEJ* **15**(4): 311–322, SPE 5101-PA.
43. Maerker, J.M. 1976: "Mechanical Degradation of Partially Hydrolyzed Polyacrylamide Solutions in Unconsolidated Porous Media," *SPEJ* **16**(4): 172–174, SPE 5672-PA.
44. Graessley, W.W., ***Polymer***, **21**, 258-262 (1980).
45. Vasconcelos, C.L, Martins, R.R., Ferreira, M.O., Pereira, M.R., Fonseca, J.L.C., *Polym. Int.*, **51**, 69-74 (2001).
46. Morris, E.R., Cutler, A.N., Ross-Murphy, D.A.R., *Carbohydr. Polym.*, **1,** 5-21 (1981).
47. Launay, B., Cuvelier, G., Martinez-Reyes, S., *Carbohydr. Polym.*, **34**, 385-395 (1998).
48. Colby, R.H., Boris, D.C., Krause, W.E., Dou, S., *Rheol Acta*, **46**, 569-575 (2007).
49. Duda, J.L., Hong, S.A., Klaus, E.E., *Ind. Eng. Chem. Fundamen.*, **22**(3), 299-305 (1983).
50. Lim. T., Uhl, J.T., Prud'homme, R.K., *SPE Reservoir Engineering*, May 2006.
51. Manz, B., Callaghan, P.T., *Macromolecules*, **30**, 3309-3316 (1997).
52. Bird, R.B., Armstrong, R.C., Hassager, O., *Dynamics of Polymeric Liquids: Fluid Mechanics*. John Wiley & Sons, New York, 1977.
53. Sonebi, M., *Cement and Concrete Research* **36**, 1609–1618 (2006).